SLAC-PUB-5210
March, 1990
(T/E)

Theory of Precision Electroweak Measurements

MICHAEL E. PESKIN*

Stanford Linear Accelerator Center
Stanford University, Stanford, California 94309

Lectures presented at the Seventeenth SLAC Summer Institute
Physics at the 100 GeV Mass Scale
Stanford, California, July 10 – 21, 1989

* Work supported by the Department of Energy, contract DE-AC03-76SF00515.

TABLE OF CONTENTS

1. Introduction

From Bequerel's discovery of radioactivity almost a century ago, the study of weak interactions has matured through a series of well-defined stages. The most recent of these began in the early 1970's with the experimental discovery of neutral currents and the theoretical discovery of renormalizable gauge theories with massive vector bosons. These discoveries led to a study of the neutral current effects through a wide variety of processes and, eventually, to a remarkable convergence of the data to the predictions of the now-standard weak interaction model of Glashow, Weinberg, and Salam.

Last summer, this era of the study of weak interactions ended and a new era began. Instead of data dominated by results on effective interactions at relatively low energy, we are beginning to see the most important data come from direct measurements of the weak gauge bosons. Instead of measurements to an accuracy in the weak interaction parameter $\sin^2 \theta_w$ of 10^{-2}, we can look forward to accuracies of 10^{-4}. And, most importantly, instead of looking forward to the convergence of all measurements to the predictions of a particular model, we can look forward to the discovery of *disagreements* between weak interaction experiments, at a level of detail that might give clues to new phenomena at higher energies.

In these lectures, I will review the theoretical concepts needed to understand the goals and implications of experiments in this new era of weak interactions. I will explain how to compute the most important order-o radiative corrections to weak interaction processes and discuss the physical implications of these correction terms. I hope that this discussion will be useful to those-experimentalists and theorists-who will try to interpret the new data that we will soon receive.

Of course, these brief lectures can only provide an overview of the the subject. The field of precision weak interactions, like any other area of precision measurement, is full of technical complication. Fortunately, one has available original papers of great beauty, beginning with the pioneering works of Sirlin[1,2] and Veltman,[3,4] and a number of recent excellent reviews. Among these, the article

of Hollik[5] is a particularly complete and instructive summary of the theory, and the 1989 LEP study volume[6] reviews the most recent numerical results. I hope that my lectures will complement these works by providing an entryway into this field not only for those who seek to be experts but for all those who would like to understand its new stage of development.

These lectures are organized as follows: In Section 2, I will review the structure of the standard weak interaction model at zeroth order. In Section 3, I will discuss the measurement of the Z^0 boson mass in e^+e^- annihilation. This measurement is affected by radiative corrections to the form of the Z^0 resonance, and so I will review the theory of the resonance line shape. In Section 4, I will briefly review the modifications of the properties of the Z^0 which would be produced by additional neutral gauge bosons. In Section 5, I will review the theory of the renormalization of weak interaction parameters such as $\sin^2 \theta_w$, concentrating especially on the contributions of the top quark and other heavy, undiscovered particles. Section 6 will give some conclusions and prospects.

2. The Standard Electroweak Model

Let us begin by recalling the basic zeroth order relations between boson masses and coupling constants in the Glashow-Weinberg-Salam weak interaction model. I will refer to this theory from here on as the standard model.

The construction of the standard model begins with the coupling of of fermions to gauge bosons of the group SU(2) x U(1). This interaction is specified by the minimal coupling

$$\mathcal{L} = \bar{f} i \not{D} f ,$$

where the gauge-covariant derivative introduces the three $SU(2)$ gauge bosons, A",, and one boson B_μ associated with the U(1):

$$D_\mu = \partial_\mu - i(g A^a_\mu \tau^a + g' B_\mu Y). \tag{2.1}$$

The parameters g, g' are the-coupling constants of the two groups, $\tau^a = \sigma^a/2$, and Y denotes the U(1) charge, or hypercharge.

The gauge bosons of the standard model acquire masses by spontaneous breaking of the gauge symmetry. The simplest way to achieve this breaking is by introducing a scalar field $\phi(x)$, the Higgs field. This is a complex doublet under $SU(2)$ with hypercharge Y = $\frac{1}{2}$. The kinetic term of the ϕ field, which contains the gauge fields via minimal coupling, then includes a term

$$\mathcal{L} = |D_\mu \phi|^2 \qquad \rightarrow \qquad \phi^\dagger (gA \cdot \tau + g' BY)^2 \phi . \tag{2.2}$$

If ϕ acquires a vacuum expectation value

$$\langle \phi \rangle = \begin{pmatrix} 0 \\ v/\sqrt{2} \end{pmatrix} ,$$

and we introduce this vacuum expectation value into (2.2), we find the gauge field

mass term

$$\frac{1}{2}\left(\left(\frac{g}{2}\right)^2\left[(A^1)^2+(A^2)^2\right]+\left[\frac{gA^3-g'B}{2}\right]^2\right)v^2.$$

The mass eigenstates are then

$$W^{\pm}=\frac{A^1\mp iA^2}{\sqrt{2}} \qquad m_W=\frac{g}{2}v$$

$$Z=\frac{gA^3-g'B}{\sqrt{g^2+g'^2}} \qquad m_Z=\frac{\sqrt{g^2+g'^2}}{2}v \tag{2.3}$$

$$A=\frac{g'A^3+gB}{\sqrt{g^2+g'^2}} \qquad m_\gamma=0\ .$$

It is convenient to define a weak interaction mixing angle θ_w by

$$\cos\theta_w=\frac{g}{\sqrt{g^2+g'^2}} \qquad \sin\theta_w=\frac{g'}{\sqrt{g^2+g'^2}}\ .$$

The standard electric charge is given by

$$e=\frac{gg'}{\sqrt{g^2+g'^2}}=g\sin\theta_w=g'\cos\theta_w\ .$$

The formulae above imply the important relation

$$\frac{m_W^2}{m_Z^2}=\cos^2\theta_w\ . \tag{2.4}$$

Experimentally, this relation holds to within 1% accuracy, and so it is important to understand its origin. In this analysis, (2.4) would seem to be a special consequence of the assumption that the Higgs field ϕ is the agent which breaks $SU(2)$ x U(1). But it may be shown that (2.4) holds at zeroth order in any model in which the field which acquires the vacuum expectation value is an isodoublet, and in a class of more general models, including models without elementary scalar fields,

characterized by Sikivie, Susskind, Voloshin, and Zakharov.[7] The essential feature of these models is the presence of an unbroken $SU(2)$ global symmetry in the Higgs sector. Throughout these lectures, I will assume that the Higgs sector is constructed in such a way that (2.4) holds at leading order. My analysis will not otherwise depend on the nature of the Higgs sector except in Section 5, where I will specifically discuss the dependence of radiative corrections of the mass of the scalar Higgs boson in the simplest symmetry-breaking scheme.

Once the theory has been defined in terms of the three parameters g, g', and v, one can work out the predictions of the theory for a whole variety of weak interaction processes. The leading-order predictions for the weak boson masses have already been given above. To discuss the interactions mediated by these bosons, it is useful to rewrite the basic gauge-covariant derivative (2.1) in terms of the mass eigenstates:

$$\begin{aligned}(gA_\mu^a\tau^a + g'B_\mu Y) = &\frac{e}{\sqrt{2}\sin\theta_w}\left(W_\mu^+\tau^+ + W_\mu^-\tau^-\right) \\ &+ \frac{e}{\sin\theta_w \cos\theta_w} Z_\mu(I^{3L} - \mathrm{Q}\sin^2\theta_w) + eA_\mu Q\end{aligned} \tag{2.5}$$

In this equation, $\tau^\pm = \tau^1 \pm i\tau^2$, I^{3L} is the third component of weak isospin, and Q = I^{3L} + Y is the electric charge. The photon then couples to the usual electromagnetic current. The W couples to the charged current of left-handed fermions

$$J_\mu^+ = \bar{L}\gamma_\mu\tau^+ L + \ldots = \bar{\nu}_L\gamma_\mu e_L + \ldots, \tag{2.6}$$

where $f_L = \frac{1}{2}(1 - \gamma^5)f$ denotes the left-handed component. The Z^0 couples to a neutral current of the particular form

$$J_\mu^Z = J_\mu^{3L} - \sin^2\theta_w J_\mu^Q, \tag{2.7}$$

in which J_μ^{3L}, J_μ^Q are, respectively, the weak isospin and electric charge currents. The unusual properties of the Z^0 and the weak neutral current all follow directly

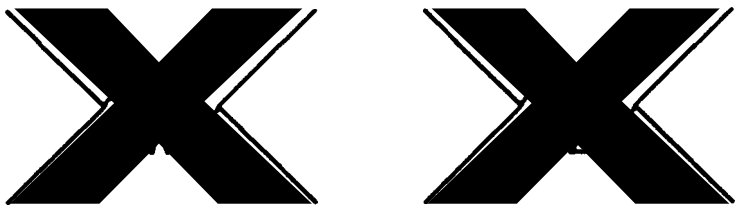

3-90 6581A1

Figure 1. Diagrams contributing to effective low-energy weak interactions.

from the chirally asymmetric Z^0 charge $(I^{3L} - \sin^2\theta_w Q)$. (I will label the weak isospin I^{3L} henceforth simply as I^3.)

At high energies, the interactions of fermions with the Z^0 and W currents are made visible in the strength and angular dependence of the weak boson decays to the various species. At energies well below the Z^0 and W masses, however, experiments probe the effective four-fermion interaction which results from Z^0 and W exchange. This interaction, corresponding to the Feynman diagrams of Fig. 1, can be written in the compact form

$$\mathcal{L}_{eff} = \frac{4G_F}{\sqrt{2}}\left[J_\mu^{+L}J_\mu^{-L} + \left(J_\mu^{3L} - J_\mu^{Q}\sin^2\theta_w\right)^2\right]. \tag{2.8}$$

Due to the relation (2.4), the prefactor in this expression is identical for the W and Z contributions:

$$\frac{G_F}{\sqrt{2}} = \frac{e^2}{8\sin^2\theta_w m_W^2} = \frac{e^2}{8\sin^2\theta_w\cos^2\theta_w m_Z^2}. \tag{2.9}$$

Over the past decade, the dependence of this effective interaction on helicity and flavor has been tested in neutrino and electron scattering processes and found to be in agreement with experiment to accuracies of 510%. The convergence of low-energy scattering data to the standard model is well described in the reviews of Kim, *et al.*,[8] Amaldi, et *al.*,[9] and Costa, *et al.*[10]

Current and future experiments work at a higher level of precision. To compare these to theory, we must replace the lowest-order relations that I have quoted so far with more complete predictions which take into account order-a radiative corrections. It is necessary to work out carefully how each of the relations I have written between underlying parameters and observables is altered by radiative effects. Already, though, we can understand the basic features that will emerge from this program of calculation.

Because the lowest-order relations contain three free parameters-g, g', and v—one must make three high-precision measurements to determine the predictions of the theory. Only the fourth measurement can give a sensitive test. Before this past summer, only two standard model observables were known with high precision. These were the value of the basic electric charge

$$\alpha = (137.0359895(61))^{-1} ,$$

obtained from precision QED measurements such as the electron (g − 2) and from the measurement of the Josephson effect, and the value of the Fermi constant, the prefactor of (2.8),

$$G_F = 1.16637(2) \times 10^{-5} \ (\mathrm{GeV})^{-2} ,$$

obtained from the muon lifetime. Now, however, experiments at SLC and LEP have reported a very precise value of the Z^0 mass [11–15]

$$m_Z = 91.150(30) \ \mathrm{GeV} . \tag{2.10}$$

This corresponds to a precision of 3×10^{-4}. Future experiments at LEP might make further small reductions of the error. At the same time, these experiments and those at the $p\bar{p}$ colliders promise the precision measurement of additional quantities-the W mass and the angular and polarization asymmetries of Z^0 decays-will finally allow the standard model to be put to a stringent test.

On the other hand, the standard model implicitly contains many parameters which do not appear explicitly in the lowest-order relations. These include the quark and lepton masses and the masses and couplings of Higgs bosons. These additional parameters affect the size of radiative corrections and thus influence the precision comparison of weak interaction experiments. This adds some uncertainty to the predictions of the standard model. But, conversely, it allows us to view these comparisons as windows into the content of the standard model, illuminating properties of heavy quarks and the Higgs sector which are otherwise difficult to view-experimentally.

3. The Z^0 Resonance Line-Shape

Before beginning a general analysis of higher-order weak interactions, I would like to discuss the specific problem of the Z^0 boson mass measurement in e^+e^- annihilation. Since the Z^0 creates an enormous resonance in the e^+e^- total cross section, one can measure the Z^0 mass at least roughly by locating the peak of this resonance. However, the shape of the resonance is distorted by radiative corrections, and this effect must be understood to use the position of the resonance in a precise determination of weak parameters. In this section, I will discuss the physics of this effect.

3.1. The Z^0 Resonance at Leading Order

It is a standard exercise to compute the cross section for e^+e^- annihilation into the various species of fermion pairs. Since this will be a useful starting point for our analysis, let me recall the basic formulae, at least in the limit where the various fermion masses can be neglected. In this limit, fermion helicity is conserved in the couplings of fermions to gauge bosons. Thus it is most convenient to quote the cross sections for e^+e^- states of definite helicity ($e_L^- e_R^+$ or $e_R^- e_L^+$) to annihilate to new fermions of fixed helicity ($f_L \bar{f}_R$ or $f_R \bar{f}_L$). These polarized cross sections are

$$\sigma(e^+e^- \to f\bar{f}) = \frac{4\pi\alpha^2}{3s} \left| Q_e Q_f + \frac{(I_e^3 - Q_e \sin^2\theta_w)(I_f^3 - Q_f \sin^2\theta_w)}{\sin^2\theta_w \cos^2\theta_w} \frac{\bar{Z} \cdot s}{(s - m_Z^2 + is\Gamma_Z/m_Z)} \right|^2 , \tag{3.1}$$

where I^3 and Q denote the weak isospin and electric charge of the fermions involved ($Q_e = -1$).

In writing (3.1), I have set the imaginary part in the denominator to $(s\Gamma_Z/m_Z)$ rather than the more usual $(m_Z\Gamma_Z)$. This reflects the fact that the imaginary part arises as the imaginary part of a loop insertion in the Z^0 propagator, as shown

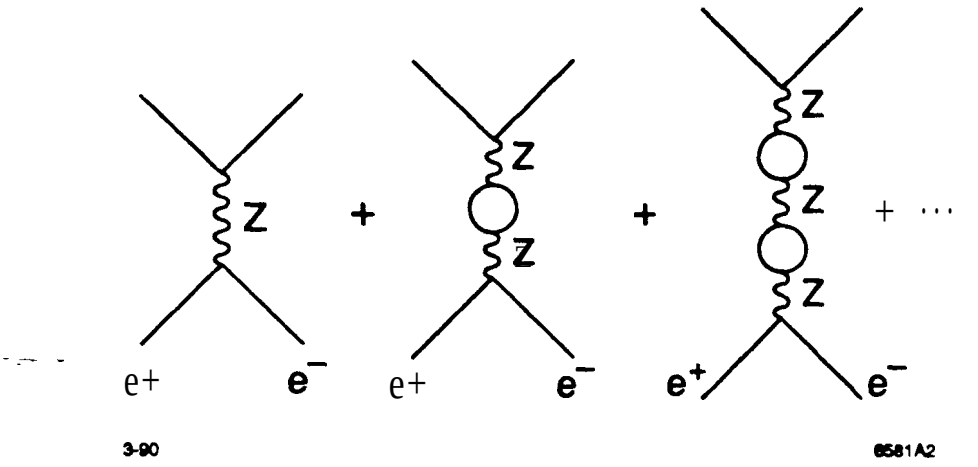

Figure 2. Feynman diagrams whose summation produces the Breit-Wigner denominator of the Z^0 propagator.

in Fig. 2. The loop diagram contains no heavy masses and is proportional to s. This produces a minor kinematical perturbation of the Z^0 resonance. I have also introduced a renormalization factor $\overline{Z}$ into the Z^0 propagator. This factor will remain very close to 1; its origin will be discussed in Section 5.7.

The total cross section for e^+e^- annihilation is built up out of the helicity cross sections according to

$$\sigma_{\text{tot}} = \frac{1}{4}\sum_{\text{pols.}}\sum_{\text{f}} \sigma(e^+e^- \to f\bar{f}) \cdot N_f \ . \tag{3.2}$$

The factor N_f denotes the effective number of species of flavor f: For leptons, N_f = 1; for quarks, N_f = 3, plus the enhancement due to QCD. More precisely, for quarks,

$$N_f = 3(1 + \frac{\alpha_s}{\pi} + \ldots) = 3.12 \pm .01 \text{ at } s = m_Z^2 \ , \tag{3.3}$$

corresponding to $\alpha_s(m_Z^2) = 0.12 \pm 0.01$, Figure 3 shows the total cross section for e^+e^- annihilation to hadrons predicted by (3.2).

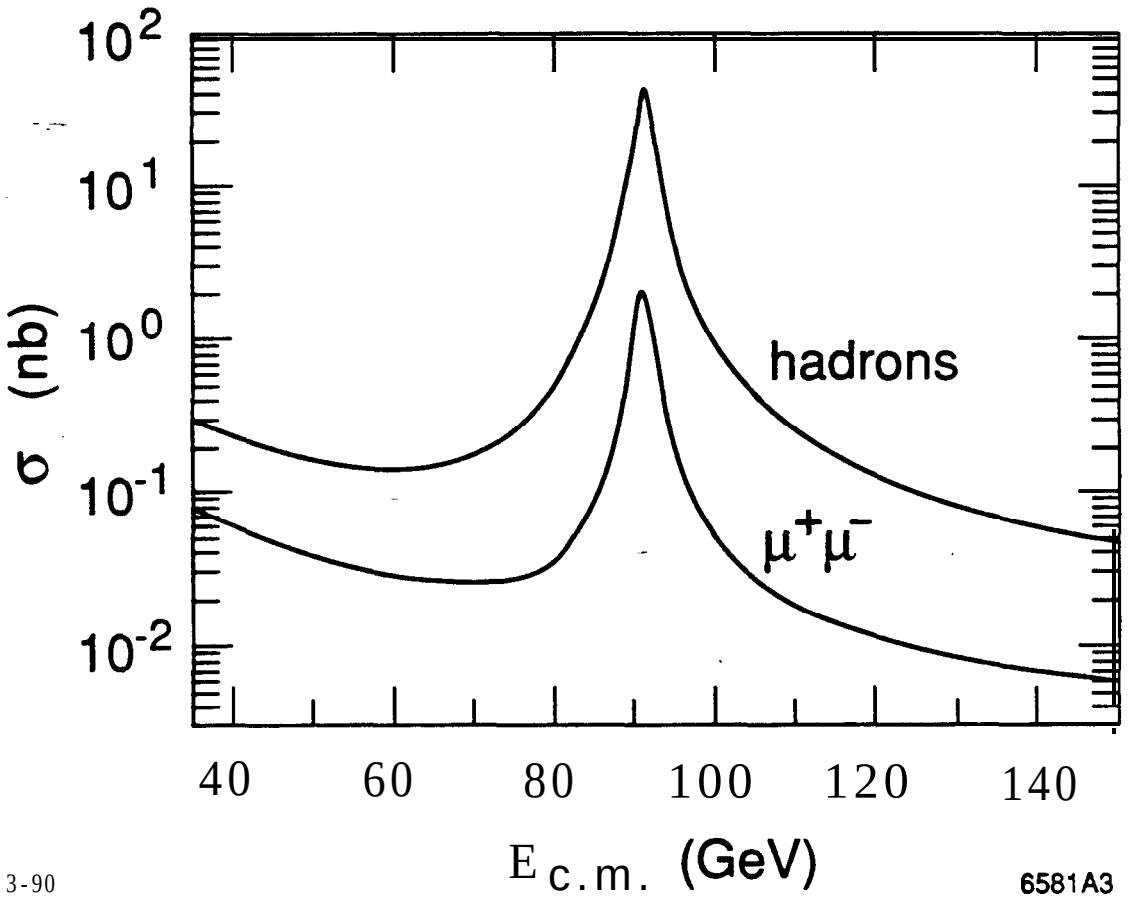

Figure 3. Total cross section, in units of R, for e^+e^- annihilation to hadrons and to muon pairs.

The helicity-dependence of the annihilation cross section also gives rise to asymmetries in fermion pair production. The forward-backward asymmetry is given by

$$A_{FB} = \frac{3}{4} \cdot \frac{(\sigma(e_L^- \to f_L) + \sigma(e_R^- \to f_R)) - (\sigma(e_L^- \to f_R) + \sigma(e_R^- \to f_L))}{\sigma(e_L^- \to f_L) + \sigma(e_R^- \to f_R) + \sigma(e_L^- \to f_R) + \sigma(e_R^- \to f_L)} . \quad (3.4)$$

The polarization asymmetry, between the cross sections of left- and right-handed electrons, may be computed as

$$A_{LR} = \frac{(\sigma(e_L^- \to f_L) + \sigma(e_L^- \to f_R)) - (\sigma(e_R^- \to f_L) + \sigma(e_R^- \to f_R))}{\sigma(e_L^- \to f_L) + \sigma(e_L^- \to f_R) + \sigma(e_R^- \to f_L) + \sigma(e_R^- \to f_R)} . \quad (3.5)$$

I will evaluate these formulae using the Z^0 mass given in (2.10) and the following values for the other parameters: $\alpha = 1/129$, $\sin^2 \theta_w = 0.235$, $\overline{Z} = 1.01$. I will defend these latter choices in Section 5.7. The dependence of these asymmetries on energy, over a wide energy range around the Z^0 resonance, is shown in Figs. 4 and 5. The leading-order values of the total cross section and the weak asymmetries just in the neighborhood of the Z^0 resonance are shown in Figs. 6, 7, and 8. Notice that, just at the Z^0 resonance, the polarization asymmetry becomes independent of the final-state flavor and simply represents the asymmetry in the left- and right-handed electron couplings to the Z^0 boson.

Equation (3.1) predicts that the Z^0 resonance has a simple Breit-Wigner form:

$$a(s) = \sigma^0_{\text{peak}} \cdot \left| \frac{s\Gamma_Z/m_Z}{s - m_Z^2 + is\Gamma_Z/m_Z} \right|^2 , \quad (3.6)$$

where the zeroth-order peak cross section is related to the total width and the partial widths into initial and final channels by

$$\sigma^0_{peak} = \frac{12\pi}{m_Z^2} \frac{\Gamma(Z^0 \to e^+e^-)\Gamma(Z^0 \to f\bar{f})}{\Gamma^2_{\text{tot}}} . \quad (3.7)$$

The various partial widths are given by

$$\Gamma_Z^f = \overline{Z} \frac{\alpha m_Z}{6 \sin^2\theta_w \cos^2\theta_w} \sum_{L,R} (I_f^3 - Q_f \sin^2\theta_w)^2 \cdot N_f . \quad (3.8)$$

The prefactor $\overline{Z}$ is the Z^0 propagator renormalization from (3.1). Evaluating these

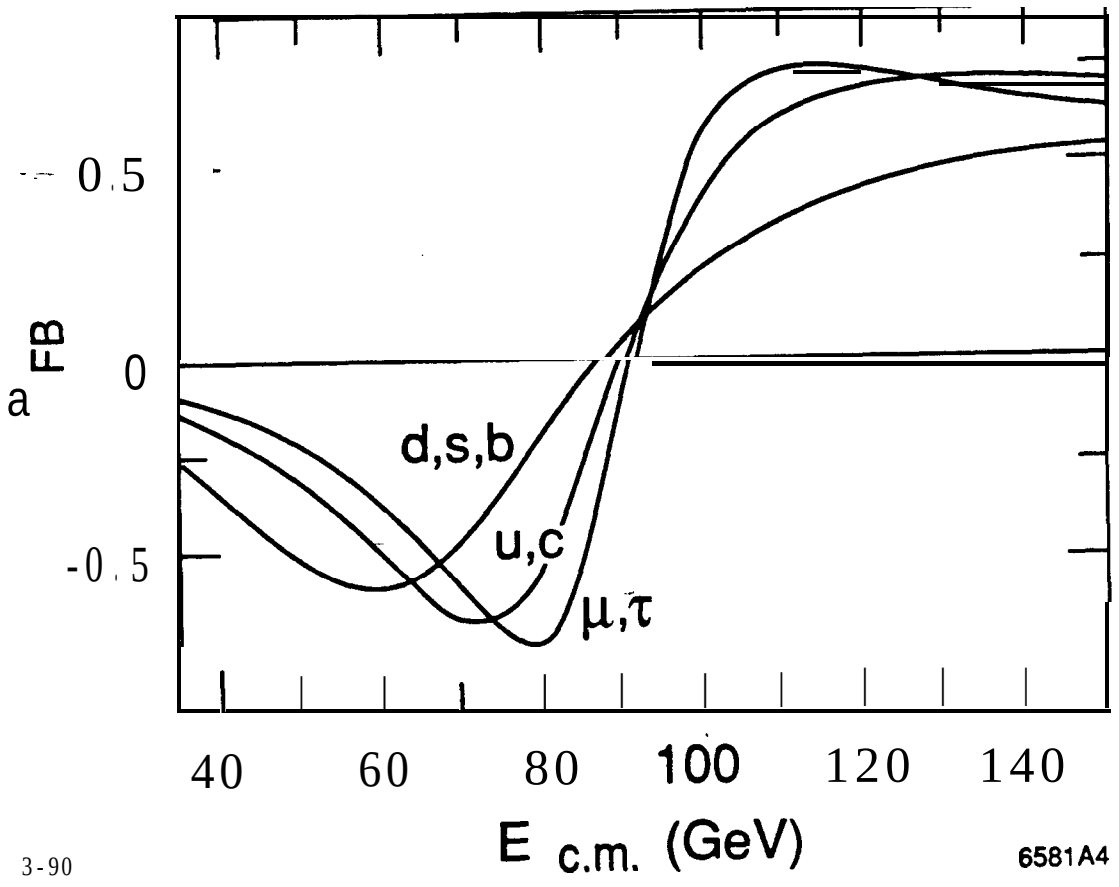

Figure 4. Forward-backward asymmetry A_{FB} for e^+e^- annihilation to charged leptons, u quarks, and d quarks.

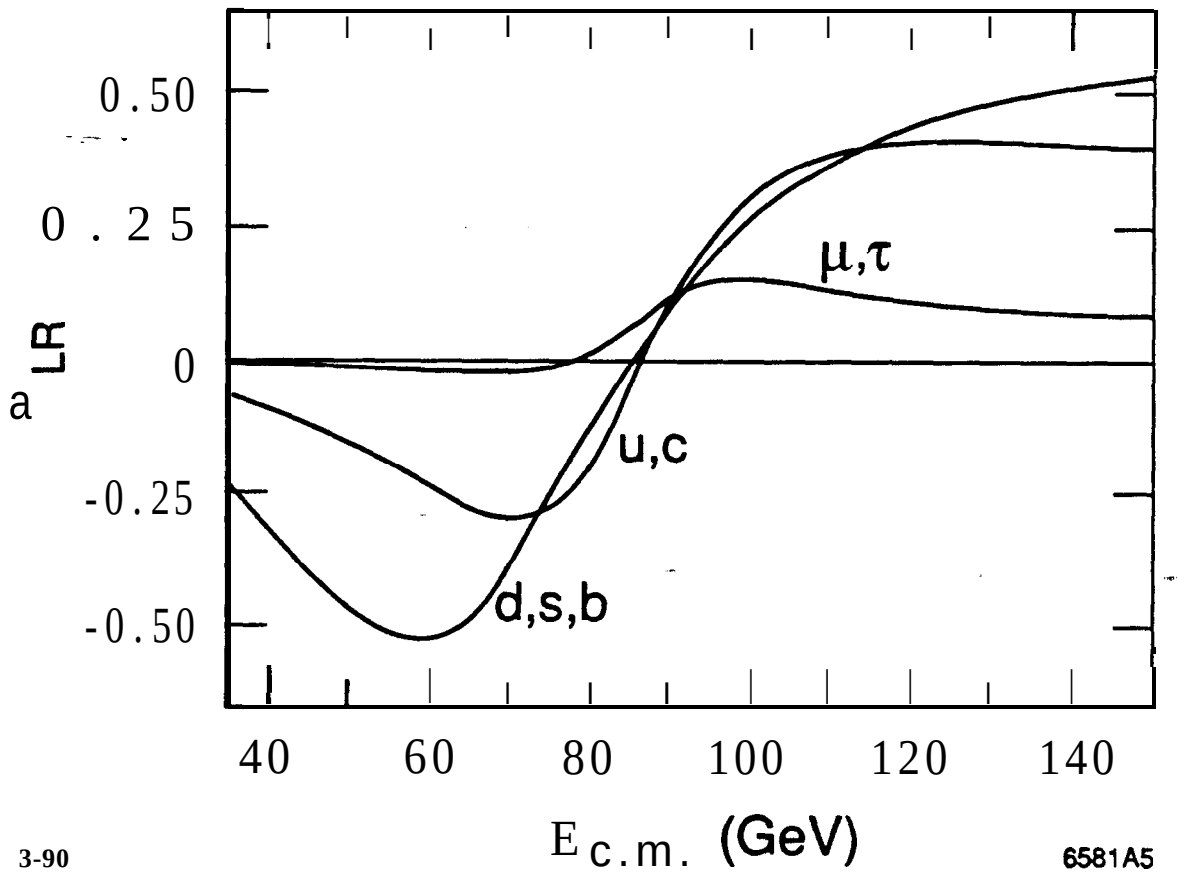

Figure 5. Polarization asymmetry A_{LR} for e^+e^- annihilation to charged leptons, u quarks, and d quarks.

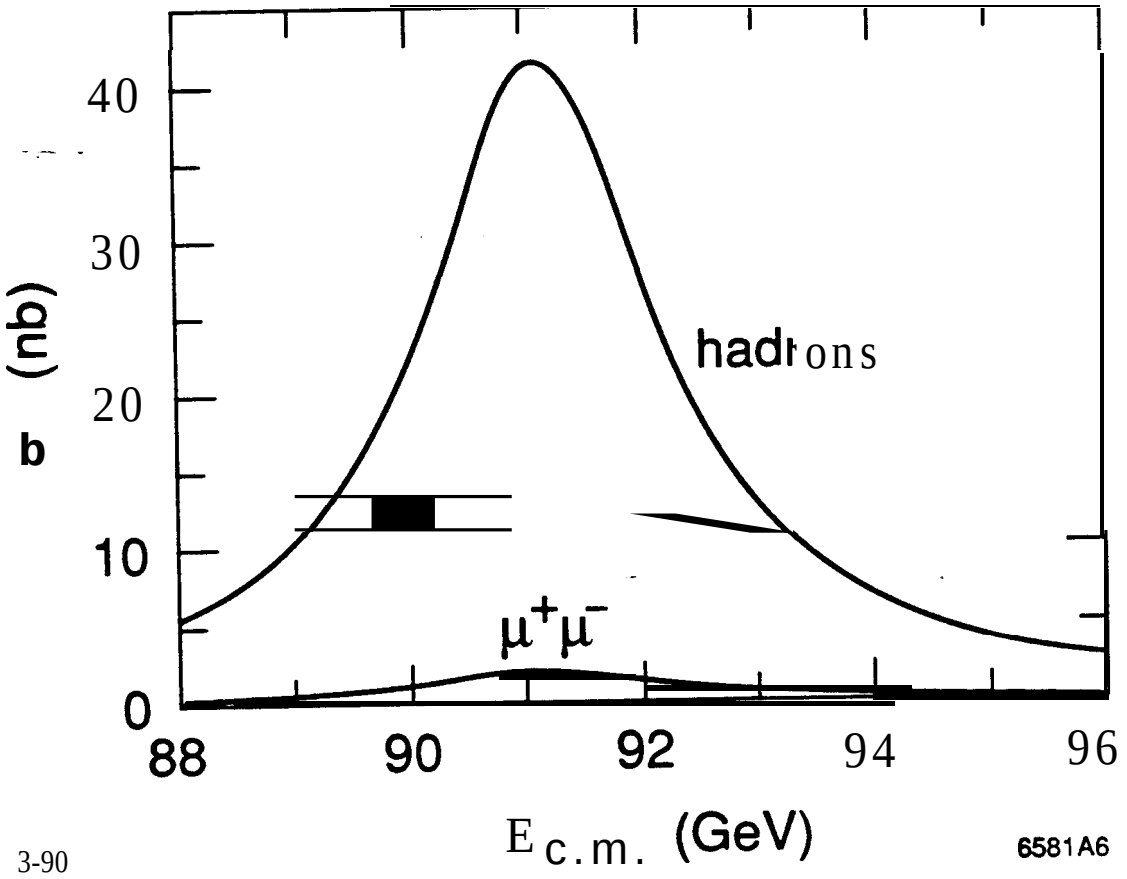

Figure 6. Total cross section for e^+e^- annihilation in the vicinity of the Z^0, to leading order in α.

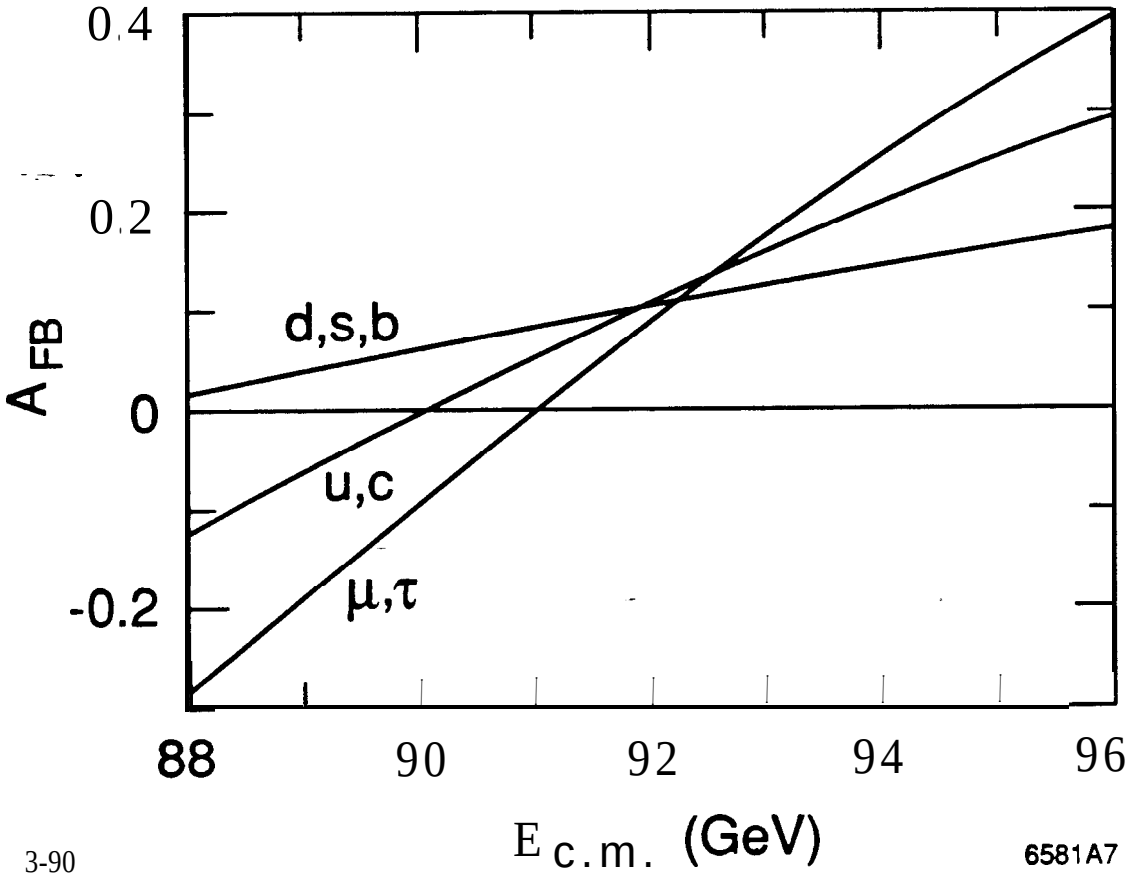

Figure 7. Forward-backward asymmetries in e^+e^- annihilation in the vicinity of the Z^0, to leading order in cr.

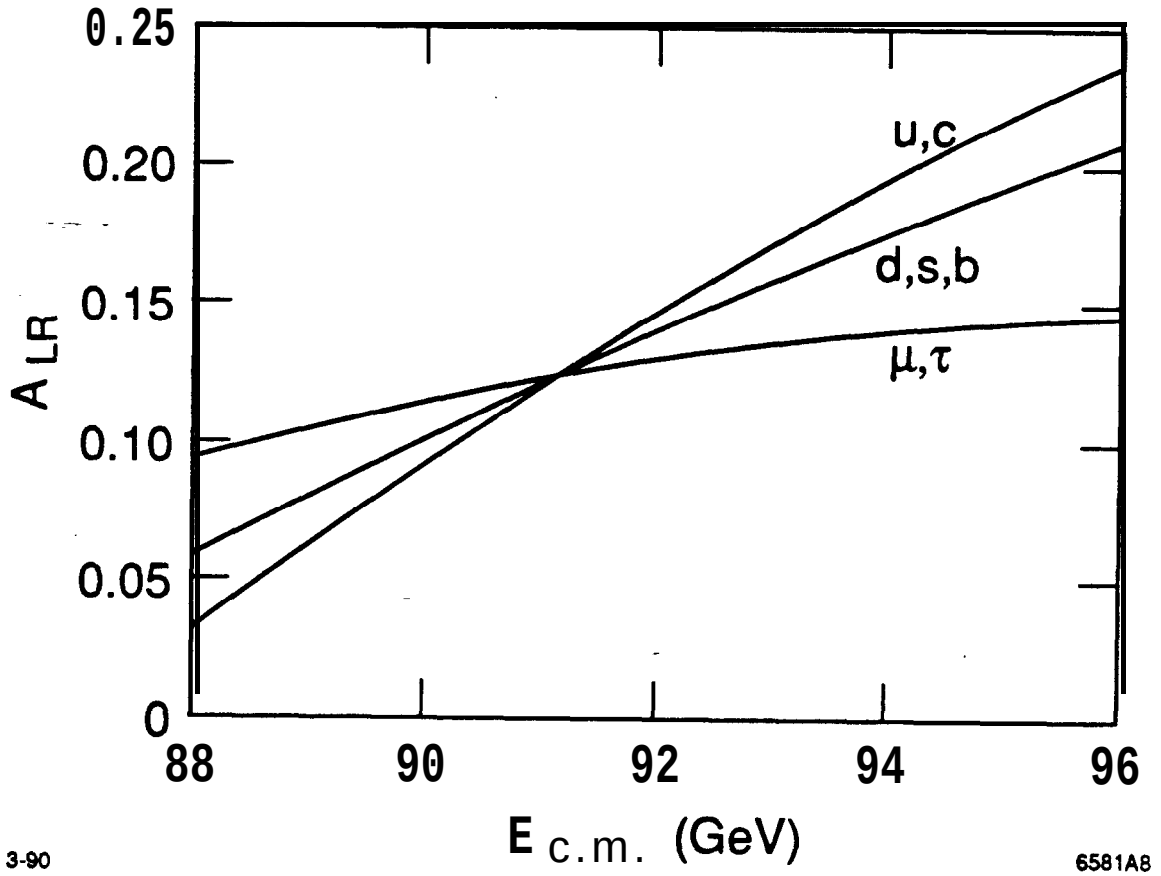

Figure 8. Polarization asymmetries in e^+e^- annihilation in the vicinity of the Z^0, to leading order in a.

formulae using the parameters listed below (3.5), we find the following the partial width for each fermion species:

e, μ, τ:	83 MeV
ν_e, ν_μ, ν_τ:	166 MeV
u, c:	294 MeV
d, s, b:	381 MeV

making up a total width of 2.48 GeV.

3.2. The General Influence of Radiative Corrections

Now that we have constructed a precise picture of the Z^0 resonance according to the leading order expressions of the standard model, we may ask how this picture is changed by radiative corrections. It is useful to think that radiative corrections produce two distinct effects: First, corrections to the Z^0 propagator and vertex shift the parameters of the resonance-the mass, the width, and the peak cross section. Second, corrections producing radiation from the initial electron and positron change the shape of the resonance by smearing out the' peak toward higher energy.

At some level, these effects blend into one another; however, the most important radiative corrections can be separated into two distinct classes. Let me label the diagrams shown in Fig. 9(a), the diagrams for real photon emission from the initial electron and positron lines, and the virtual photon diagram needed to cancel their infrared divergences, as 'soft' radiative corrections. These diagrams are essentially QED effects, since the typical momentum of virtual lines is much less than m_Z. Let me label the diagrams shown in Fig. 9(b), the diagrams involving Z^0 propagator corrections and the weak interaction contributions to the vertex, as 'hard'. In these diagrams, the typical momentum of virtual lines is of order m_Z, so that weak and electromagnetic contributions appear on the same footing. As the figure suggests, the hard radiative corrections give renormalized resonance parameters which provide the input to the calculation of the smearing of the peak

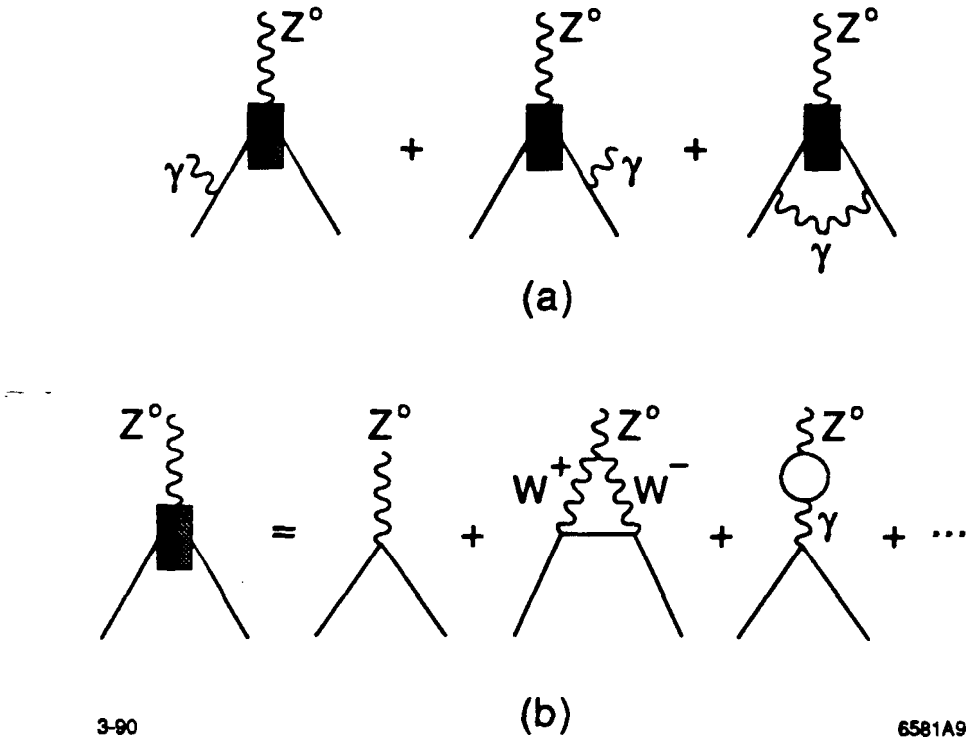

Figure 9. Classes of diagrams contributing to the shape of the Z^0 resonance: (a) 'soft' radiative corrections discussed in Section 3; (b) 'hard' radiative corrections discussed in Section 5.

by radiation. In this section, I will treat these resonance parameters as fixed and discuss the effect of radiation in determining the Z^0 line shape. We will return to the hard contributions, and determine their effect, in Section 5.

3.3. Soft Radiative Corrections: Order α

At leading order in α, QED affects the Z^0 resonance through the diagrams of Fig. 10. The evaluation of these diagrams leads to the famous Bonneau-Martin formula[16] for radiative corrections to a narrow resonance. In quoting this formula, I will drop the contributions from vacuum polarization diagrams, for example, the last diagram of Fig. 9(b); As that figure indicates, I will include these later with the hard corrections.

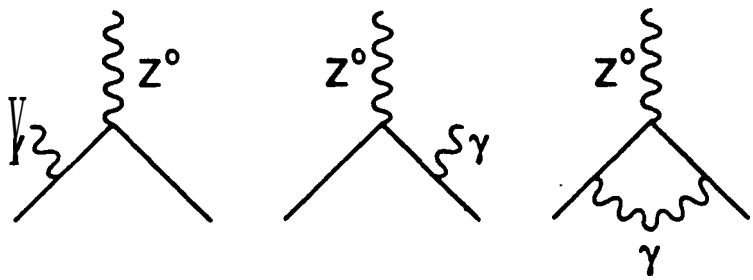

3-90 6581A10

-- ` Figure 10. QED corrections to the Z^0 line shape, in the leading order in α.

The first two diagrams of Fig. 10 produce the following correction to the total cross section:

$$\Delta\sigma(s) = 2\int_0^1 dx \left[\frac{\alpha}{2\pi}\left(\log\frac{s}{m_e^2} - 1\right)\left(\frac{1+(1-x)^2}{x}\right)\right]\sigma_0(s(1-x)) \,. \qquad (3.9)$$

The quantity in brackets is just the Weiszacker-Williams radiation spectrum expected in any electromagnetic scattering process; the variable x is the photon momentum fraction: x $= k/E$, where k is the photon momentum and E is the electron beam energy. The actual e^+e^- annihilation takes place at the reduced -center-of-mass energy given by $\hat{s} = s(1 - x)$. The integral in (3.9) diverges at the limit x $\rightarrow$ 0. This is a standard phenomenon in QED; the divergence can be removed by performing an analysis to all orders in a, but, more simply, it cancels in the total cross section at any given order. Let us temporarily control it by introducing a fictitious photon mass λ, which gives an artificial lower limit to the integral. The divergence as $\lambda \rightarrow 0$ is cancelled in the total cross section by the contribution of the third diagram of Fig. 10, which diverges as

$$-2\cdot\frac{\alpha}{2\pi}\,(\log\text{-}\$\text{-}1)\cdot 2\log\frac{E}{\lambda}\cdot\sigma_0(s) \qquad (3.10)$$

for small λ. Collecting the full contribution from the three diagrams, we find

$$\sigma_{tot}(s) = \left[1 + \frac{2\alpha}{\pi}\left\{(\log\frac{s}{m_e^2} - 1)(\log\frac{\lambda}{E} + \frac{3}{4}) + (\frac{\pi^2}{6} - \frac{1}{4})\right\}\right]\sigma_0(s) + \frac{\alpha}{\pi}(\log\frac{s}{m_e^2} - 1)\int_{\lambda/E}^{1}\frac{dx}{x}(1 + (1-x)^2)\,\sigma_0(s(1-x))\,, \tag{3.11}$$

which is finite in the limit $\lambda \to 0$.

The Bonneau-Martin formula (3.11) is compared to the zeroth-order Z^0 line shape in Fig. 11. The correction is formally of order a but, even after the cancellation of infrared divergences, it is enhanced by two large logarithms. First, there is the logarithm from the Weiszacker-Williams formula, which implies that the strength of the radiation is given by the dimensionless parameter

$$\beta = \frac{2\alpha}{\pi}(\log\frac{s}{m_e^2} - 1)\Big|_{s=m_Z^2} = 0.108\,. \tag{3.12}$$

There is a second logarithm which arises from-the fact that the two lines of (3.11) are mismatched when s is on the resonance but $s(1 - x)$ is not. The full size of the correction is then

$$-\beta \cdot \log\frac{m_Z}{\Gamma_Z} \cong -0.39\,. \tag{3.13}$$

This is indeed a very large correction; it indicates that we must compute to higher order in α to understand the Z^0 line shape quantitatively.

3.4. Multiple Photon Radiation

The systematic calculation of QED diagrams to the next order in a is a very complicated task. To make a precise analysis, one must of course perform the complete calculation. However, it would aid our understanding more to isolate those contributions which are producing the large corrections, understand their origin, and sum them up, if possible, to all orders in α.

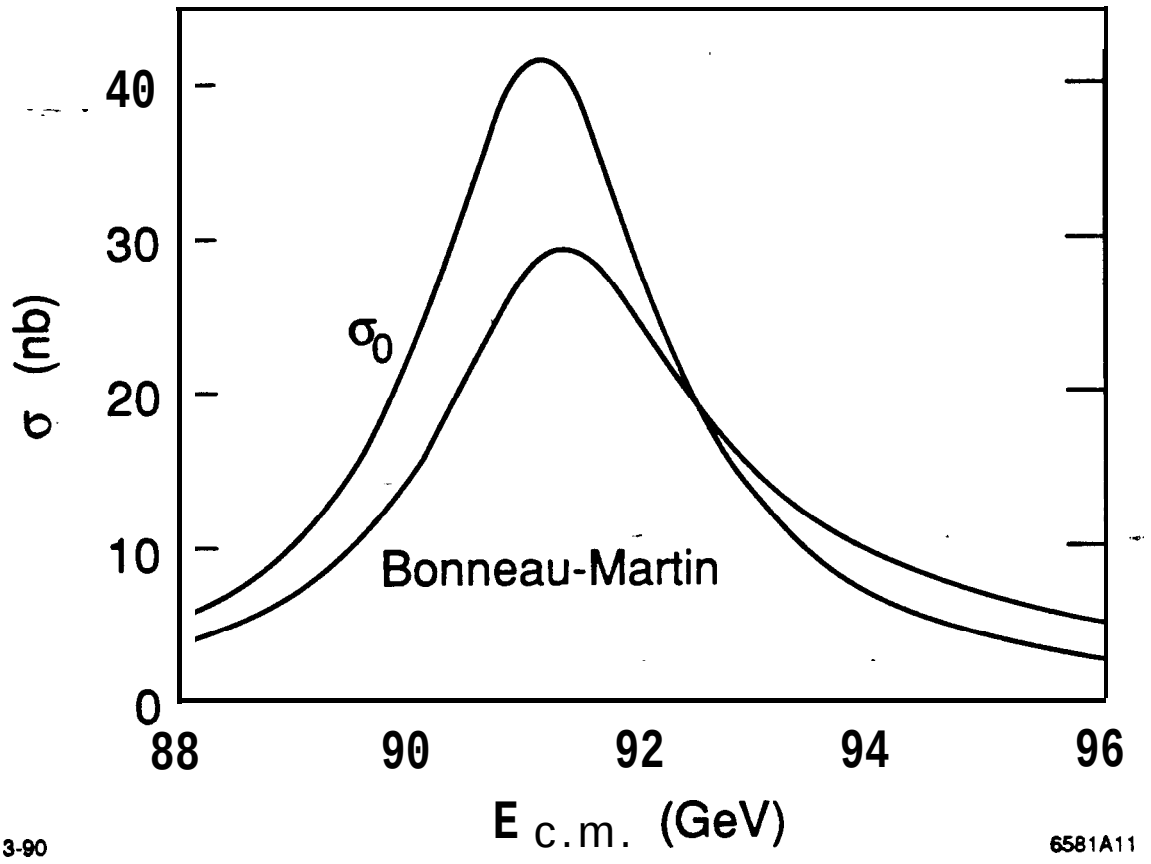

Figure 11. The effect of order α initial-state radiation corrections on the Z^0 line shape. The order α curve is computed from (3.11).

Why is the QED correction so large? The problem is not with the size of α, which is as small as one could wish; rather, it is that α is enhanced by large logarithms. In quantum field theory, large logarithms always have a physical origin; they arise when one compares quantities with two very different characteristic energies in an indelicate way. By understanding the origin of the large logarithms, we can see how to tame them.

The identification and summation of large logarithms is a major part of our understanding of perturbative QCD. Let me give two examples. Consider first the QCD correction to the total cross section for $e^+e^- \to$ hadrons, given by the diagrams of Fig. 12(a). In these diagrams, all particles have typical momenta of order the electron beam energy. Since all momenta are at the same scale, no large logarithms should appear. Indeed, the standard QCD result for the total hadronic cross section is

$$\sigma = \frac{4\pi\alpha^2}{3s} \sum Q_f^2 \cdot 3 \cdot \left(1 + \frac{\alpha_s}{\pi} - \frac{33 - 2n_f}{12}(\frac{\alpha_s}{\pi})^2 \log \frac{s}{\mu^2} + \ldots\right) \cdot \quad (3.14)$$

The term of order α_s has no large logarithm. The next term in the expansion does have a large logarithm if α_s is defined at a scale μ very different from s, to account for the scale-dependent renormalization of this coupling constant. The related process of Drell-Yan production of electron pairs, $p\bar{p} \to e^+e^-$ has an additional complication. In this process, as a result of the diagrams shown in Fig. 12(b), the quark and antiquark which annihilate have typical transverse momentum of order $\sqrt{q^2}$, where q is the momentum of the virtual photon. The amplitude for a quark in the proton, with typical transverse momentum 300 MeV, to give rise to such a highly virtual state contains powers of the logarithm of the ratio of these transverse momentum scales. The effect of these logarithms is to produce an evolution of the quark distribution in the proton with log q^2; this evolution is just that described by the Altarelli-Parisi equations.[17]

The problem of computing the Z^0 line shape is the QED analogue of this latter situation. The large logarithms in (3.13) appear when we relate the off-shell

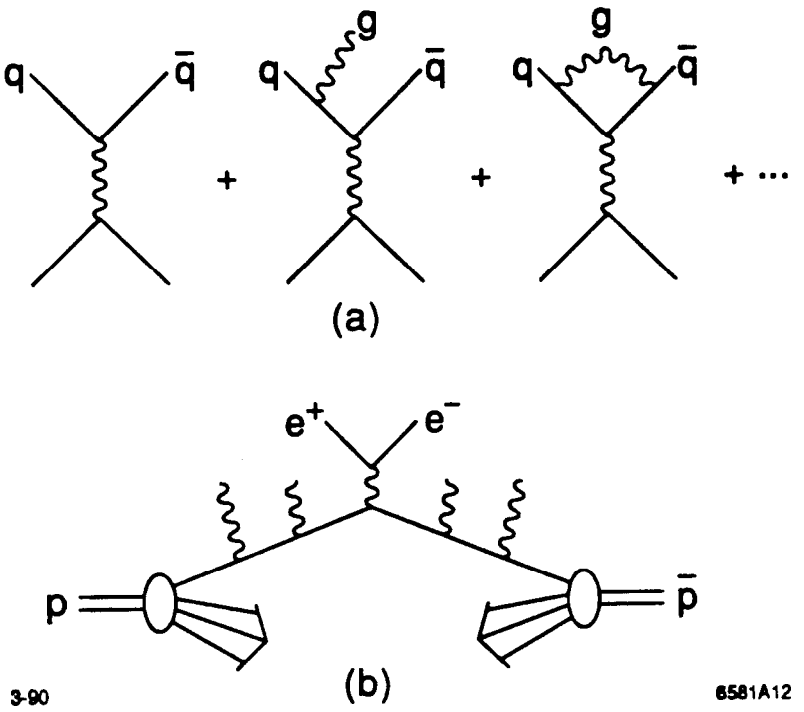

Figure 12. Two examples from QCD of the summation of large logarithms: (a) $e^+e^- \to$ hadrons; (b) $p\bar{p} \to e^+e^-$.

electron which finally annihilates into the Z^0 to the on-shell electron from which the process begins. To control these logarithms, we should reinterpret (3.11) as the first step of an evolution process by which the virtual electron emerges from the external electron. This strategy for calculating the Z^0 line shape was first advocated by **Fadin** and **Kuraev.**[18] However, it should be noted that these authors, and also Altarelli and **Parisi,** took their inspiration from the QED evolution equation constructed by Gribov and Lipatov[19] in their classic work on deep inelastic scattering.

Let $D_e(z, s)$ be the electron distribution function, the probability that the annihilating electron has fraction z of the original beam energy. If there is no radiation from the initial electron, we would have

$$D_e(z) = \delta(z - 1) \ . \tag{3.15}$$

Order by order in α, this result receives radiative corrections. I will now argue that (3.11) may be interpreted as providing the order a correction to (3.15). In this reinterpretation, we view (3.11) as a step in a process rather than as a simple correction; this will allow us to represent this process by an evolution equation which will generate the most important corrections to all order.

To make this reinterpretation of (3.11), let us divide this equation into three parts. The second line of the equation represents the effect of radiation in moving electrons and positrons from the full energy to an energy fraction $(1-x)$. Assigning half of this contribution to the electron and half to the positron, we may represent it as

$$\Delta D_e(z) = \int dx \left[\frac{\beta}{4} \cdot \frac{1+(1-x)^2}{x}\right] D_e\left(\frac{z}{(1-x)}\right) . \tag{3.16}$$

As electrons radiate photons and move to lower energy, we should expect to find fewer electrons at the full beam energy. The fractional depletion should be found by integrating over x the probability of radition to energy fraction $(1-x)$:

$$\frac{\Delta D_e(z,s)}{D_e(z,s)} = -\frac{\beta}{4}\int_{\lambda/E}^{1} \frac{dx}{x}\left(1+(1-x)^2\right) = -\frac{\beta}{4}\left(\log\frac{E}{\lambda} + \log\frac{E}{\lambda} - \frac{3}{2}\right) . \tag{3.17}$$

Indeed, (3.11) contains exactly this depletion, in the term

$$\Delta\sigma(s) = -\beta\left(\log\frac{E}{\lambda} - \frac{3}{4}\right)\sigma_0(s) . \tag{3.18}$$

The magnitude of (3.18) is double that of (3.17) in order to account the effect on the electron and on the positron. We have now given a physical interpretation to most of the pieces in (3.11). The only pieces of (3.11) not included in the above accounting are the terms

$$\Delta\sigma(s) = \left(1+\frac{2\alpha}{\pi}\left(\frac{\pi^2}{6}-\frac{1}{4}\right)\right)\sigma_0(s) ; \tag{3.19}$$

these last terms give a correction to the e^+e^- annihilation vertex which is explicitly of order α, with no enhancement by large logarithms.

The two terms (3.16) and (3.18) may be considered as the contributions of first order in β to an evolution process in which an electron radiates and moves down to lower energy fraction. The evolution parameter is β, and thus the evolution progresses further the higher the energy or the further the electron must go off-shell. We may assemble the two pieces as the kernel of an integral equation for $D_e(z,s)$:

$$\frac{\partial}{\partial\beta}D_e(z,s) = \frac{1}{4}\int_0^{(1-z)} dx\left[\frac{1+(1-x)^2}{x} - A\delta(x)\right]\cdot D_e\left(\frac{z}{(1-x)},s\right) . \qquad (3.20)$$

The subtracted term depletes the electron distribution at the higher energy, the Weizsacker-William term fills in the distribution of electrons after radiation. Both terms are singular at x = 0, and, though this singularity is difficult to write mathematically, it is easy to describe and implement in a computation. After one cuts off the divergences *in* some way, the coefficient A is fixed by the requirement that the total probability does not change:

$$\int dz D_e(z,s) = 1 , \qquad (3.21)$$

for any value of s.

In QCD, we have no explicit solution of the evolution equation for quark distributions. In QED, however, the situation is much more promising. First, the initial condition for the evolution equation is known: at β = 0, $D_e(z)$ reduces to the delta function in (3.15). Second, the evolution parameter β is still rather small at the Z^0, so we can imagine solving the (3.20) in an expansion in β.

We can obtain a good first approximation to the solution by concentrating on the region near z = 1. Let us try as an **ansatz**

$$D_e^{(0)}(z,s) = \frac{\beta}{2}(1-z)^{\beta/2-1} . \qquad (3.22)$$

This function satisfies (3.21) and contracts to a delta function at z = 1 when

$\beta \to 0$. Its derivative is

$$\frac{\partial}{\partial \beta} D_e^{(0)} = \frac{\beta}{4} \log(1-z) \cdot (1-z)^{\beta/2-1} + \frac{1}{2}(1-z)^{\beta/2-1} . \qquad (3.23)$$

The most singular term of the integral in (3.20) is

$$\frac{1}{2} \int_{\eta}^{(1-z)} \frac{dx}{x} D_e\left(\frac{z}{(1-x)}\right) . \qquad (3.24)$$

In writing this expression, I have cut off the integral at a lower limit η. Inserting $D_e^{(0)}$ into this term, and approximating near $z = 1$, we find

$$\frac{1}{2} \int_{\eta}^{(1-z)} \frac{dx}{x} \frac{\beta}{2} \left((1-z)-x\right)^{\beta/2-1} \sim \frac{\beta}{4} \log \frac{(1-z)}{\eta} (1-z)^{\beta/2-1} \qquad (3.25)$$

The logarithm of $(1-z)$ matches the desired form (3.23); the logarithm of η is a rescaling of the original distribution function and so is naturally cancelled when A in (3.20) is chosen to preserve the normalization of $D_e(z)$. In fact, since $D_e^{(0)}(z,s)$ satisfies (3.21), the correct choice of A will reproduce the second term of (3.23). In this way, we can see that the function $D_e^{(0)}(z,s)$ actually gives the correct dependence on z in the limit $z \to 1$ and thus is a good first approximation to the exact electron distribution.

Fadin and Kuraev began with this function as a first approximation and systematically computed corrections to it as a series in β:

$$D_e(z,s) = \frac{\beta}{2}(1-z)^{\beta/2-1}\left(1 + \frac{3}{8}\beta\right) - \frac{1}{4}\beta(1+z) + \cdots . \qquad (3.26)$$

The distribution function (3.26) is displayed, and compared to the Weiszacker-Williams distribution, in Fig. 13. An exact evaluation of the distribution function $D_e(z)$ would also include effects of pair-production (Fig. 14), which require additional terms in the evolution equation. The first such contributions are of order α^2 and so are omitted here, though they may be found in Ref. 18.

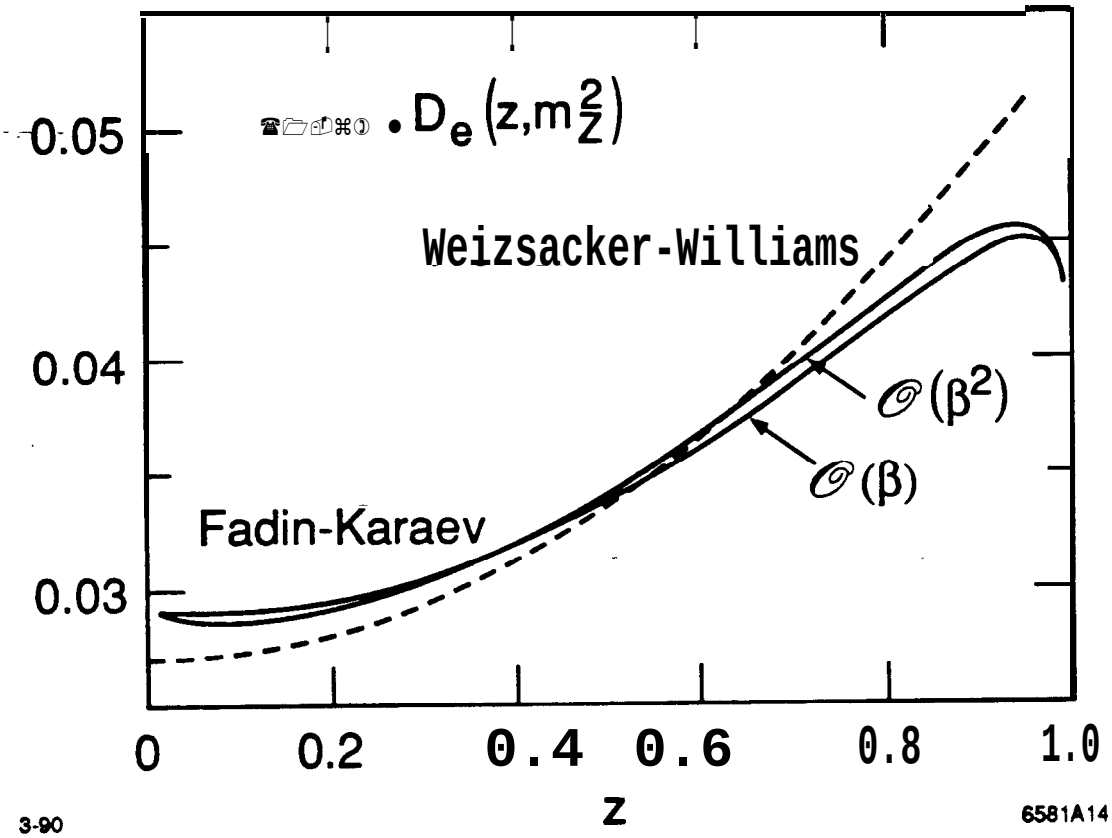

Figure 13. The distribution $D_e(z,s)$ of the energy fraction carried by a virtual electron.

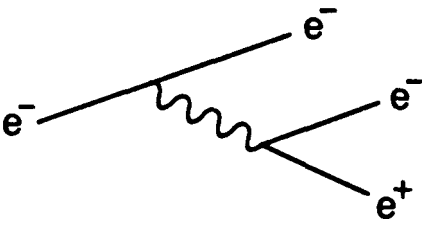

Figure 14. An additional contribution to the electron distribution function from pair-production.

To compute the Z^0 line shape, we must compute the cross section as a function of s, given this distribution in energy fraction for the electron and position. That is,

$$\sigma = \int_0^1 dz_1 \; D_e(z_1) \int_0^1 dz_2 \; D_e(z_2)\, \sigma^0(\hat{s}) \,, \tag{3.27}$$

where $\hat{s} = z_1 z_2 s$. It is useful to work out more explicitly the distribution of the effective electron-positron collision energy. This may be described by computing

$$\begin{aligned} &\int_0^1 dz_1 \; D_e(z_1) \int_0^1 dz_2 \; D_e(z_2)\, \delta((1-x) - z_1 z_2) \\ &\qquad = \beta x^{\beta-1}(1 + \frac{3}{4}\beta) - \beta(1 - \frac{x}{2}) + \cdots . \end{aligned} \tag{3.28}$$

In (3.28), I have inserted x to represent the fraction of total radiated energy. Using the distribution function in x, and restoring the order-o correction to the annihilation vertex written in (3.19), we find the following formula for the radiatively corrected cross section:

$$\sigma = \int_0^1 dx \left[\beta x^{\beta-1}(1 + \frac{3}{4}\beta) - \beta(1 - \frac{x}{2})\right] \cdot [1 + \frac{2\alpha}{\pi}\left(\frac{\pi^2}{6} - \frac{1}{4}\right)]\, \sigma_0\,(s(1-x)) \,. \tag{3.29}$$

One might view this as an improved version of the Bonneau-Martin formula (3.11)

in which the logarithms are exponentiated to powers of x. The formula (3.29) is compared to the zeroth- and first-order approximations to the cross section in Figs. 15 and 16. Cahn[20] has pointed out that the integral over x in (3.29) can be carried out analytically for a Breit-Wigner resonance, and the resulting formula has been useful in analyzing data on the shape of the Z^0 resonance.

In the past few years, there has been considerable further theoretical effort to refine the calculation fo QED effects on the Z^0 line shape. Fadin and Kuraev actually carried out this analysis to order α^2. The complete order-o corrections to $e^+e^- \to \mu^+\mu^-$ have been computed by Berends, Burgers, and van Neerven.[21] Other higher-order analyses have been carried out by many authors and are reviewed by Berends in Ref. 22. A useful comparison of calculations of the Z^0 line shape at various levels of approximation has been given by Alexander, Bonvicini, Drell, and Frey.[23] Their results (computed assuming $m_Z = 93$ GeV) are reproduced in Fig. 17. These authors estimate the theoretical errors in the extraction of the mass, width, and peak cross section of the Z^0 arising from residual uncertainties in this calculation at well below 1%.

3.5. Extraction of the Resonance Parameters

Since the QED radiative corrections broaden the Z^0 peak and smear it asymmetrically, it is not useful to quote the resonance parameters in terms of the observed peak position or the visually extracted width. Rather, one should parametrize a zeroth-order cross section in terms of a resonance position, width, and peak height, integrate this cross section together with the effects of radiation by inserting it into (3.29) (or a higher-order formula for the soft radiative corretions), and compare the result to the data. Since (3.29) does not include hard radiative corrections, the effects of these corrections will be included in the fitted resonance parameters. These effects must be taken into account in comparing the extracted parameters to other weak interaction measurements and to deeper theoretical predictions.

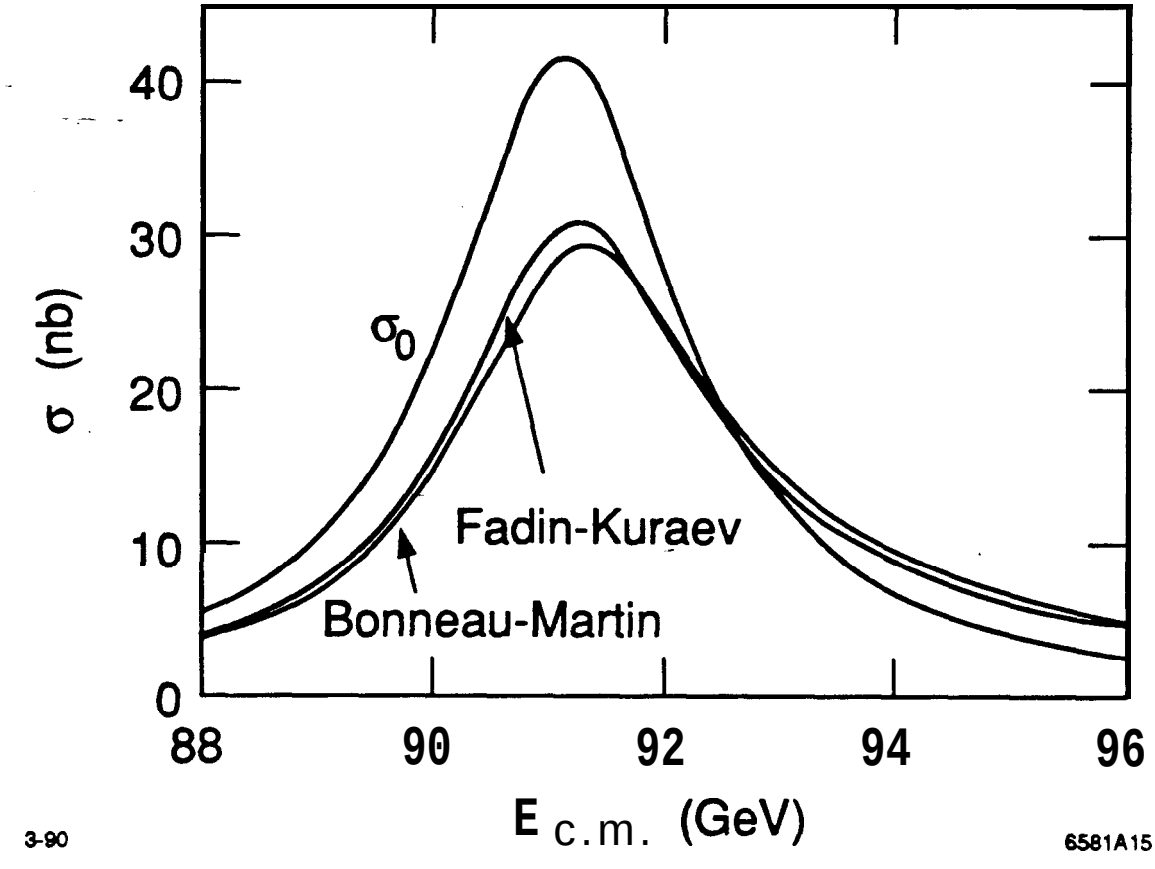

Figure 15. Total cross section for e^+e^- annihilation to hadrons in the vicinity of the Z^0, computed in zeroth order, first order (eq. (3.11)), and from the Fadin-Kuraev formula (3.29).

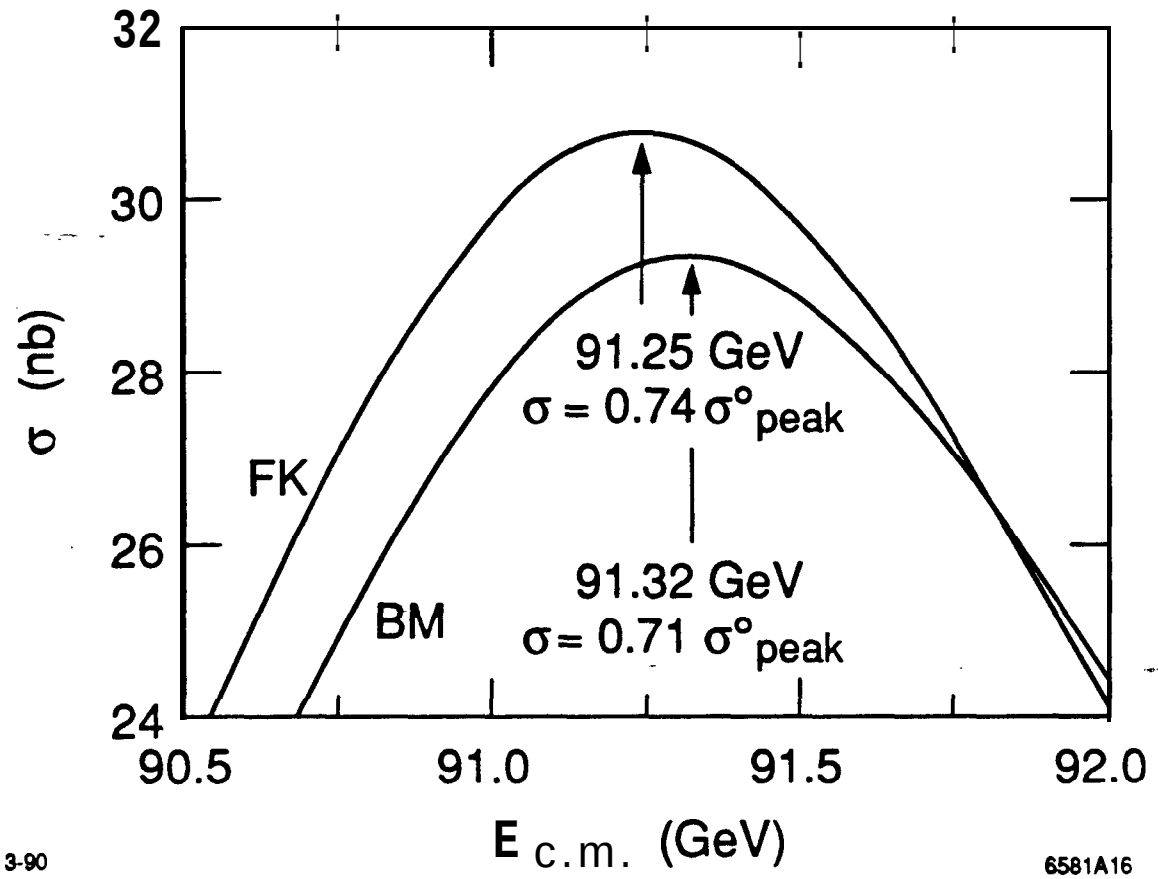

Figure 16. Magnification of Fig. 15 in the vicinity of the Z^0 peak. For each of the two radiative correction formulae, I have indicated the shift of the location of the peak and the decrease in the peak height from the zeroth-order value.

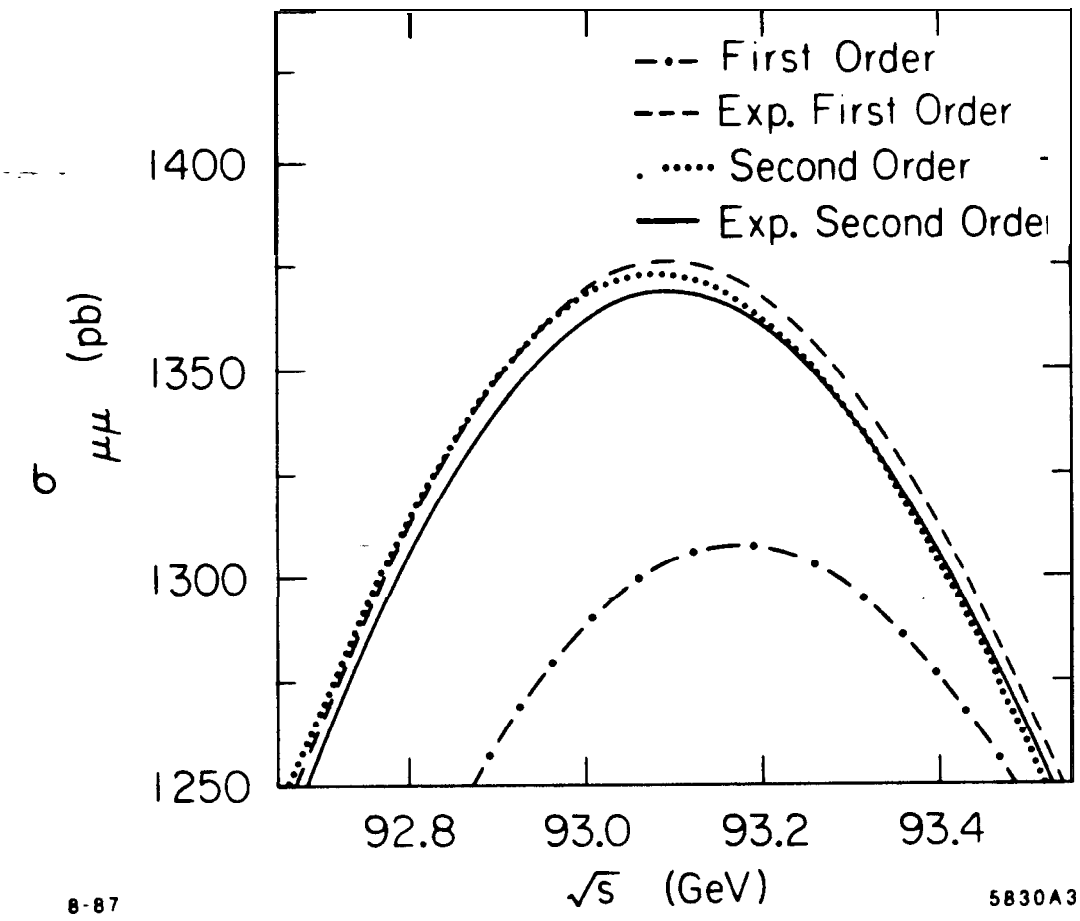

Figure 17. Comparison of the Z^0 line shape calculation at different levels of approximation, from Ref. 23.

To show the utility of this theory, I have displayed in Fig. 18 a calculation of the total cross section for e^+e^- annihilation to hadrons in the vicinity of the Z^0, obtained by inserting (3.1), with the parameters used in Section 3.1, into the radiative correction formula (3.29). The result is compared to the recent cross section measurements of the ALEPH experiment.[13] The mass of the Z^0 has, of course, been obtained from fitting such a curve to the data; however, the peak height and width of the Z^0 have been calculated from the standard model. The detailed agreement of theory and experiment for the line shape is quite remarkable.

In addition to its effects on the resonance line shape, initial-state radiation has other important effects on weak interaction experiments at the Z^0. In experiments which depend on specific exclusive final states, the effect of experimental cuts may be modified by radiation. For example, in the measurement of the forward-backward asymmetry in $e^+e^- \to \mu^+\mu^-$, a strict collinearity cut changes the shape of the Z^0 resonance slightly by suppressing its tail. The values of asymmetries measured at the Z^0 peak are affected by the smearing of the e^+e^- annihilation energy which arises from radiation. In Figs. 19 and 20, I have redrawn the plots of A_{FB} and A_{LR} versus beam energy taking into account the effects of radiation by computing the various helicity cross sections using (3.29) before forming the asymmetry. Notice that the various quantities A_{LR} are relatively weakly affected by radiation, but that the forward-backward asymmetry in $e^+e^- \to \mu^+\mu^-$ is very strongly perturbed. This effect was pointed out by Bohm and Hollik in ref. 24.

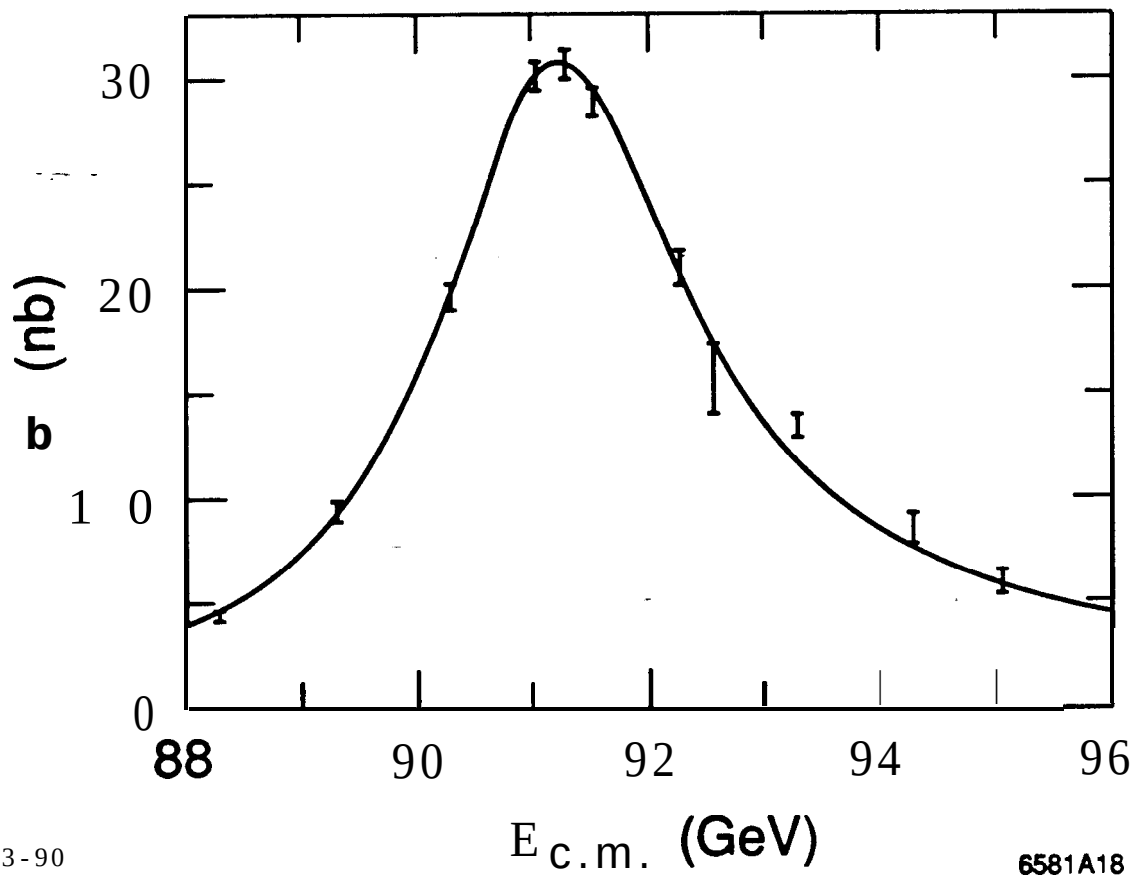

Figure 18. Total cross section measurements on the Z^0 peak reported by the ALEPH experiment,[13] compared to the line shape computed from (3.29).

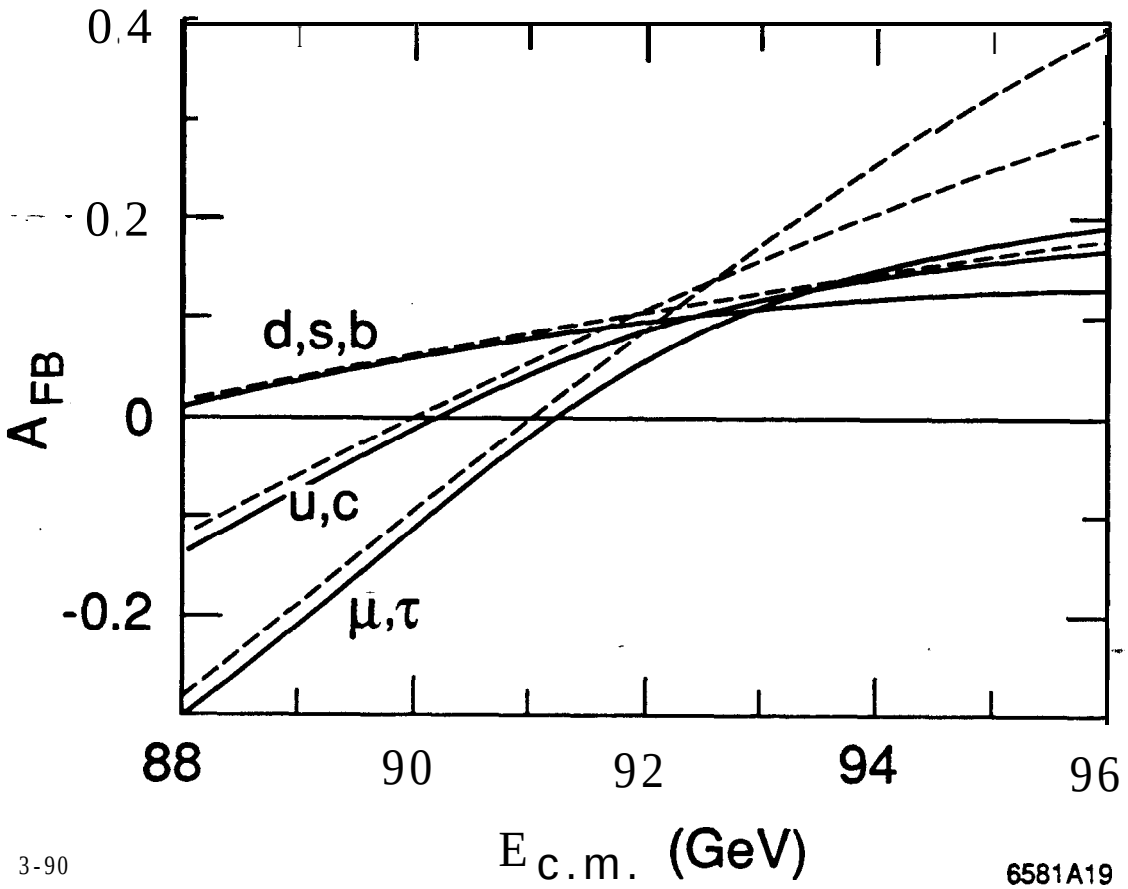

Figure 19. Forward-backward asymmetries in the vicinity of the Z^0 resonance, computed at lowest order (dashed curves) and including soft radiative corrections according to (3.29) (solid curves).

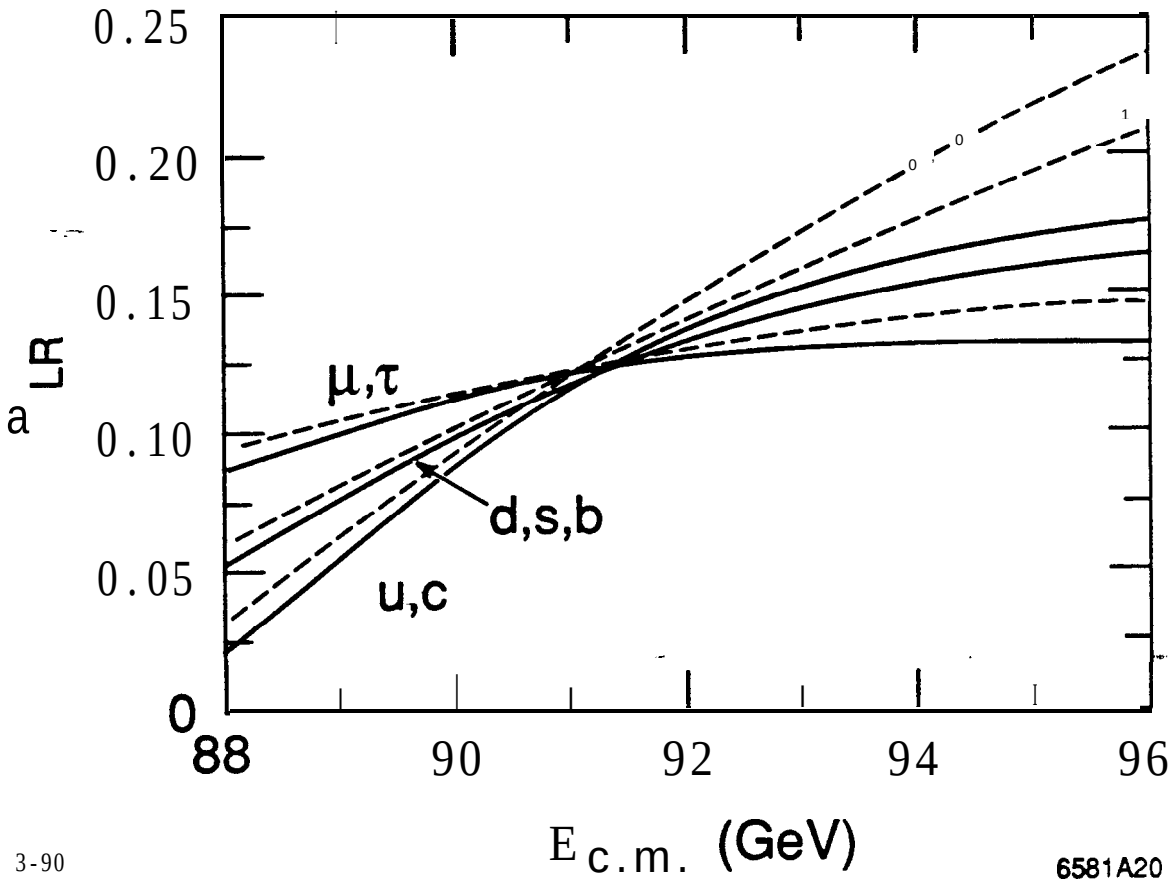

Figure 20. Polarization asymmetries in the vicinity of the Z^0 resonance, computed at lowest order (dashed curves) and including soft radiative corrections according to (3.29) (solid curves).

4. Extension of the Weak Interaction Gauge Group

Now that we have seen how to obtain the values of the Z^0 resonance parameters, we should analyze the implications of the values of these parameters for the standard model and its variants. In principle, any particle which couples to $SU(2) \times U(1)$ can appear in loop diagrams correcting the weak boson propagators and vertices and thus can modify the leading-order predictions of the standard model in order α. In the next section, I will discuss such loop corrections in a systematic framework. However, it is possible-even with our present detailed experimental knowledge-that the gauge group of the weak interactions is somewhat larger than that of the standard model. In this case, one expects variations from the standard model predictions even at leading order in α. In this section, I will briefly discuss the effects of a new heavy weak boson in modifying the properties of the Z^0 resonance.

4.1. An Extension from E_6 Grand Unification

If there does exist a second weak vector boson $Z^{0\prime}$, it should mix, at some level, with the standard Z^0. This mixing will induce a modification of the zeroth-order Z^0 current; instead of (2.7), the physical Z^0 will couple to a rotated current

$$J_\mu^Z = \cos\theta_m \left[J_\mu^{3L} - \sin^2\theta_w J_\mu^Q \right] + \sin\theta_m J_\mu^{Q'} , \qquad (4.1)$$

where the second term is the current of a charge Q' which is orthogonal (in some extended space) to the $SU(2) \times U(1)$ charges of the standard model. This addition will cause modifications of the Z^0 asymmetries and partial widths. These modifications are independent of the mass of the $Z^{0\prime}$, depending only on the mixing angle θ_m. Of course, they also depend on the explicit form chosen for Q'.

It would be wonderful to understand the systematics of the effect of the modified current (4.1) for the most general charges Q'; however, I do not know how to present such an analysis compactly. Instead, I will restrict myself to a specific class

of models which have been used by many authors as a laboratory for exploring the effects of a $Z^{0\prime}$. As is well known, grand unification in $SU(5)$ contains precisely the gauge bosons of the standard model, plus additional heavy bosons which mediate proton decay. However, this grand unification group may be extended to $SO(10)$ and further to E_6, producing at each stage one extra neutral boson whose charge commutes with the standard model gauge group. These bosons, or at least some linear combination of them, might well have a mass in the region of a few hundred GeV. Langacker, Robinett, and Rosner[25] have presented a specific scheme in which they consider one arbitrary linear combination of these two addition neutral bosons to represent the $Z^{0\prime}$. The linear combination is characterized as second mixing angle θ, which is essentially unconstrained. This leads to a family of models with

$$Q' = \sin\theta_w \left(\cos\theta \cdot \frac{1}{2\sqrt{6}}\chi + \sin\theta \cdot \frac{1}{6}\sqrt{\frac{5}{2}}\psi \right) . \qquad (4.2)$$

In this formula, χ and ψ are quantum numbers, which, for the various species of fermion, take the values

	$(\nu, e)_L$	e_R	$(u, d)_L$	u_R	d_R
χ	3	1	- 1	1	- 3
ψ	1	- 1	1	- 1	- 1

(A transparent derivation of these quantum numbers from E_6 may be found in Ref. 26.) By adjusting the parameter θ in (4.2), we can sweep through a variety of structures for the $Z^{0\prime}$ charges. This gives some robustness to this scheme of phenomenology.

I should note that there are strong experimental constraints on the size of the mixing angle θ_m. For most values of θ ($\cos\theta \geq 0$), low-energy neutral current experiments restrict θ_m to roughly the range $-0.05 < \theta_m < 0$. The precise allowed regions, for some specific choices of θ, are displayed in the papers of Amaldi, et al., Ref. 9 and Costa, et al., Ref. 10.

In addition, the recent precise measurements of the W boson mass by the

CDF and UA2 collaborations[27] put a further, and rather model-independent, constraint on θ_m. It is expected that a second charged weak boson cannot appear with a mass below a few TeV, since otherwise it would give a large enhancement of K_L–K_S mixing.[28] Assuming, then, that there is no new light W, the mass of the W should be unperturbed from its standard model value, while the mass of the Z^0 is affected by mixing with the $Z^{0\prime}$. The unperturbed mass of the Z^0, m_{Z0}, may then be recovered from m_Z, $m_{Z'}$, and the mixing angle θ_m using the simple properties of two-level mixing. One finds:

$$m_{Z0}^2 = m_Z^2 \cos^2\theta_m + m_{Z'}^2 \sin^2\theta_m \,. \tag{4.3}$$

The value of m_{Z0} obtained in this way must be related to the measured value of m_W through the usual standard model calculation (reviewed in Section 5.6). To understand this constraint, I have taken the average of the CDF and UA2 values of m_W:

$$m_W = 80.22 \pm 0.35 \text{ GeV} \,, \tag{4.4}$$

raised the value by 1 σ, computed the corresponding unperturbed Z^0 mass as described in the next section, and plotted in Fig. 21 the contour in the plane of $\sin\theta_m$ versus $m_{Z'}$ along which this calculation agrees with the value of m_{Z0} from (4.3). The region inside the contour is allowed at probable confidence. This constraint turns out to be quite sensitive to the value of the top quark mass, since, as I will explain in Section 5.6, a heavy top quark tends to decrease the Z-W mass splitting. This method for constraining θ_m was introduced by Langacker in Ref. 29; he pointed out there that this same constraint is an upper bound on θ_m in models with several $Z^{0\prime}$s if $m_{Z'}$ is taken to be the mass of the lightest $Z^{0\prime}$.

A second effect of the mixing between the Z^0 and $Z^{0\prime}$ is a change in the relation between m_Z and the value of $\sin^2\theta_w$ which enters the prediction of the Z^0 resonance cross sections and asymmetries. In the results of the next section, I have taken this effect into account by computing m_{Z0} from (4.3) and using this value to

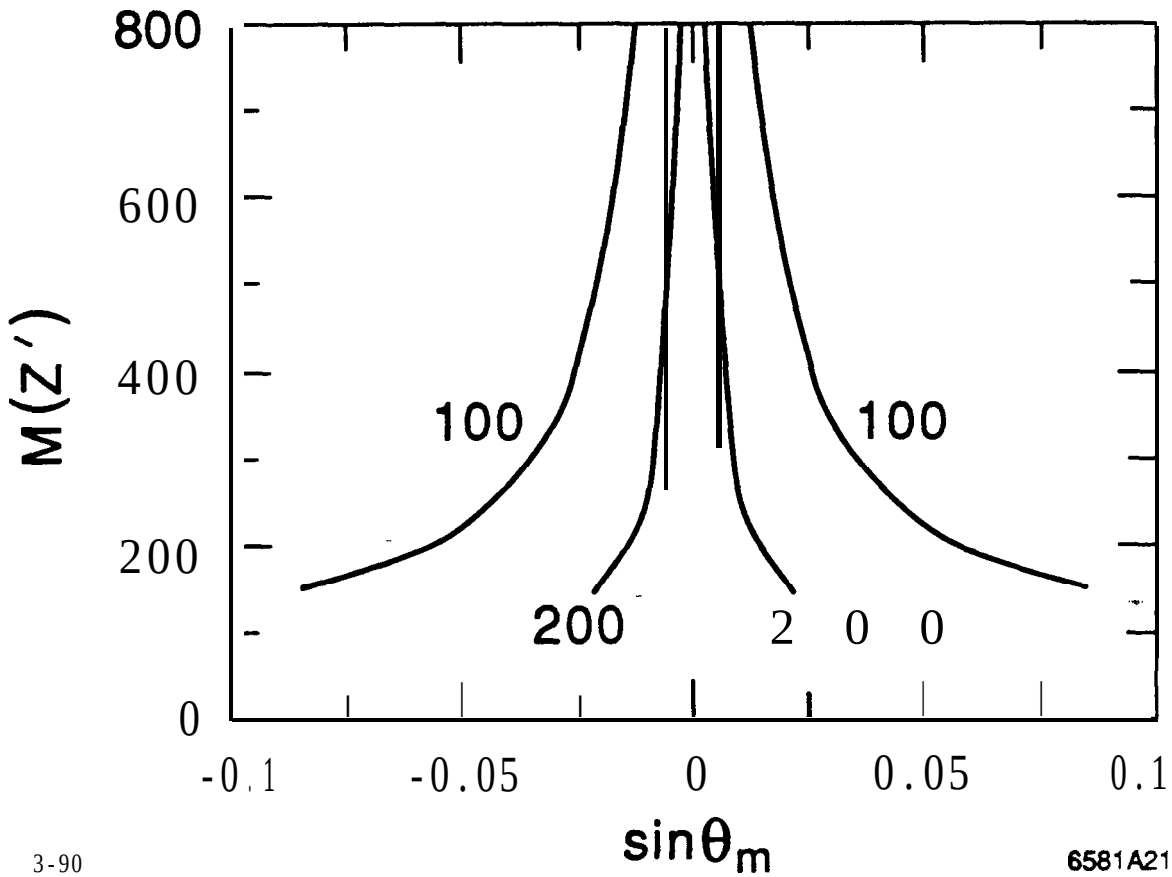

Figure 21. Probable confidence allowed region for θ_m, for m_t = 100, 200 GeV, based on the value (4.4) for the W mass.

extract $\sin^2 \theta_w$, assuming $m_{Z'} = 500$ GeV. This correction has only a minor effect on these calculations.

4.2. Observable Consequences of an Extended Gauge Group

Now that we have defined a model with extended gauge symmetry, let us compute the effects of this model on the properties of the Z^0. Cvetič and Lynn[30] have suggested that the Z^0 asymmetries are particularly sensitive to the mixing of the Z^0 with a $Z^{0\prime}$. More recently, Altarelli and collaborators[31] have sketched out a systematic program of experiments to search for the effects of a $Z^{0\prime}$. My analysis will concentrate on the simplest observables that they discuss.

If, for each left- or right-handed species, we let

$$Q_Z = \cos\theta_m (I^3 - Q \sin^2 \theta_w) + \sin\theta_m Q' \tag{4.5}$$

the relation (3.8) for the Z^0 partial widths is modified to

$$\Gamma_Z^f = \frac{\alpha m_Z}{6 \sin^2\theta_w \cos^2\theta_w} \sum_{L\,R} (Q_Z)^2 \cdot N_f . \tag{4.6}$$

From this equation, we can compute the zeroth-order peak cross section of the Z^0, using (3.7), and the polarization asymmetries into various species, using

$$A_{LR}^f = \frac{\Gamma(Z \to f_L \bar{f}_R) - \Gamma(Z \to f_R \bar{f}_L)}{\Gamma(Z \to f_L \bar{f}_R) + \Gamma(Z \to f_R \bar{f}_L)} . \tag{4.7}$$

On the Z^0 pole, the forward-backward asymmetries are given by the simple relations

$$A_{FB}(e^+e^- \to f\bar{f}) = \frac{3}{4} A_{LR}^e A_{LR}^f . \tag{4.8}$$

In comparing the predictions of models with extended gauge groups to experiment, it is important to compute quantities which are directly observable, avoiding

as much as possible the necessity for using standard model calculations of unmeasured quantities. For example, since the partial width of the Z^0 to neutrinos depends on the mixing with the $Z^{0\prime}$, one should compare the directly measured ratio of leptonic to hadronic branching fractions of the Z^0, rather than using the Z^0 branching fraction to leptons, which is inferred from this quantity by adding the calculated neutrino partial width to the denominator. In this spirit, I have considered the effects of the $Z^{0\prime}$ on four of the most accessible Z^0 resonance parameters-the zeroth-order total hadronic cross section, the total width of the resonance, the ratio of leptonic to hadronic branching fractions, and the polarization asymmetry from e^+e^-. In Figs. 22, 23, and 24, I have plotted these quantities against one another for $(-\pi/2) \leq \theta \leq (\pi/2)$, for the values θ_m = -0.01, -0.02, -0.03. The standard model reference values, obtained for m_t = 100 GeV, m_H = 100 GeV, $\alpha_s(m_Z^2)$ = 0.11 $\pm$ 0.01, is indicated by the stars. The lines through these stars indicate the variation of the standard model prediction as m_t is varied from 50 to 200 GeV. This dependencewill be discussed in detail in Section 5.7. Notice that observables involving leptons are particularly sensitive to the effects of a $Z^{0\prime}$, since the couplings of the charged leptons to the standard Z^0 are relatively weak. The standard and nonstandard predictions are compared to recent measurements from LEP. It is clear that measurements at the Z^0 will soon dramatically constrain, and may perhaps discover, the influence of a $Z^{0\prime}$.

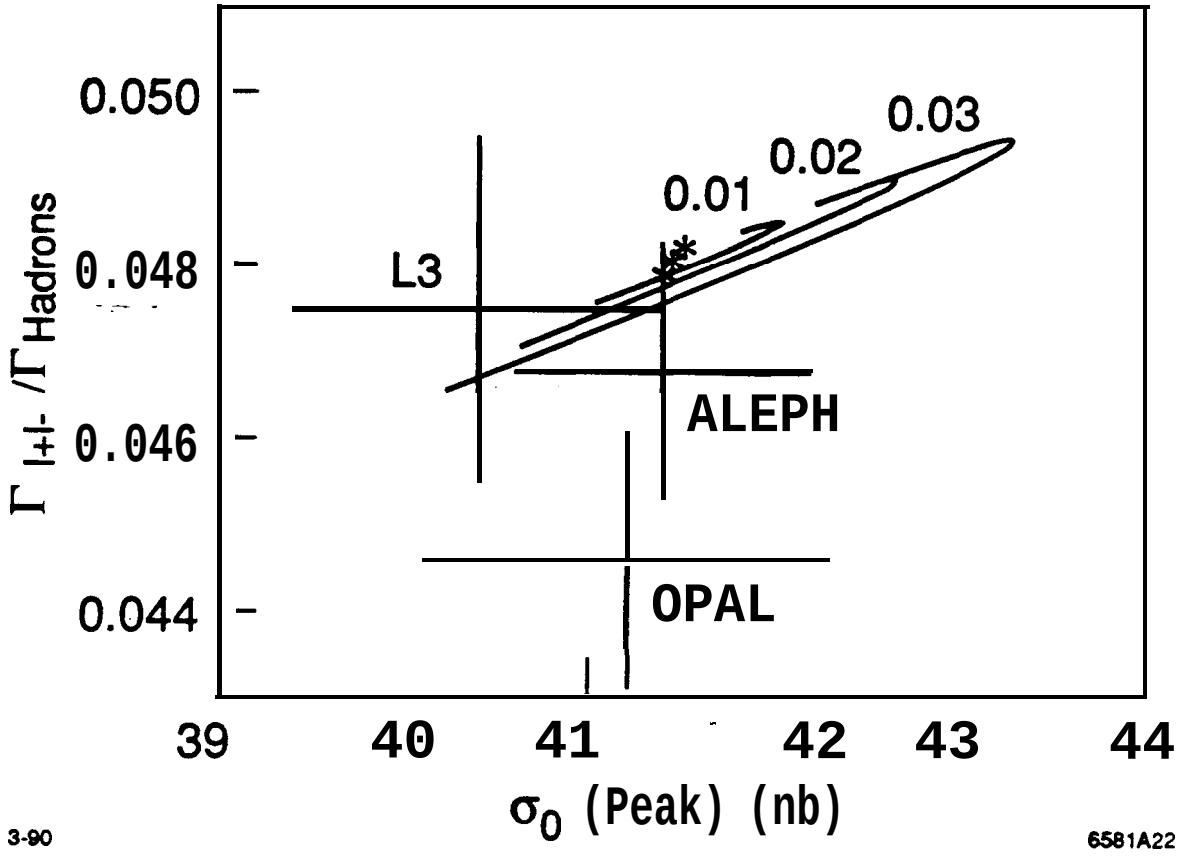

Figure 22. Effect of Z^0–$Z^{0\prime}$ mixing on the rapport between the Z^0 peak hadronic cross section and the ratio of leptonic and hadronic branching fractions. The stars denote the range of the standard model predictions. The three curves correspond to θ_m = -0.01, -0.02, -0.03; each sweeps out the region -n/2 < θ < n/2. The predictions are compared to data from recent publications of the ALEPH[13], L3,[14] and OPAL[15] experiments at LEP.

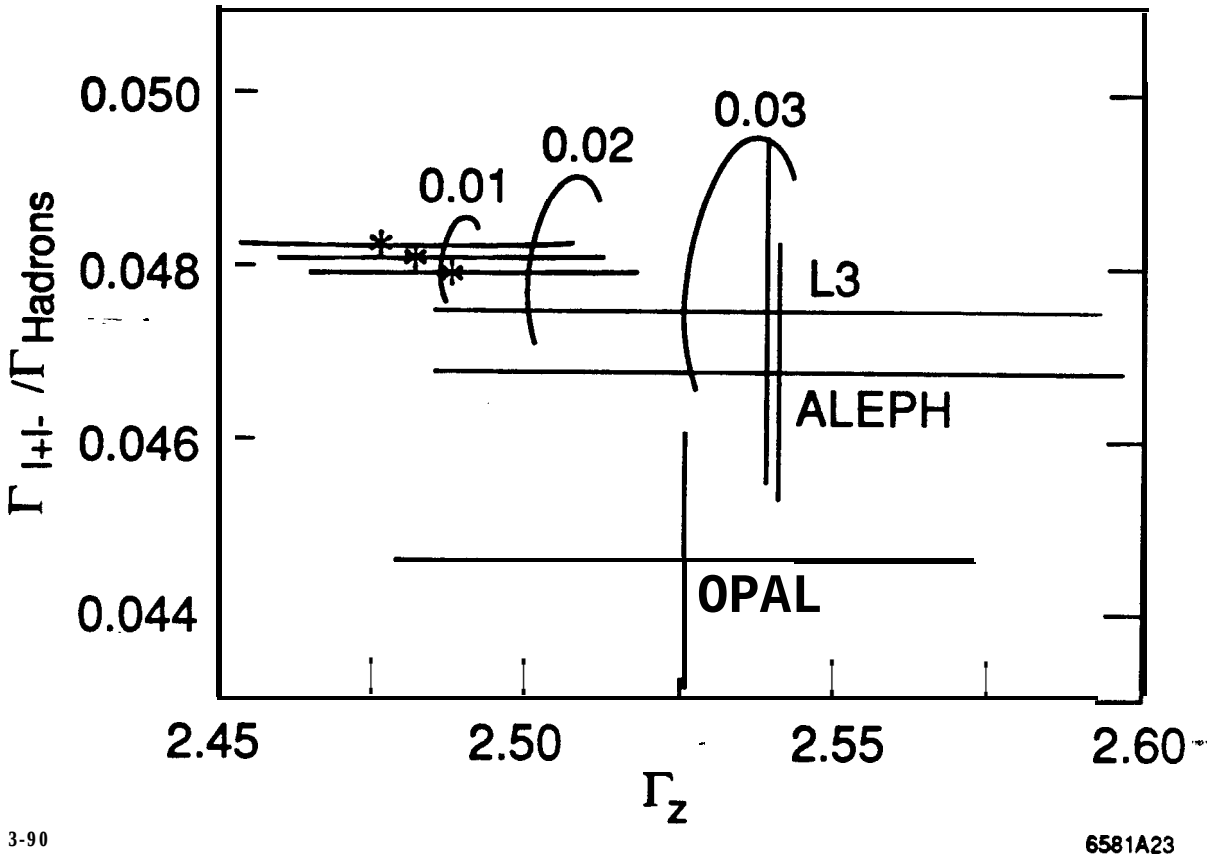

Figure 23. Effect of Z^0–$Z^{0\prime}$ mixing on the rapport between the Z^0 total width and the ratio of leptonic and hadronic branching fractions. The notation is as in Fig. 22. The horizontal lines show the effect on the standard model prediction of a variation in m_t from 50 to 200 GeV and a variation in $\alpha_s(m_Z^2)$ from 0.10 to 0.12. The stars indicate the cases $m_t = 100$ GeV. The m_t effect was included in Fig. 22, but it was almost invisible there.

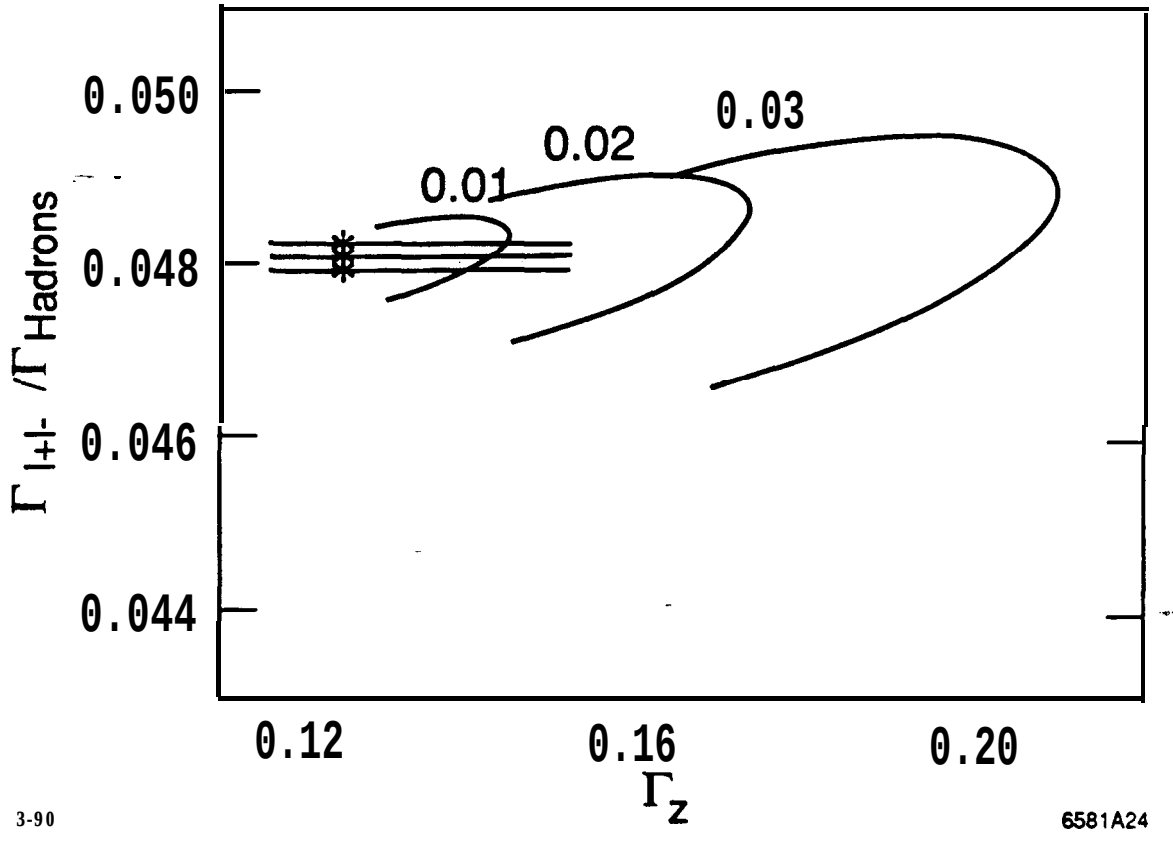

Figure 24. Effect of Z^0–$Z^{0\prime}$ mixing on the rapport between the polarization asymmetry A_{LR} and the ratio of leptonic and hadronic branching fractions. The notation is as in Fig. 23.

5. Renormalization of Weak Interaction Parameters

For the remainder of these lectures, I will assume that the standard $SU(2) \times$ U(l) model is the correct picture of weak interactions at zeroth order. However, the new precision experiments make it necessary to compute order a radiative corrections in order to allow a detailed comparison of theory with experiment. This gives us an opportunity to use these radiative corrections to probe the standard model in detail, and even to look beyond it. The opportunity comes from two sources. First, the typical size of radiative corrections is no longer a small number in the era of weak boson experiments. Indeed,

$$\frac{\alpha}{4\pi} \cdot m_Z \sim 100 \text{ MeV} , \tag{5.1}$$

an accuracy already reached for the Z^0 mass and soon within reach for the W mass. Second, as I will explain in this section, radiative corrections from specific sources are often larger than this simple estimate, as a result of the essential chirality of the standard model. These two points apply equally-and the second may apply even more strongly-to radiative corrections due to undiscovered heavy species.

In this section, I will review the theory of these order-α corrections to weak interaction parameters, the corrections which I termed 'hard' in the discussion of Section 3.2. I will explain how these corrections may be calculated and how they influence measureable quantities. The effect of the top quark in weak radiative corrections is particular easy to understand. Since its influence is large and also quite topical, I will use this effect as my main illustrative example.

5.1. Renormalization of α

The prototype of hard radiative corrections is the electromagnetic vacuum polarization. Let us begin by studying this correction, which gives a momentum-dependent renormalization of the electric charge. This correction provides a conceptually simple renormalization effect to introduce our program. It also has some practical significance for precision calculations in weak interactions.

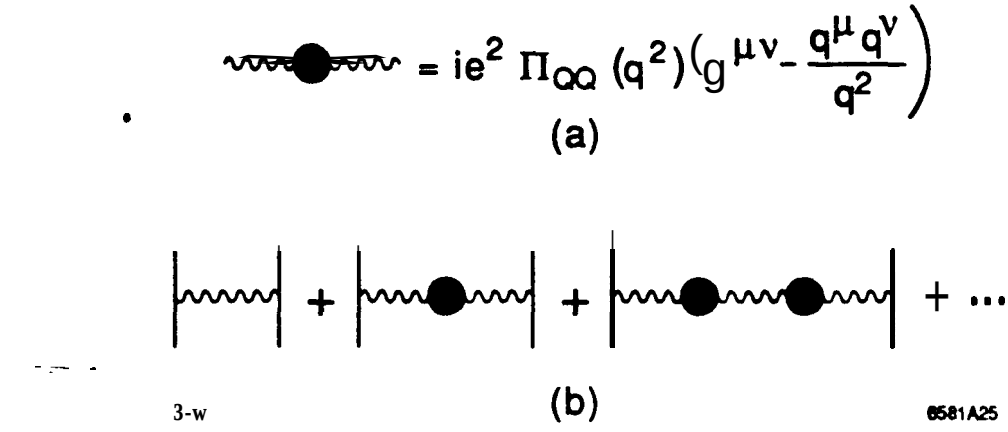

Figure 25. Conventions for the electromagnetic vacuum polarization.

I will define the electromagnetic vacuum polarization $\Pi_{QQ}(q^2)$ as the coefficient of $g^{\mu\nu}$ in the photon self-energy, as indicated in Fig. 25(a). I have extracted from Π_{QQ} the coupling constant e^2; throughout this section, unembellished coupling constants e, g will refer to *bare* parameters from the standard model Lagrangian. The full kinematic structure $(g^{\mu\nu} - q^\mu q^\nu/q^2)$ follows from the conservation of the electromagnetic current. Since the photon self-energy has no zero-mass pole, we must have $\Pi_{QQ} \sim q^2$ *as* $q^2 \to 0$. Then it is convenient to define

$$\Pi'_{QQ}(q^2) = \frac{\Pi_{QQ}}{q^2} \,. \tag{5.2}$$

(In textbooks on QED, it is $(e^2\Pi'_{QQ})$ that is usually called the vacuum polarization. My notation differs from this in order to treat vacuum polarization diagrams for the photon and the heavy gauge bosons on the same footing.)

If the photon self-energy corrections are summed up to all orders, as suggested in Fig. 25(b), one finds the complete photon propagator

$$\frac{-ie^2}{q^2}\left(1 + e^2\Pi_{QQ}\frac{1}{q^2} + \dots\right) g^{\mu\nu} = \frac{-ig^{\mu\nu}}{q^2} \cdot \frac{e^2}{(1 - e^2\Pi'_{QQ})} \,. \tag{5.3}$$

The form of this equation suggests that we should define a running electric charge

$$e_*^2(q^2) = \frac{e^2}{1 - e^2\Pi'_{QQ}(q^2)} . \tag{5.4}$$

The value of a measured from the electron (g − 2) or the Josephson effect is the coefficient of $1/q^2$ in the photon propagator at $q^2 = 0$; that is $4\pi\alpha = e_*^2(q^2 = 0)$. Replacing the bare coupling constant e by α using this relation, and also setting $4\pi\alpha_*(q^2) = e_*^2(q^2)$, *we* have

$$\frac{1}{4\pi\alpha_*(q^2)} = \frac{1}{4\pi\alpha} - [\Pi'_{QQ}(q^2) - \Pi'_{QQ}(0)] . \tag{5.5}$$

The vacuum polarization Π'_{QQ} due to a fermion loop is ultraviolet divergent; however, this divergence cancels in the difference of vacuum polarization amplitudes which appears in (5.5). This equation can thus be the basis for concrete physical predictions.

It is interesting to use (5.5) to compute the change in the value of the effective electric coupling as q^2 changes from 0 to m_Z^2. Let us approximate Π_{QQ}, for each fermion flavor, by the simplest l-loop diagram, and evaluate this diagram in the limit $m_Z^2 >> m^2$. (I will present a more general formula in the next section.) This gives

$$\frac{1}{\alpha_*(m_Z^2)} - \frac{1}{\alpha} \cong -\sum_f \frac{1}{3\pi} Q_f^2 N_f \left[\log \frac{m_Z^2}{m_f^2} - \frac{5}{3}\right] , \tag{5.6}$$

where Q_f is the electric charge and N_f is the factor (3.3). Evaluating this expression for the various quarks and leptons (using current algebra masses for the quarks), we find

	e	μ	τ	u	d	s	c	b
mass (MeV)	0.5	106	1784	5.5	8	150	1200	5000
$\Delta(\alpha_*^{-1})$	2.4	1.3	0.7	2.5	0.6	0.4	1.0	0.1

so that in all $\alpha^{-1} - \alpha_*^{-1}(m_Z^2) \sim 8$. A more accurate estimate, presented just below, gives a 6% upward renormalization of cr. Intuitively, one would expect that it is the value of a at m_Z^2, rather than at 0, which should enter the evaluation of standard model predictions for the weak boson masses. For example, the relation between the Fermi constant and the W mass, in leading order, is

$$\frac{G_F}{\sqrt{2}} = \frac{e^2}{8 \sin^2 \theta_w m_W^2} . \tag{5.7}$$

If $\alpha_*(m_Z^2)$ is used in this relation instead of α to compute m_W from G_F, the prediction for m_W is shifted upward by 3%. Almost ten years ago, Marciano and Sirlin[32,33] showed by detailed calcuation that this large shift indeed appears in the standard model radiative corrections to m_W.

Since the electromagnetic vacuum polarization is such an important contribution to weak interaction radiative corrections, it is worth a digression to explain how it may be evaluated more exactly. Our estimate above was adequate for the leptons, but for the quarks it was little more-than a guess. However, the quark contribution to Π_{QQ} can be evaluated accurately by using the optical theorem to relate the hadronic corrections to forward Bhabha scattering, indicated in Fig. 26(a), to the total cross section for $e^+e^- \to$ hadrons. This yields

$$\text{Im } \Pi'_{QQ}(q^2) = \frac{1}{12\pi} R(q^2) \tag{5.8}$$

where $R(q^2)$ is the usual ratio of e^+e^- cross sections to hadrons versus muon pairs. Thus, Π'_{QQ}aquires an imaginary part for real positive values of q^2. It follows that, when this function is considered as an analytic function of q^2, it has a discontinuity across the real q^2 axis given by Disc $\Pi'_{QQ} = 2i\text{Im } \Pi'_{QQ}$. This allows us to use (5.8) to evaluate a Cauchy integral for Π'_{QQ} about the contour in the q^2 plane indicated in Fig. 26(b):

$$\Pi'_{QQ}(q^2) = \oint \frac{ds'}{2\pi i} \frac{1}{s' - q^2} \Pi_{QQ}(s') . \tag{5.9}$$

Inserting (5.8) into (5.9), and subtracting the same integral evaluated at $q^2 = 0$

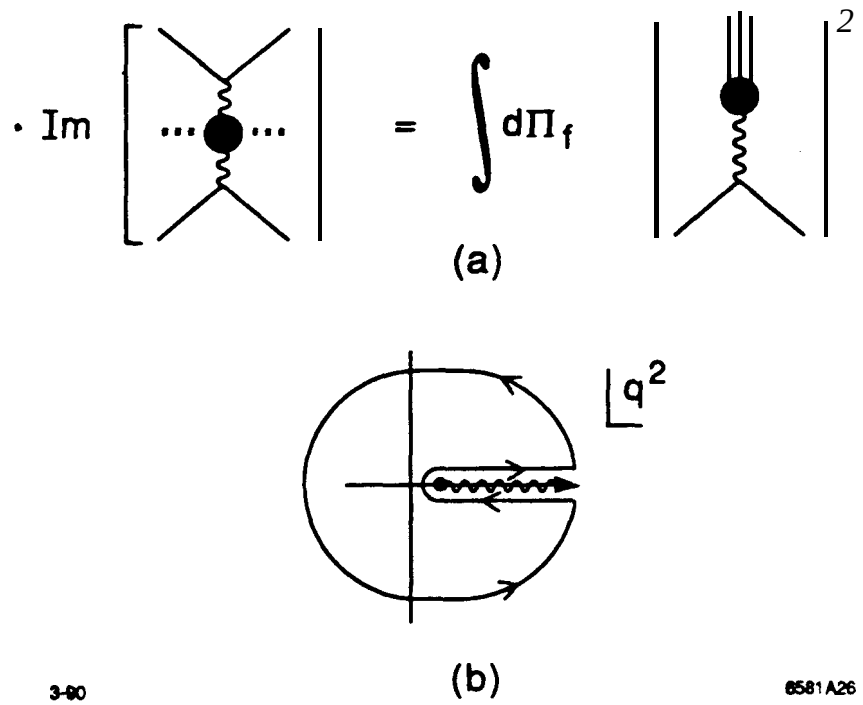

Figure 26. Evaluation of the hadronic contribution to the electromagnetic vacuum polarization.

we find

$$e^2\Pi'_{QQ}(q^2) - e^2\Pi'_{QQ}(0) = \frac{\alpha}{3\pi} P \int_0^\infty ds' R(s') \left[\frac{1}{s' - q^2} - \frac{1}{s'}\right]. \tag{5.10}$$

A recent evaluation of the integral (5.10) from the measured e^+e^- annihilation cross section by Burkhardt, Jegerlehner, Penso, and Verzegnassi[34] gives the result

$$\left[\alpha^{-1} - \alpha_*^{-1}(m_Z^2)\right]_{\text{hadronic}} = 3.95 \pm 0.12 . \tag{5.11}$$

Combining this with a more accurate evaluation of the lepton vacuum polarization diagrams, one finds

$$\alpha_{*,o}^{-1}(m_Z^2) = 128.77 \pm 0.12 . \tag{5.12}$$

(The subscript o indicates that this value of α_* takes into account only the renor-

malization effects due to observed quarks and leptons, and not the possible additional effects due to the top quark and other heavy species.) The relative error in $\alpha_{*,o}(m_Z^2)$ is 9 x 10^{-4}. This error is dominated by the uncertainties in the e^+e^- total cross section measurements from 2 GeV to the J/ψ and from 4 GeV to the highest energies of SPEAR.

In calculating weak interaction radiative corrections, we will also encounter vacuum polarization diagrams for weak gauge bosons, and these contain similar corrections from hadronic intermediate states. However, as Lynn, Penso, and Verzegnassi [35] have explained, the most important of these contributions are actually proportional to (5.11). The remaining terms are small and are dominated by contributions from the well-studied vector mesons w and ϕ.

5.2. The Structure of Vacuum Polarization Amplitudes

To evaluate more general weak radiative corrections, we will need to discuss a wider variety of vacuum polarization amplitudes. Thus, in Fig. 27, I have presented in a standard notation the vacuum polarization amplitudes of the photon, Z^0, and W, and the amplitude for photon–Z^0 mixing. In this figure, and henceforth, I use the abbreviations

$$\sin^2\theta_w \rightarrow s^2\,, \quad \cos^2\theta_w \rightarrow c^2$$

in writing the values of loop amplitudes. It is most useful to break up the Z^0 vacuum polarizations into the contributions of electromagnetic and weak isospin currents (replacing the Z^0 current by (2.7)), and this has been done in setting the conventions shown. For later convenience, I have written the W vacuum polarization as a matrix element of weak isospin currents J_μ^{1L}.

If we wish to evaluate the effect of the top quark on weak interaction parameters, we must compute the contributions to this vacuum polarization amplitudes from top and bottom quark loops. In general, the contribution from heavy fermions is well approximated by the simplest fermion loop diagram, shown in Fig. 28(a).

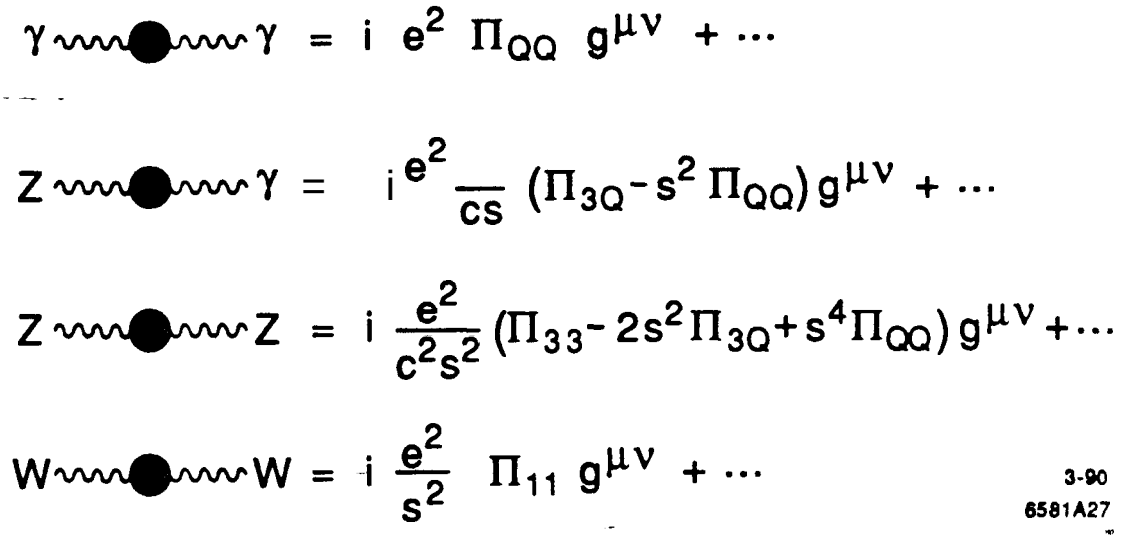

Figure 27. Vacuum polarization diagrams arising in the evaluation of weak interaction radiative corrections.

The evaluation of this diagram for vector currents is a standard exercise in QED. However, for the weak interactions, we also need to consider chiral currents, and these add some interesting complications. Let me, then, display separately the contributions to the fermion loop diagram from left- and right-handed currents, and allowing the particle and antiparticle in the diagram to have different masses. These terms take *a* relatively simple form when expressed as Feynman parameter integrals

$$\Pi_{LL}(m_1^2,m_2^2,q^2) = \Pi_{RR}(m_1^2,m_2^2,q^2)$$

$$= -\frac{4}{(4\pi)^2}\int_0^1 dx\,\log\left[\frac{\Lambda^2}{M^2 - x(1-x)q}\right]\cdot\left(x(1-x)q^2 - \frac{1}{2}M^2\right)$$

$$\Pi_{LR}(m_1^2,m_2^2,q^2) = \Pi_{RL}(m_1^2,m_2^2,q^2)$$

$$= -\frac{4}{(4\pi)^2}\int_0^1 dx\,\log\left[\frac{\Lambda^2}{M^2 - x(1-x)q^2}\right]\cdot\left(\frac{1}{2}m_1 m_2\right)\ , \tag{5.13}$$

where

$$M^2 = xm_1^2 + (1-x)m_2^2\ . \tag{5.14}$$

The parameter A is an ultraviolet cut-off (though actually these expressions are most easily obtained using dimensional regularization). Adding these four contributions, with equal mass fermions, we find the vacuum polarization of vector currents

$$\Pi_{VV}(m^2,m^2,q^2) = \left(-\frac{4}{}\right)\int_0^1 dx\,\log\left(\frac{\Lambda^2}{m^2 - x(1-x)q^2}\right)\cdot x(1-x)q^2 \tag{5.15}$$

which is the standard QED result. The approximate formula (5.6) is simply obtained from the limit $q^2 >> m^2$ of this expression. The integrals in (5.13) and (5.15) are straightforward to evaluate analytically; detailed expressions are given, for example, in ref. 5.

The various vacuum polarization amplitudes shown in Fig. 27 are straightforwardly reconstructed from these functions. For a fermion doublet of weak isospin $\frac{1}{2}$, fermion masses m,, m_d, and electric charges Q_u, Q_d ($Q_u = Q_d + 1$), the four

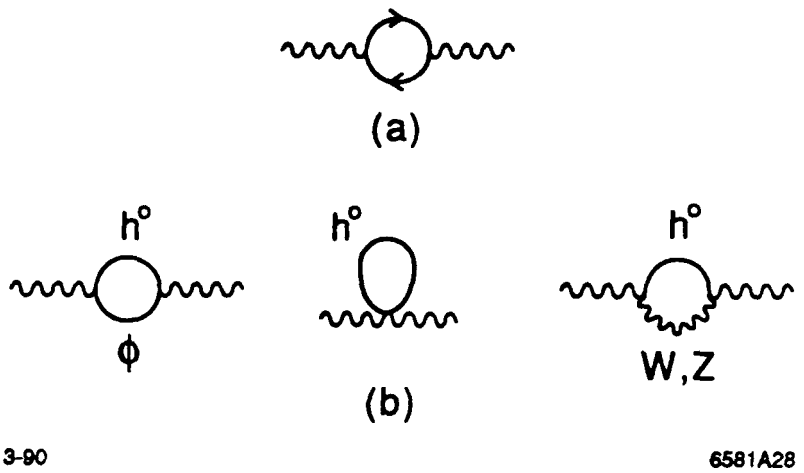

Figure 28. Contributions to the vacuum polarization amplitudes from (a) heavy fermions, (b) the Higgs boson of the minimal standard model.

amplitudes are given by

$$\begin{aligned}
\Pi_{QQ}(q^2) &= Q_u^2\,\Pi_{VV}(m_u^2, m_u^2, q^2) + Q_d^2\,\Pi_{VV}(m_d^2, m_d^2, q^2) \\
\Pi_{3Q}(q^2) &= \frac{1}{2}Q_u\,(\Pi_{LL}+\Pi_{LR})(m_u^2, m_u^2, q^2) - \frac{1}{2}Q_d\,(\Pi_{LL}+\Pi_{LR})(m_d^2, m_d^2, q^2) \\
&= \frac{1}{4}\left[Q_u\,\Pi_{VV}(m_u^2, m_u^2, q^2) - Q_d\,\Pi_{VV}(m_d^2, m_d^2, q^2)\right] \\
\Pi_{33}(q^2) &= \frac{1}{4}\left[\Pi_{LL}(m_u^2, m_u^2, q^2) + \Pi_{LL}(m_d^2, m_d^2, q^2)\right] \\
\Pi_{11}(q^2) &= \frac{1}{2}\,\Pi_{LL}(m_u^2, m_d^2, q^2)\ .
\end{aligned} \tag{5.16}$$

For quarks, multiply these expressions by 3 colors.

The amplitude Π_{VV} in (5.15) vanishes at $q^2 = 0$, in accordance with our earlier argument. In fact, only one vector current is needed to achieve this cancellation, so Π_{LV}, and therefore the term Π_{3Q} in the photon–Z^0 mixing amplitude, also vanishes at $q^2 = 0$. However, the purely chiral vacuum polarizations do not in general vanish at zero momentum. From (5.13), we see that the zero-momentum

limit of Π_{LL} is not only nonzero but actually increases with the masses of the fermions in the loop:

$$\Pi_{LL}(m_t^2, m_t^2, q^2) \cong \frac{2}{(4\pi)^2} m_t^2 \log \frac{\Lambda^2}{m_t^2}$$
$$\Pi_{LL}(m_t^2, m_b^2, q^2) \cong \frac{2}{(4\pi)^2} m_t^2 \left(\log \frac{\Lambda^2}{m_t^2} + \frac{1}{2} \right) , \tag{5.17}$$

for $m_t^2 >> q^2, m_b^2$. This unusual behavior has important physical consequences, as we will see below.

For completeness, I also display the contributions to the various vacuum polarizations from the Higgs boson of the minimal standard model, which appears in the diagrams shown in Fig. 28(b). These are

$$\Pi_{QQ}(q^2) = \Pi_{3Q}(q^2) = 0$$

$$\Pi_{33}(q^2) = -\frac{1}{4(4\pi)^2} \int_0^1 dx \log \left[\frac{\Lambda^2}{x m_H^2 + (1-x) m_Z^2 - x(1-x) q^2} \right]$$
$$\cdot \left((1-2x)^2 q^2 + 4 m_Z^2 + (1-2x)(m_Z^2 - m_H^2) \right) \tag{5.18}$$

$$\Pi_{11}(q^2) = -\frac{1}{4(4\pi)^2} \int_0^1 dx \log \left[\frac{\Lambda^2}{x m_H^2 + (1-x) m_W^2 - x(1-x) q^2} \right]$$
$$\cdot \left((1-2x)^2 q^2 + 4 m_W^2 + (1-2x)(m_W^2 - m_H^2) \right) ,$$

where m_H is the mass of the Higgs scalar.

5.3. RENORMALIZATION OF WEAK INTERACTION ASYMMETRIES: I

Armed with this technical information, we are ready to study the radiative correction to some particular experiment. Let begin with a rather simple example, the correction due to the top quark to the prediction of weak interaction asymmetries at the Z^0 resonance. In particular, I would like to focus on the renormalization of the polarization asymmetry A_{LR}, defined as

$$A_{LR} = \frac{\sigma(e_L^- e^+ \to Z) - \sigma(e_R^- e^+ \to Z)}{\sigma(e_L^- e^+ \to Z) + \sigma(e_R^- e^+ \to Z)} . \tag{5.19}$$

The particular asymmetry A_{LR} is an important quantity for two reasons. First, it is observable not only in its own right but also as an ingredient in the various forward-backward asymmetries at the Z^0. The leading order relation

$$A_{FB}^f = \frac{3}{4} A_{LR}^e A_{LR}^f \tag{5.20}$$

is true to all orders for the contribution of the Z^0 resonance. More generally, I will argue below, all weak interaction asymmetries measure the same radiative correction amplitude, up to some unimportant residual effects. A_{LR} is thus representative of a class of radiative corrections that we would like to investigate.

Second, among the various weak asymmetries, A_{LR} is the most sensitive to radiative corrections. The formula for A_{LR} in the standard model at leading order is

$$A_{LR} = \frac{8\left(\tfrac{1}{4} - \sin^2\theta_w\right)}{1 + \left(1 - 4\sin^2\theta_w\right)^2} \cong 8(\tfrac{1}{4} - \sin^2 0,) . \tag{5.21}$$

Evaluating this expression with the parameters of Section 3.1, we find $A_{LR} \cong 0.13$. But A_{LR} is an asymmetry, and, better, the asymmetry of a total cross section with respect to changes in the polarization of a physically isolated source. This means that almost all systematic errors cancel in the measurement of A_{LR}, so that, with enough statistics, it should be possible to measure this asymmetry to 1% or so of

its value. To convert this error to an error on $\sin^2\theta_w$, one should divide by the factor of 8 in (5.21), giving the possibility of achieving an accuracy

$$\delta \sin^2\theta_w \sim 2 \times 10^{-4} \ . \qquad (5.22)$$

With this promised precision in mind, let us evaluate the contribution of the top quark to A_{LR}. The basic ingredients of the calculation are displayed in Fig. 29. The leading order vertex for e^+e^- annihilation into a Z^0 follows directly from (2.7). The corrected polarization asymmetry may be found from the ratio of the terms proportional to I^{3L} and Q in the complete, radiatively corrected vertex. In the second line of 29, this ratio has been labelled s_*^2. The corrected value of A_{LR} is obtained by replacing $\sin^2\theta_w$ by s_*^2 in (5.21). This complete vertex gets contributions from the various diagrams shown in the third line of 29, some of which are rather complicated to compute. However, since there are no direct couplings between the top quark and the electron, the top quark enters the renormalization of this vertex only through the last diagram shown in Fig. 29, the vacuum polarization diagram involving photon--Z' mixing.

This particular simplification occurs quite generally for radiative corrections due to heavy or exotic particles. Because exotic particles often have no direct couplings to light fermions, and in all other cases these couplings are highly constrained, it is usually true that the only important effects of heavy particles on the weak interactions of light quarks and leptons occur by the indirect effects of these particles through their vacuum polarization amplitudes. An interesting example is the case of supersymmetric particles.[36,37] The diagrams involving the direct coupling of leptons to their superpartners turn out to be quite small, while the largest corrections come from the vacuum polarization of the t quark and the $\tilde{t}$ squark. In Ref. 38, contributions arising through vacuum polarization amplitudes were termed 'oblique' radiative corrections. As we continue this analysis, we will see that such corrections are not only numerically important but also quite easy to understand in a systematic way.

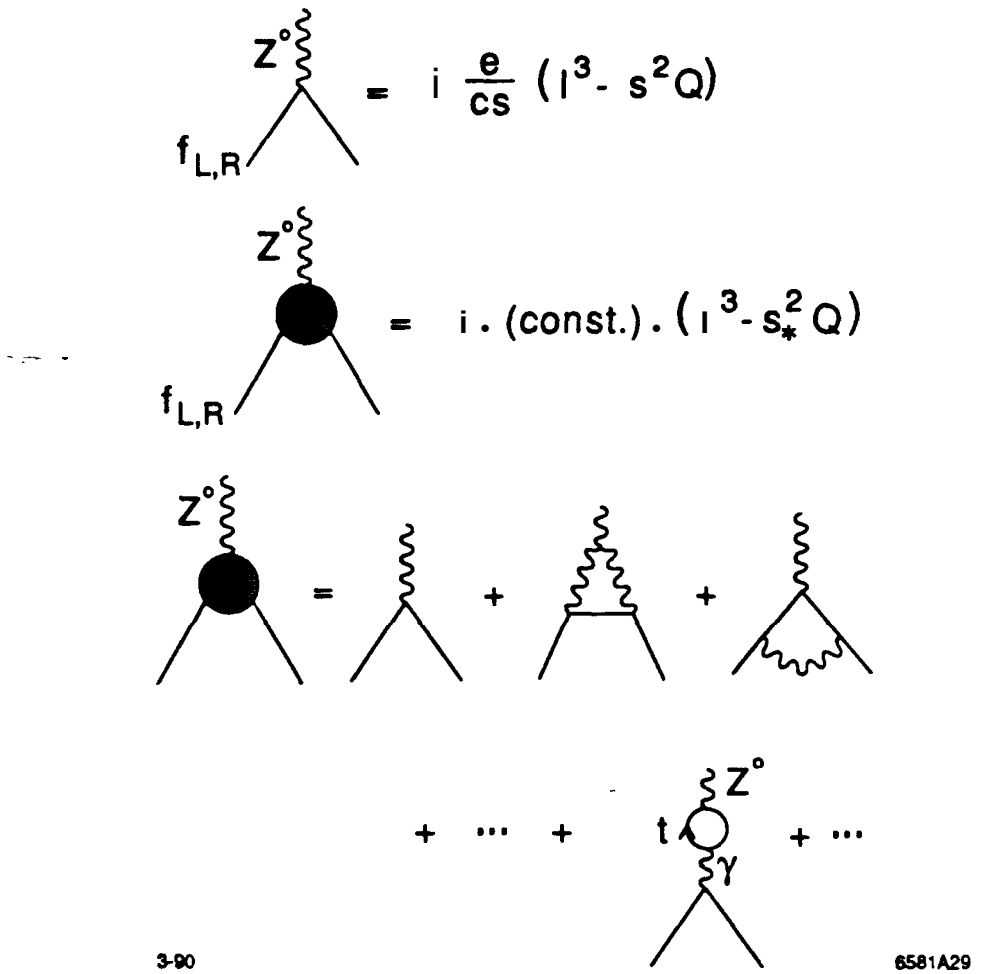

Figure 29. Calculation of the l-loop renormalization of weak interaction asymmetries at the Z^0.

In principle, we might try to illustrate this in the calculation of A_{LR}, by adding together the leading order diagram and the oblique contribution of the vacuum polarization amplitude for photon-Z^0 mixing. The result is

$$\frac{e}{cs}\left(I^3 - [s^2 - e^2(\Pi'_{3Q} - s^2\Pi'_{QQ})]Q\right), \qquad (5.23)$$

and so we can identify

$$s_*^2 = \sin^2\theta_w - e^2(\Pi'_{3Q}(m_Z^2) - \sin^2\theta_w \Pi'_{QQ}(m_Z^2)) . \qquad (5.24)$$

Unfortunately, this result is a disaster; the two vacuum polarization amplitudes are both ultraviolet divergent, and so the answer makes no physical sense.

5.4. An Exhortation on $\sin^2\theta_w$

In a renormalizable quantum field theory, the appearance of ultraviolet divergences in a physical amplitude is a sign that we are asking the wrong question. In the previous section, we computed the radiative correction to the polarization asymmetry by computing the shift of the left-right asymmetry of electron-positron-Z^0 vertex from its value in leading order. But this leading order value is a ratio of bare parameters; it cannot be measured directly. To make a physically meaningful statement, we must predict the value of the asymmetry from other measureable weak interaction quantities.-

One straightforward way to structure such a prediction is the following: First, imagine measuring $\sin^2\theta_w$ using other observables of the weak interactions, for example, α, G_F, and m_Z. We may consider the evaluation (5.21) using this value of $\sin^2\theta_w$ as giving a reference value. We may then predict the deviation of the actual value of A_{LR} from this reference value by computing a set of Feynman diagrams. This process depends, in its intermediate stages, on the exact definition of $\sin^2\theta_w$ in terms of observable quantities. Many different definitions are possible, and I will discuss a few of these below. The final result of the process is a prediction for A_{LR} in terms of α, G_F, and m_Z, and this result will of course be independent of the definition of $\sin^2\theta_w$ used. In principle, we might simply discard $\sin^2\theta_w$ and speak only about relations between directly measureable quantities. This purist attitude has been advocated recently by Passarino.[39] I must admit, though, that I find the value of $\sin^2\theta_w$ a useful point of reference, if I know exactly what it means.

The most common definition of $\sin^2\theta_w$ in the literature on weak interaction radiative corrections is one introduced by Sirlin,[2] which elevates the leading order

mass relation (2.4) to a definition

$$\sin^2\theta_w|_S \equiv 1 - \frac{m_W^2}{m_Z^2} . \tag{5.25}$$

This definition is technically very useful, but I feel uncomfortable with it, for two reasons. First, the mass of the W cannot be measured with the highest precision, so that in practice one must compute m_W in terms of m_Z, a, and G_F in order to apply this definition. This problem is exacerbated by the fact that the Feynman diagrams which renormalize the W-Z mass splitting depend rather strongly on the top quark mass, through the relation (5.17). Thus, the use of this definition introduces a strong dependence on m_t into processes such as the weak asymmetries at the Z^0, which do not otherwise contain this singular dependence. Similarly, the value of $\sin^2\theta_w|_S$ depends on other new physics which might be added to the standard model.

Another possibility is to define $\sin^2\theta_w$ as a ratio of coupling constants renormalized by minimal subtraction.[32,40] In this way, we define the weak interaction couplings just as the strong interaction coupling α_s is defined in QCD. This definition has the advantage of removing the strong dependence on the top quark mass. It has a further advantage for theorists who wish to predict the value of $\sin^2\theta_w$ from grand unified theories, since that computation is done most naturally in this framework.[41] However, this definition gives up the clear physical picture which is available when $\sin^2\theta_w$ is constructed from quantities which are directly measureable. In some sense, using $\sin^2\theta_w|_{\overline{MS}}$ introduces into the weak interactions all the conceptual problems that experimenters—and theorists-have in understanding the meaning of α_s or $\Lambda_{\overline{MS}}$

As a compromise between these two viewpoints, let me propose a new standard for $\sin^2\theta_w$—the Z^0 standard: Define θ_w and $\sin^2\theta_w$ by the formula:

$$\sin 2\theta_w|_Z \equiv \left(\frac{4\pi\alpha_{*,o}(m_Z^2)}{\sqrt{2}G_F m_Z^2} \right)^{1/2} . \tag{5.26}$$

In this formula, $\alpha_{*,o}(m_Z^2)$ is the value of α_* at the Z^0 mass, including the renor-

malization due to observed quarks and leptons, as determined in Section 5.2. Regardless of the definition of a, the formula is a correct lowest-order relation in the standard model and may then be the basis for a definition to all orders. The use of $\alpha_{*,o}(m_Z^2)$ rather than α incorporates into the formula the Marciano-Sirlin renormalization effect described below (5.7); this is the largest renormalization effect coming from the conventional states of the standard model.

The value of $\sin^2\theta_w|_Z$ is now known extremely precisely; in fact, the error in this-quantity is a good measure of the real accuracy of our understanding of the standard model, before theoretical uncertainties due to the top quark mass and other types of new physics are included. Using the value of the Z^0 mass given in (2.10) and the value of $\alpha_{*,o}(m_Z^2)$ from (5.12), we have

$$\sin^2\theta_w|_Z = 0.2317(4)\,. \qquad (5.27)$$

The error in $\sin^2\theta_w|_Z$ arises from

$$A\sin^2\theta_w|_Z \cong 0.3\left(\frac{A\,\%}{\alpha_*},\ \frac{\Delta m_Z}{2\,m_Z}\right) = (3.1,\ 2.2)\times 10^{-4}\,. \qquad (5.28)$$

Let me stress again that, by definition, $\sin^2\theta_w|_Z$ is independent of the mass of the top quark, the Higgs boson, or any other type of new physics. The dependence on these parameters is introduced when $\sin^2\theta_w|_Z$ is used to predict the values of other observables of the weak interactions, such as the W boson mass or the polarization asymmetry A_{LR}.* It is my hope that the use of $\sin^2\theta_w|_Z$ as a standard will clarify conceptually the process of using precision weak interaction measurements to constrain or to discover new physical processes.

★ **This sentiment accords with Taylor's Dogma:[42] "One should not apply to the data a radiative correction which depends on the masses of undiscovered particles."**

5.5. RENORMALIZATION OF WEAK INTERACTION ASYMMETRIES: II

Now that we have clarified the meaning of the parameter $\sin^2\theta_w$, we can see that the calculation we were performing at the end of Section 5.3 was misguided. There, we tried to compute the difference between s_*^2, the measureable ratio of the I^3 and Q terms in the weak neutral current, to the bare parameter $\sin^2\theta_w$, which is not directly observable. A more meaningful calculation would be to compute the-difference of two quantities which are completely defined by experiment, for example, to compute

$$s_*^2 - \sin^2\theta_w|_Z \,. \tag{5.29}$$

Let us, then, assemble the complete contribution to (5.29) arising from top and bottom quark loop diagrams.

We may take the shift of s_*^2 from its bare value to be that given in (5.24). With no extra effort, we might evaluate this vertex at a general value of q^2, where q is the momentum of the Z^0. The parameter $s_*^2(q^2)$ is given by

$$s_*^2 = \frac{g'^2}{g^2+g'^2} - e^2[\Pi'_{3Q}(q^2) - s^2\Pi'_{QQ}(q^2)] \,. \tag{5.30}$$

But to compute (5.29), we must also work out the shift of $\sin^2\theta_w|_Z$ from its bare value. To do this, we need the shifts of α, G_F, and m_Z. Figure 30(a) shows the shift of α:

$$4\pi\alpha = e^2(1 + e^2\Pi'_{QQ}(0)) \,. \tag{5.31}$$

(To be careful, we should exclude here the contribution of the b quark loop to (5.31), since this effect was already included when we exchanged α for $\alpha_{*,o}(m_Z^2)$.) Figure 30(b) shows the shift of m_Z^2:

$$m_Z^2 = \frac{1}{4}(g^2+g'^2)v^2\left(1 + \frac{1}{m_Z^2}\frac{e^2}{s^2c^2}(\Pi_{33} - 2s^2\Pi_{3Q} + s^4\Pi_{QQ})(m_Z^2)\right). \tag{5.32}$$

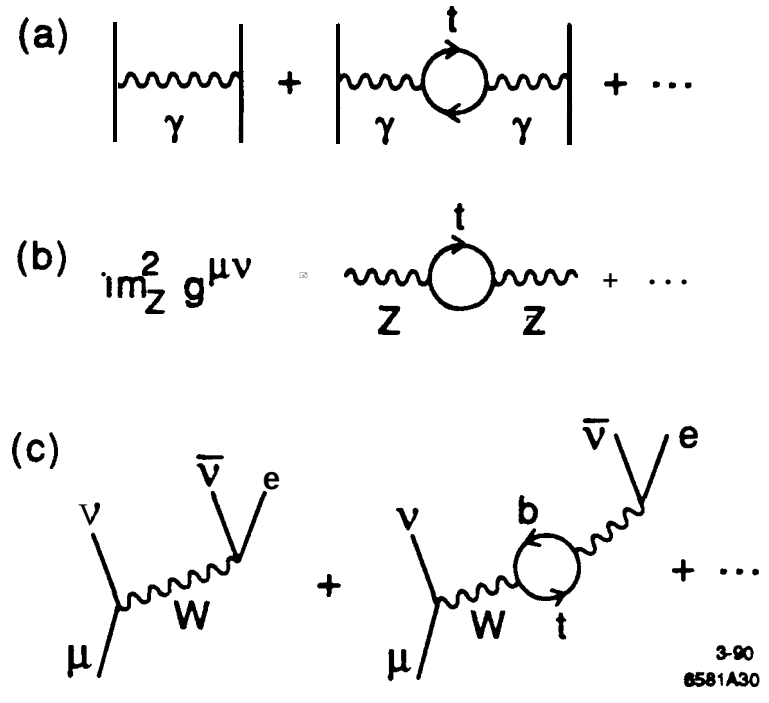

Figure 30. Shifts of the quantities needed to define $\sin^2\theta_w|_Z$ generated by l-loop diagrams involving the t quark.

Figure 30(c) shows the shift of G_F, as it would be extracted from μ decay:

$$\frac{G_F}{\sqrt{2}} = \frac{1}{2v^2}\left(1 - \frac{1}{m_W^2}\,\frac{e^2}{s^2}\,\Pi_{11}(0)\right) . \tag{5.33}$$

Note that in each case, the contribution of t and b comes only from vacuum polarization diagrams. In the language of Section 5.3, all of these contributions are purely 'oblique'.

We can now compute the shift of $\sin^2\theta_w|_Z$ from its bare value with only a bit of algebra. In general,

$$\delta(\sin^2\theta_w) = 2sc\delta\theta_w = \frac{2sc}{2\cos 2\theta_w}\,\delta\sin 2\theta_w = \frac{2s^2c^2}{c^2 - s^2}\,\frac{\delta\sin 2\theta_w}{\sin 2\theta_w} . \tag{5.34}$$

Then, inserting the shifts of α, G_F, and m_Z^2,

$$\sin^2\theta_w|_Z = \frac{g'^2}{g^2+g'^2} + \frac{2s^2c^2}{c^2-s^2}\cdot\frac{1}{2}\left(\frac{\delta\alpha}{\alpha} - \frac{\delta G_F}{G_F} - \frac{\delta m_Z^2}{m_Z^2}\right)$$

$$= \frac{g'^2}{g^2+g'^2} + \frac{s^2c^2}{c^2-s^2}$$

$$\cdot\left[e^2\Pi'_{QQ}(0) + \frac{e^2}{s^2c^2}\,\frac{\Pi_{11}(0)}{m_Z^2} - \frac{e^2}{s^2c^2m_Z^2}(\Pi_{33} - 2s^2\Pi_{3Q} + s^4\Pi_{QQ})(m_Z^2)\right] . \tag{5.35}$$

By combining this result with (5.30), we find following contribution to (5.29) from l-loop diagrams involving the top quark:

$$s_*^2(q^2) = \sin^2\theta_w|_Z$$

$$+\left\{\frac{e^2}{c^2-s^2}\left[\frac{\Pi_{33}(m_Z^2) - 2s^2\Pi_{3Q}(m_Z^2) - \Pi_{11}(0)}{m_Z^2} - (c^2-s^2)\,\frac{\Pi_{3Q}(q^2)}{q^2}\right]\right.$$

$$\left. + \frac{e^2s^2}{c^2-s^2}\left[s^2\Pi'_{QQ}(m_Z^2) - c^2\Pi'_{QQ}(0) + (c^2-s^2)\,\Pi'_{QQ}(q^2)\right]\right\} . \tag{5.36}$$

In fact, this formula did not make of any special property of the top quark, other than that it does not couple directly to light quarks and leptons. The formula (5.36) holds for any oblique weak interaction radiative correction.

We should immediately check that our new analysis solves the problem of ultraviolet divergences which was raised at the end of Section 5.3. Recall from Section 5.2 that the vacuum polarization amplitudes $\Pi_{33}(q^2)$ and $\Pi_{11}(q^2)$ contain two separate divergent terms, in their value at $q^2 = 0$ and in their first derivative at this point. However, each divergence of Π_{33} is related to a divergent term in Π_{11} by weak isospin symmetry. In particular,

$$\Pi_{33}(0) = \Pi_{11}(0) + \text{finite}\,; \quad \Pi_{3Q}(0) = \Pi_{QQ}(0) = 0\,. \tag{5.37}$$

This formula insures that the divergent terms from $\Pi_{33}(0)$ and $\Pi_{11}(0)$ cancel in (5.36). The divergences in the first derivatives are also related by weak isospin

symmetry:

$$\frac{d}{dq^2}\,\Pi_{33}(0) = \frac{d}{dq^2}\,\Pi_{11}(0) = \frac{d}{dq^2}\,\Pi_{3Q}(0)\ . \tag{5.38}$$

The last part of this relation follows from the fact that Q = I^3 + Y; thus Π_{3Q} = $\Pi_{33} + \Pi_{3Y}$. Since the weak hypercharge is orthogonal to I^3, the second piece of this expression has no divergence in its first derivative. The first derivative of any II at a different value of q^2 differs from the value at $q^2 = 0$ only by finite terms. Then the-relation (5.38) implies that (after a bit of algebra) these divergent terms also cancel out of (5.36). Finally, the divergent terms in the last line of (5.36) assemble into differences of first derivatives of Π_{QQ}, and these are again finite. Thus, the relation (5.36) is a completely well-defined theoretical prediction, which may now be compared to experiment.

Let us, then, evaluate (5.36) and examine the properties of this relation, The formula is easily evaluated numerically by inserting the formula of Section 5.2 for vacuum polarization amplitudes. In Fig. 31, I have plotted the prediction for $s^2_*(m^2_Z)$ in the standard model as a function of-the top quark mass, for fixed Higgs boson mass, and as a function of the Higgs mass, for fixed m_t.

The next few sections contain many figures similar to Fig. 31 which give the dependence of various weak interaction parameters on m_t and m_H, so it is worth pausing to clarify the conventions reflected in these figures. The figures include not only the effects of m_t and m_H but also the additional l-loop corrections of the standard model. However, these additional corrections are added in a rather simplistic way, by introducing fixed shifts of s^2_* and other basic quantities. The explicit procedure is spelled out in Section 5.10. This gives a simple calculational scheme, which I hope that you can straightforwardly reproduce. However, the simplicity of the method limits the accuracy to about 0.5% in $\sin^2\theta_w$. The best current calculations of weak readiative corrections are reported in Ref. 6; these results are typically good to 0.1% in $\sin^2\theta_w$. A calculation at this level is not recommended as an educational exercise, but it is essential to extract the full information from a precision experiment. The three curves in each set reflect

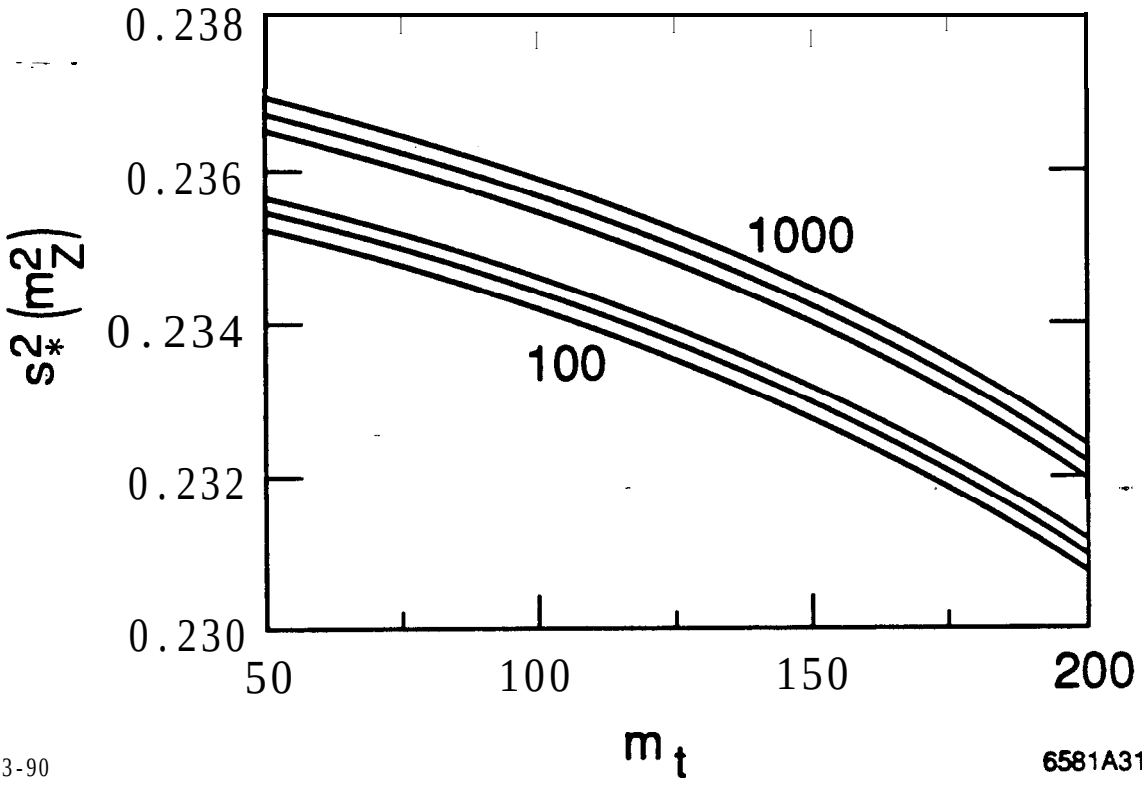

Figure 31. Dependence of $s^2_*(m^2_Z)$ on m_t and m_H predicted by (5.36), using the known value of m_Z. The two bands show the result of varying m_t, with m_H held fixed at the two values 100 GeV, 1000 GeV. The width of each band reflects the 1 σ error in m_Z.

the 1 σ uncertainty in the Z^0 mass value (2.10). In the present situation, where the dominant uncertainty in $\sin^2 \theta_w|_Z$ comes from the renormalization of α, this understates the true errors by about a factor of two. Hopefully, new data on low-energy e^+e^- annihilation cross sections will decrease this uncertainty and make these errors appropriate for future comparisons.

The results of Fig. 31 may be translated into predictions for the weak asymmet&s. Thus, in Figs. 32 and 33 I display the predictions for A_{LR} and for the forward-backward asymmetries at the Z^0 in $e^+e^- \to b\bar{b}$ and $e^+e^- \to \mu^+\mu^-$. The solid curves apply to the idealized situation in which the hard amplitudes are evaluated at the resonance peak. The dashed curves show the effect of including soft radiative corrections according to (3.29) and evaluating the expressions at the true peak cross section $m_Z + 100$ MeV. This soft radiative correction is a small perturbation of A_{LR} and A^b_{FB}, but is has a large effect on A^μ_{FB}.

We argued in Section 5.3 that A_{LR} is exceptionally sensitive to effects which perturb $\sin^2 \theta_w$, and that is borne out here. Since the polarization asymmetry for b quarks at the Z^0 is close to 1, we would expect from (5.20) that this forward-backward asymmetry would behave quite similarly to A_{LR}, and this, again, is clear from Fig. 32. In principle, this forward-backward asymmetry might be used as a substitute for the measurement of A_{LR}. The use of this measurement brings two new difficulties. First, the b forward-backward asymmetry is diluted by B–$\bar{B}$ mixing; for a precision measurement, the mixing parameter x of the B_d–$\bar{B}_d$ system and the fraction of B_s production must be known to about 10%. Second, this asymmetry suffers a QCD correction:[43]

$$A^b_{FB} \to A^b_{FB} \cdot \left(1 - \frac{\alpha_s}{\pi}\right) . \tag{5.39}$$

Neither of these effects would seem to be an obstacle to measuring A^b_{FB} to an accuracy of 3 x 10^{-3}. Another possible substitute for a precision measurement of A_{LR} is the forward-backward asymmetry to lepton pairs. However, we see from Fig. 33 that this quantity is unfortunately very small, so that its measurement will be hindered at an earlier stage. by systematic errors.

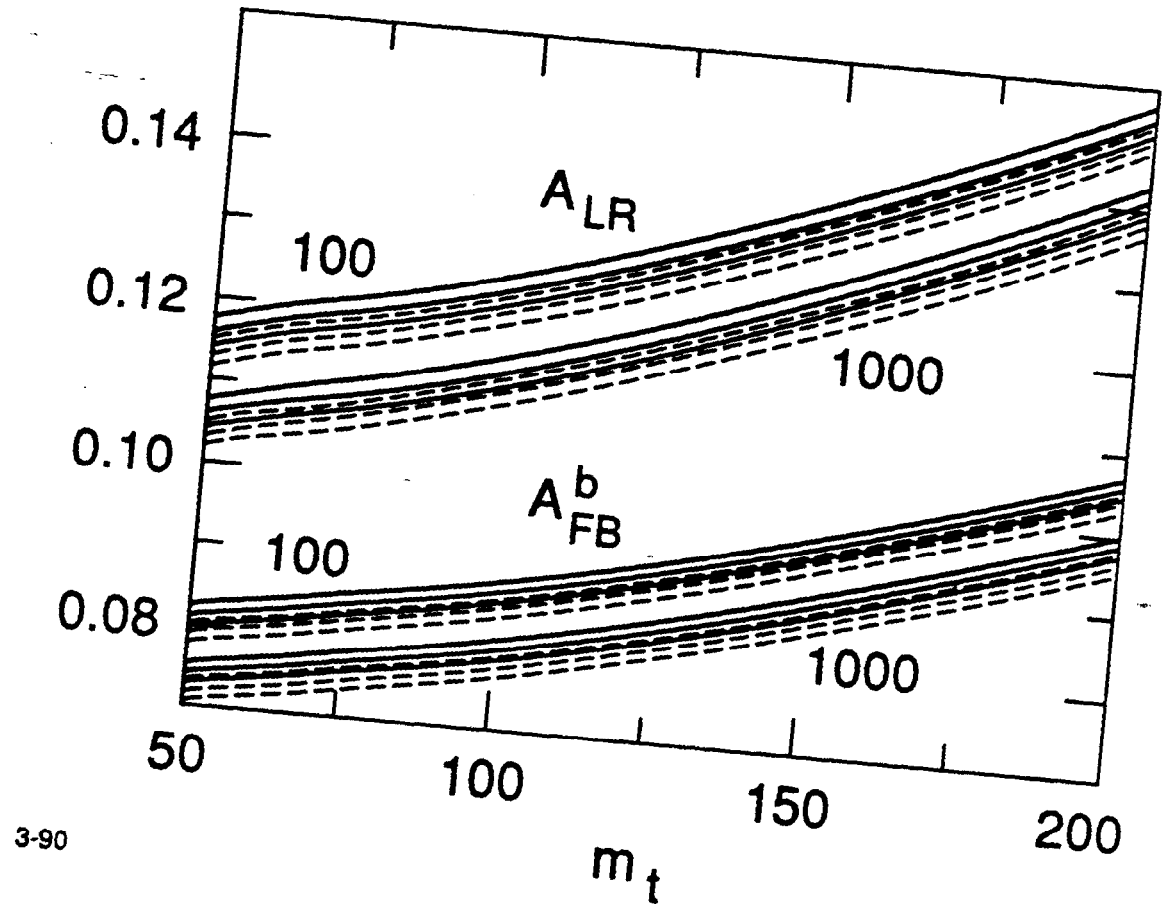

Figure 32. Dependence of A [illegible] on m_t and m_H. The notation is as in Fig. 31. The dashed curves reflect the inclusion of soft radiative corrections, computed with (3.29).

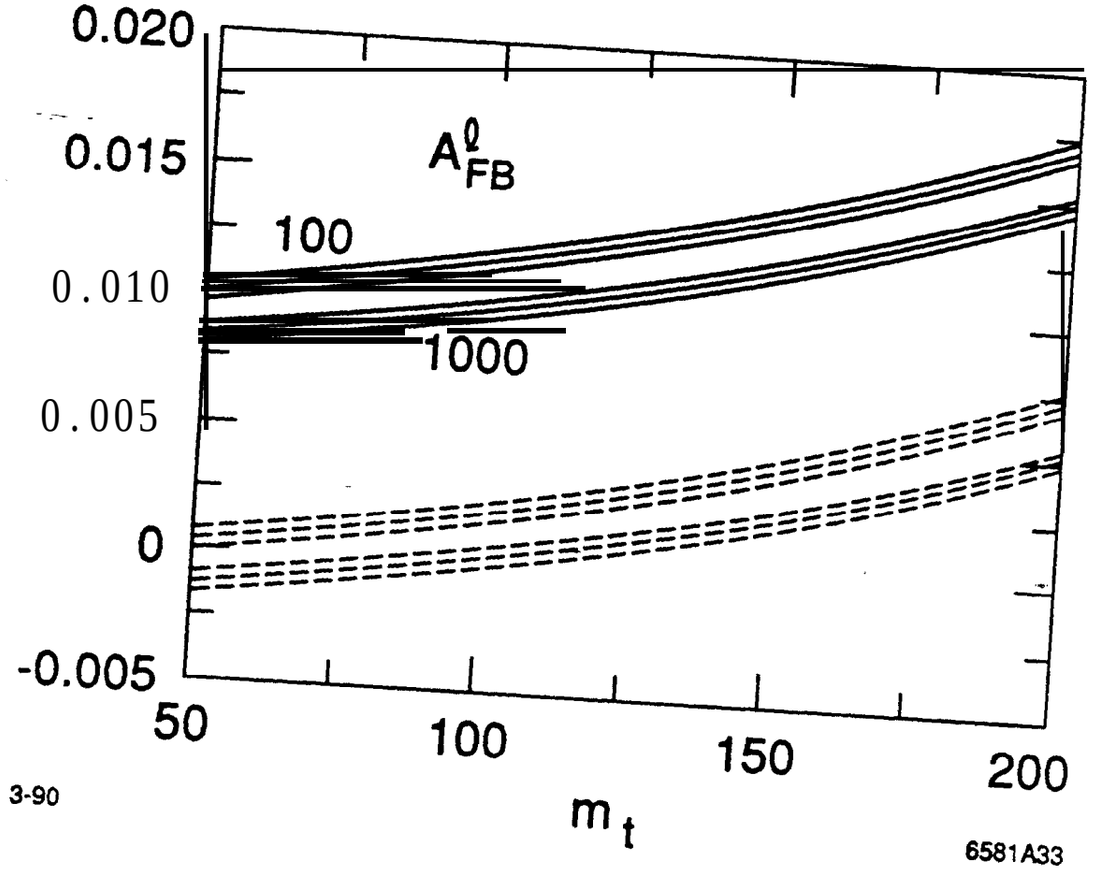

Figure 33. Dependence of A_{FB}^{ℓ}, the lepton forward-backward asymmetry, on m_t and m_H. The notation is as in Fig. 32.

For large values of the top quark mass, the parameter s_*^2 decreases quadratically with m_t. Let us evaluate this dependence using the relation

$$e^2(\Pi_{33}(0) - \Pi_{11}(0)) \cong -\frac{3\alpha}{16\pi} m_t^2 , \tag{5.40}$$

which follows from (5.17). This singular dependence on m_t cancels out of all other differences of vacuum polarization amplitudes. Thus,

$$s_*^2(m_Z^2) \cong \sin^2 \theta_w|_Z - \frac{3\alpha}{16\pi} \frac{1}{(c^2 - s^2)} \frac{m_t^2}{m_Z^2} . \tag{5.41}$$

Because this dependence comes from vacuum polarizations which originate in the renormalization of m_Z and G_F, rather than in (5.30), this quadratic sensitivity to m_t may properly be considered an artifact of the definition of $\sin^2 \theta_w|_Z$. This dependence does not appear, for example, in the comparison of s_*^2 with $\sin^2$ 8,. However, this dependence is also a true aspect of the precision calculation of s_*^2 from m_Z and, as I have pointed out, the effect is quite observable experimentally'- for large m_t. The quadratic dependence on m_t is expected to be independent of q^2. This is illustrated in Fig. 34, where I have displayed the dependence on m_t and m_H of $s_*^2(0)$. This quantity is measureable from the ratio of cross sections for neutrino-electron and antineutrino-electron scattering. It also plays a role in the radiative corrections to deep-inelastic neutrino scattering, as I will discuss below.

The physical origin of this quadratic dependence *on* m_t is easily described. In the standard model, a heavy top quark cannot be weakly coupled. Since the mass of the top quark originates from the top quark coupling λ_t to the Higgs field, its coupling must grow with m_t according to

$$m_t = \frac{\lambda_t}{\sqrt{2}} v , \tag{5.42}$$

where v is the Higgs field vacuum expectation value. If the weak bosons were replaced by Higgs fields, the top quark vacuum polarization diagrams would be of

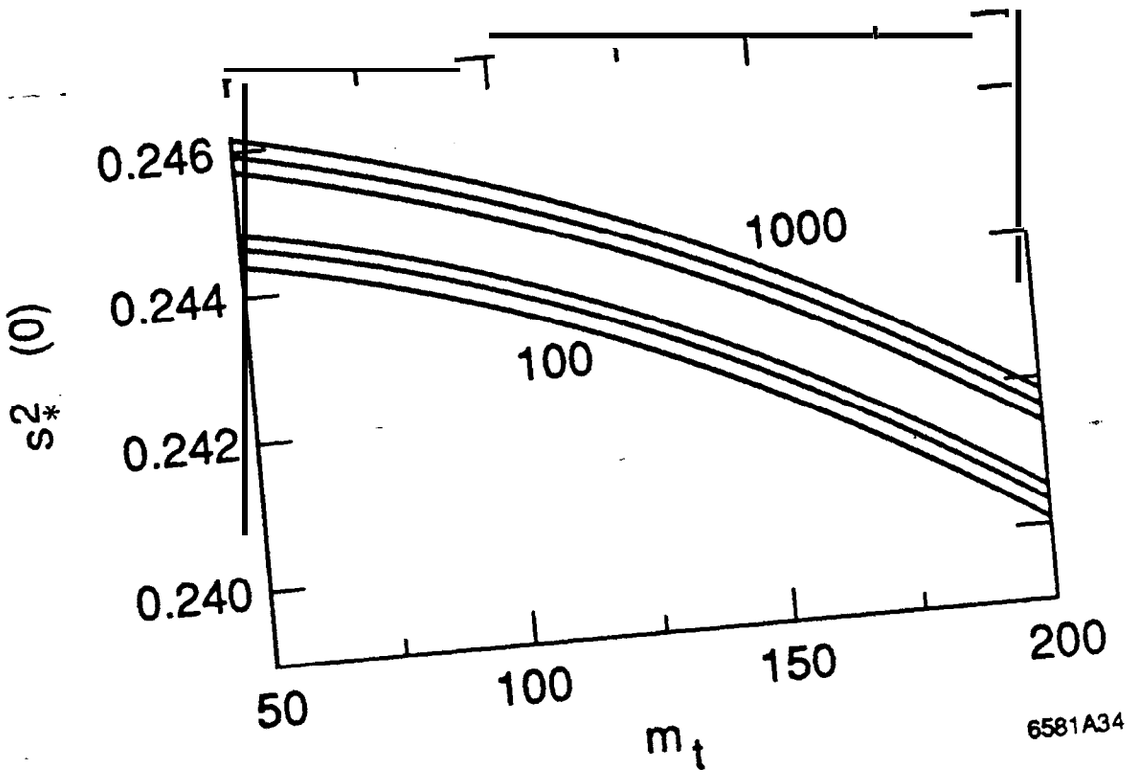

3-90

Figure 34. Dependence of $s^2_*(0)$ on m_t and m_H. The notation is as in Fig. 31.

order

$$\frac{\lambda_t^2}{4\pi} = \frac{2m_t^2}{4\pi v^2} = \frac{g^2}{8\pi}\frac{m_t^2}{m_W^2} . \qquad (5.43)$$

But, when the weak bosons receive mass through the Higgs mechanism, they do absorb components of the Higgs multiplet to form their longitudinal polarization states. Thus, (5.43) should also correctly estimate the contribution of a heavy top quark-to the vacuum polarization diagrams of weak gauge bosons. Indeed, (5.41) is precisely of this order.

From (5.40), one might conclude that the large radiative corrections due to m_t are a manifestation of weak isospin violation. However, (5.36) has the curious property that, even if the masses oft and *bare* set equal and then taken to infinity, the effect of this doublet of quarks does not vanish. Rather, it approaches the constant value

$$s_*(m_Z^2) = \sin^2\theta_w|_Z + \frac{3\alpha}{24\pi}\frac{1}{(c^2 - s^2)} . \qquad (5.44)$$

The asymptotic value is quite closely approximated already when $m_t = m_b = m_Z$. In principle, then, after the top quark mass is known so that this contribution may be computed and subtracted, the measurement of s_*^2 from A_{LR} will be sensitive to additional generations of quarks and leptons, all of whose members are very heavy. The error quoted in (5.22) is slightly less than the contribution of one new quark doublet.

It would be wonderful if (5.36) were also sensitive to the mass of the Higgs boson. Unfortunately, the antisymmetric factor (l-22) under the integral in (5.18) implies that the quadratic dependence on m_H cancels out. Indeed, Veltman [3] has demonstrated a screening *rule* which states that no l-loop corrections to processes involving light fermions depend more strongly than logarithmically on m_H.

5.6. RENORMALIZATION OF THE W BOSON MASS

Using the method of the previous section, we can assemble the effect of the top quark loop diagrams-or any other oblique correction-on the W boson mass. The direct renormalization of m_W is

$$m_W = \frac{g^2 v^2}{4} + \frac{e^2}{s^2}\Pi_{11}(m_W^2) \ . \tag{5.45}$$

However, to make a physical prediction, we must compare m_W to another physically observable quantity. To do this, we may make use of the simple lowest-order relation (2.4) between m_W, m_Z, and $\cos^2\theta_w$. Taking the shift of m_Z from (5.32) and the shift of $\cos^2\theta_w|_Z$ from (5.35), we may compute

$$\begin{aligned} m_W^2 = {} & m_Z^2 \cos^2\theta_w|_Z \\ & - \frac{e^2 c^2}{s^2(c^2-s^2)}\left[\Pi_{33}(m_Z^2) - 2s^2\Pi_{3Q}(m_Z^2) - \frac{s^2}{c^2}\Pi_{11}(0) - \frac{c^2-s^2}{c^2}\Pi_{11}(m_W^2)\right] \\ & - \frac{e^2 s^2 m_W^2}{c^2-s^2}\left[\Pi'_{QQ}(m_Z^2) - \Pi'_{QQ}(0)\right] . \end{aligned} \tag{5.46}$$

By using (5.37) and (5.38), you may easily show that this expression is free of ultraviolet divergences, just as we found for (5.36).

The dependence of m_W on m_t and m_H is plotted in Fig. 35. Once we have computed m_W from m_Z, we can construct $\sin^2\theta_w|_S$, the value of $\sin^2\theta_w$ as defined from the ratio of weak boson masses. The dependence of this quantity of the top quark and Higgs boson masses at fixed m_Z is shown in Fig. 36. The dependence on m_t is much more pronounced than that of s_*^2. By applying (5.40), it is easy to see that the quadratic dependence on m_t is

$$m_W^2 - m_Z^2\cos^2\theta_w|_Z \cong \frac{3\alpha}{16\pi}\frac{c^2}{s^2(c^2-s^2)}m_t^2 . \tag{5.47}$$

The formula (5.46) may be viewed as a formula for the difference $(\sin^2\theta_w|_S - \sin^2\theta_w|_Z)$ as a function of m_t, m_Z, and other parameters. Using this formula, it is

easy to convert the relation (5.36), which governs the radiative corrections to weak asymmetries, to a formula based on $\sin^2\theta_w|_S$. I will quote only the asymptotic dependence of this relation for large m_t:

$$s^2_*(q^2) - \sin^2\theta_w|_S \cong +\frac{3\alpha}{16\pi}\frac{1}{s^2}\frac{m_t^2}{m_W^2} \ . \qquad \textit{(5.48)}$$

-'-Another measure of the ratio of the W and Z^0 masses is the relative strength -of the charged and neutral weak currents near $q^2 = 0$. If we include the l-loop oblique corrections to the lowest-order formula (2.8), this equation is modified to the form

$$\mathcal{L}_{eff} = \frac{4G_F}{\sqrt{2}}\left[J_\mu^{+L}J_\mu^{-L} + \rho_*(0)\left(J_\mu^{3L} - J_\mu^Q s^2_*(0)\right)^2\right]. \qquad (5.49) \ .$$

The overall coefficient is, by definition, G_F. The factor $\rho_*(0)$ arises from the difference between vacuum polarization corrections to the W and Z propagators. Since $\Pi_{3Q}(0) = \Pi_{QQ}(0) = 0$, this difference reduces to

$$\rho_*(0) = 1 - \frac{e^2}{s^2c^2m_Z^2}(\Pi_{33}(0) - \Pi_{11}(0)) \ . \qquad \textit{(5.50)}$$

This quantity is quite sensitive to large m_t, behaving as

$$\rho_*(0) \cong 1 + \frac{3\alpha}{16\pi}\frac{1}{s^2c^2}\frac{m_t^2}{m_Z^2} \ . \qquad (5.51)$$

I hesitated to use the symbol ρ in the previous paragraph. Veltman [4] originally defined the 'p-parameter'

$$\rho = \frac{m_W^2}{m_Z^2\cos^2\theta_w} \qquad \textit{(5.52)}$$

to call attention to the zeroth-order relation $\rho = 1$ in the standard model (eq. (2.4)), and to compute the corrections to this relation, using yet another definition of $\sin^2\theta_w$. Since that time, the literature on weak interaction radiative corrections

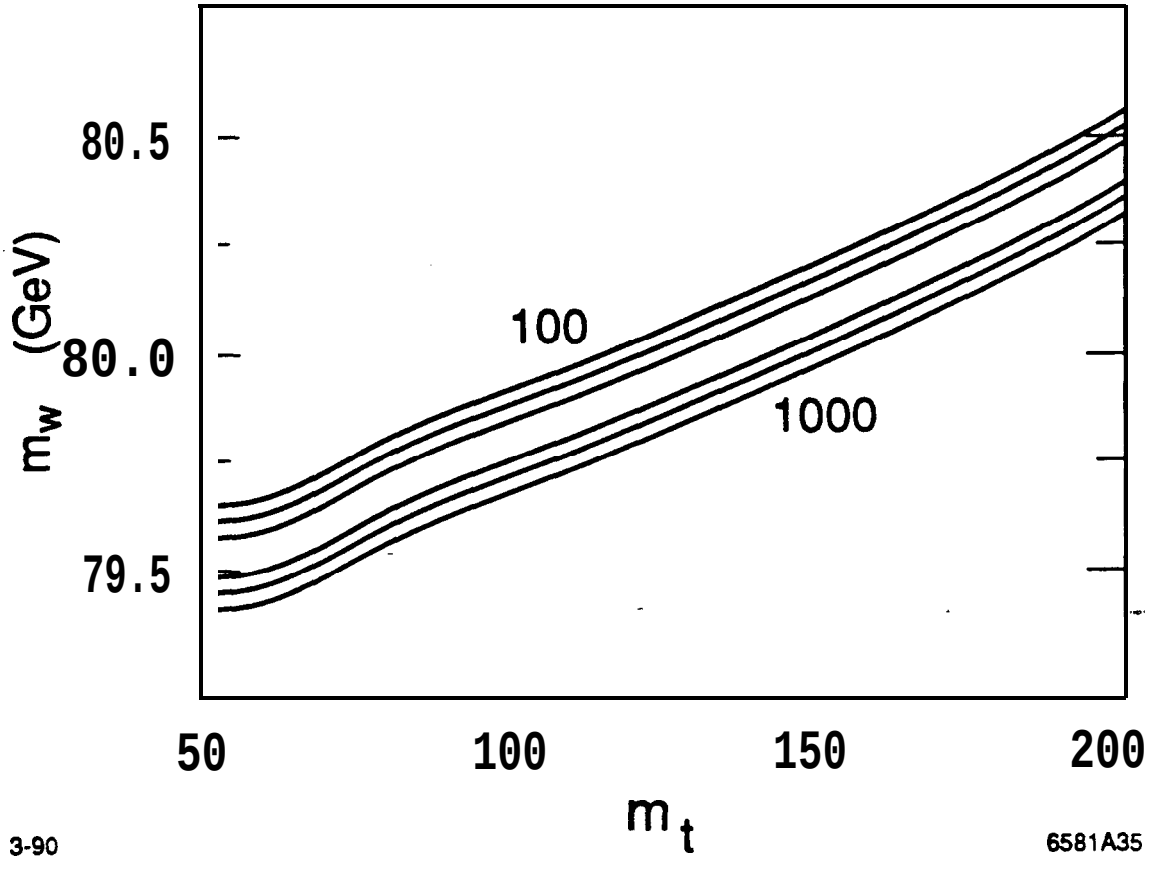

Figure 35. Dependence of m_W *on* m_t and m_H, for m_Z fixed at its measured value. The notation is as in Fig. 31.

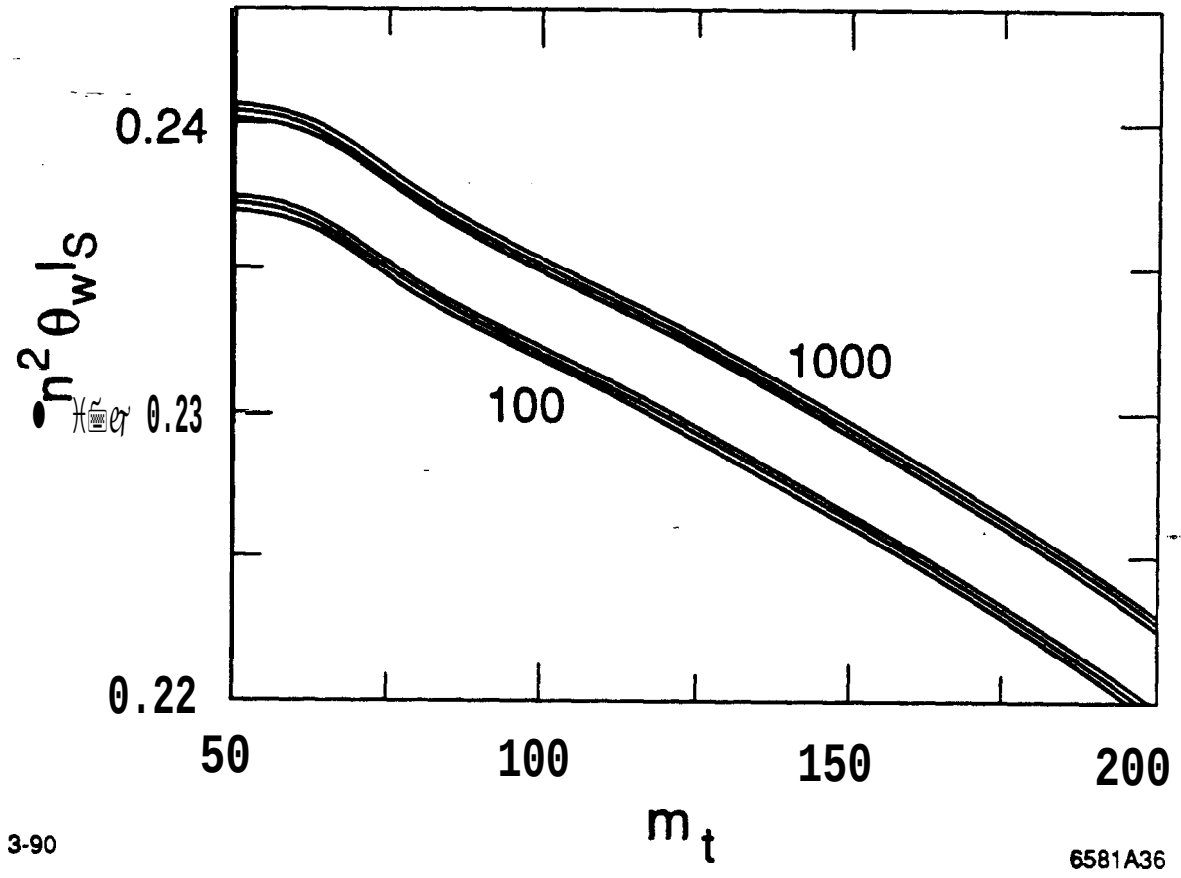

Figure 36. Dependence of $\sin^2\theta_w|_S$ on m_t and m_H, for m_Z fixed at its measured value. The notation is as in Fig. 31.

has been filled with a bewildering variety of definitions of ρ as ratios of the W and Z^0 propagators at many different kinematic points. By this time, it is probably most sensible to drop the use of ρ altogether, except (as in the usage of Amaldi, et al., Ref. 9) to parametrize models in which the relation (2.4) is violated at zeroth order. I ask your indulgence, though, for my use of $\rho_*(0)$ to represent a particular, precisely defined, amplitude which is measureable in the ratio of neutral to charged current neutrino scattering. The notation meshes with a general analysis of the weak neutral current which I will present in the next section.

5.7. Renormalization of Neutral Current Amplitudes

As we analyze the observables of the weak interactions one by one, it is natural. to raise the question of whether different observables measure essentially the same weak interaction **renormalizations**, or, conversely, which observables we must measure to cover the complete set of possible renormalization effects. This question is most easily addressed by turning to a somewhat more abstract framework.'- Kennedy and Lynn[44] have shown how to construct a general formalism for treating the renormalization of any process which involves photon or weak boson exchange between light fermions by writing an effective interaction which generalizes the zeroth order formula (3.1). In the notation of Kennedy and Lynn, we would write the effective neutral current amplitude in the form

$$\mathcal{M}_{\text{eff}}^{NC} = e_*^2 Q \frac{1}{q^2} Q' + \frac{e_*^2}{c_*^2 s_*^2} (I_3 - s_*^2 Q) \frac{Z_*}{q^2 - M_*^2} (I^{3\prime} - s_*^2 Q') \tag{5.53}$$

where $(I^3$, Q) and $(I^{3\prime}$, Q') are the quantum numbers of the external fermions and all starred quantities are functions of q^2.

It is straightforward to verify that (5.53) takes account of all l-loop oblique corrections to the scattering of two light fermions by the photon and the Z^0. The diagrams we must consider are shown in Fig, 37. To lowest order, the parameters

e_*^2, s_*^2, M_*^2, Z_* in (5.53) may be taken to equal $4\pi\alpha$, $\sin^2\theta_w|_Z$, m_Z^2, and 1, respectively; we define $c_*^2 = 1 - s_*^2$ to all orders. If we expand the starred functions to first order in their deviations from these values, add in the l-loop diagrams which shift $\sin^2\theta_w|_Z$ according to (5.35), and compare the resulting expression to the l-loop corrections, shown in Fig. 37, we find a general expression for the four starred functions in terms of vacuum polarization amplitudes. For $e_*^2(q^2)$ and $s_*^2(q^2)$, we find exactly the relations (5.5) and (5.36). The remaining functions $M_*^2(q^2)$ and $Z_*(q^2)$ may be readily worked out. If we introduce

$$\Pi_{ZZ} = \frac{e^2}{s^2c^2}(\Pi_{33} - 2s^2\Pi_{3Q} + s^4\Pi_{QQ}) , \tag{5.54}$$

these functions may be expressed as

$$\begin{aligned} q^2 - M_*^2(q^2) &= (q^2 - m_Z^2)\left(1 + \frac{d}{dq^2}\Pi_{ZZ}\Big|_{q^2=m_Z^2}\right) - \left(\Pi_{ZZ}(q^2) - \Pi_{ZZ}(m_Z^2)\right) \\ Z_*(q^2) &= 1 + \frac{e^2}{s^2c^2}\frac{d}{dq^2}(\Pi_{33} - 2s^2\Pi_{3Q} + s^4\Pi_{QQ})\Big|_{q^2=m_Z^2} \\ &\quad - e^2\Pi'_{QQ}(0) - \frac{e^2(c^2 - s^2)}{s^2c^2}(\Pi'_{3Q}(q^2) - s^2\Pi'_{QQ}(q^2)) . \end{aligned} \tag{5.55}$$

The function $M_*^2(q^2)$ has been arranged to satisfy

$$M_*^2(m_Z^2) = m_Z^2 \quad ; \qquad \frac{d}{dq^2}M_*^2\Big|_{q^2=m_Z^2} = 0 . \tag{5.56}$$

These two functions provide two new and independent finite combinations of vacuum polarization amplitudes.

In writing these formulae-and the formulae for s_*^2 above, I have assumed that the various vacuum polarization integrals are real. If this is not true (that is, if some intermediate state can be produced at the Z^0, we should take the real part of each vacuum polarization integral II except for the term $\Pi_{ZZ}(q^2)$ in the first line

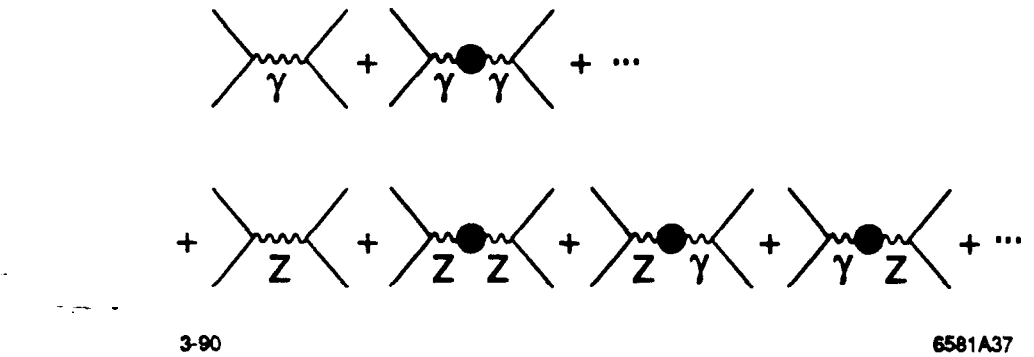

Figure 37. Feynman diagrams contributing l-loop oblique corrections to the scattering of light fermions by the photon and the Z^0.

of (5.55). The imaginary part of this correction will then generate the Z^0 width, which would then appear in (5.53)as

$$M_*(m_Z^2) = m_Z^2 + im_Z\Gamma_Z \ . \tag{5.57}$$

Kennedy and Lynn have shown that, even though the standard model weak radiative corrections involve vertex and box diagrams as well as vacuum polarization graphs, the most important of these corrections can also be written in the form (5.53). Terms which cannot be shoehorned into this form (for example, nontrivial form factors of box diagrams) are small-a several tenths percent corrections-at the Z^0 and below. (The one important counterexample to this general statement will be discussed in Section 5.8.) Thus, the effective neutral current amplitude (5.53) is a very useful way to summarize the effect of radiative corrections both from within the standard model and from new physical processes.

The Kennedy-Lynn effective amplitude is sometimes described as merely a 'scheme', that is, yet another definition of $\sin^2\theta_w$. I hope this discussion, and the analysis to follow, clarifies that it is actually a general phenomenology of weak interaction renormalizations, and a very useful one. The starred parameters can be predicted in any scheme by trading $\sin^2\theta_w|_Z$ in the formulae above for any other definition of $\sin^2$ 8,.

The effective amplitude (5.53) clarifies which aspects of the neutral current coupling can be measured with precision at the Z^0. In essence, experiments at the Z^0 measure values of the starred parameters at $q^2 = m_Z^2$, and, of these, the only nontrivial ones are $s_*^2(m_Z^2)$ and $Z_*(m_Z^2)$. We have already seen that $s_*^2(m_Z^2)$ governs the weak interaction asymmetries at the Z^0. The factor $Z_*(m_Z^2)$ renormalizes the Z^0 propagator; it also multiplies the Z^0 width. In fact, the effective amplitude justifies the expressions (3.1) and (3.8) for the total cross section and the partial widths at the Z^0, with the parameters of this formula evaluated as

$$\alpha \to \alpha_*(m_Z^2)\,; \quad \sin^2\theta_w \to s_*^2(m_Z^2)\,; \quad \overline{Z} \to Z_*(m_Z^2)\,. \tag{5.58}$$

The values quoted in Section 3.1 correspond to $m_t = m_H = 100$ GeV.

It is unfortunately difficult to extract the value of Z_* from experiment. It is much easier to obtain an accurate value of the peak cross section of the Z^0 resonance than to obtain an accurate value of the width. (It is the measurement of the peak cross section, for example, which gives the strong constraint on the number of neutrino generations.) But the factor $Z_*(m_Z^2)$ cancels out of the peak cross section, because it appears in the numerator of the second term of (5.53), as well as in the factor Γ_Z in the denominator.

The dependence of the Z^0 width on m_t and m_H is shown in Figs. 38 and 39. In Fig. 38, 1 have blown up the standard model prediction from Fig. 23, showing the theoretical uncertainty due to the QCD corrections to the effective number of colors N_f and the variation as m_t is raised from 50 to 200 GeV. In Fig. 39, I have plotted directly the variation of Γ_Z with the top quark and Higgs boson masses.

The rather narrow focus of Z^0 resonance experiments, in terms of their sensitivity to the parameters of the weak effective amplitude, highlights the importance of obtaining orthogonal measures of weak interaction radiative corrections from other sources, by precision measurements of m_W and of the low-energy parameters $s_*^2(0)$ and p,(O). However, even though the Z^0 experiments must concentrate on the extraction of the single parameter $s_*^2(m_Z^2)$, it is likely that this measurement will

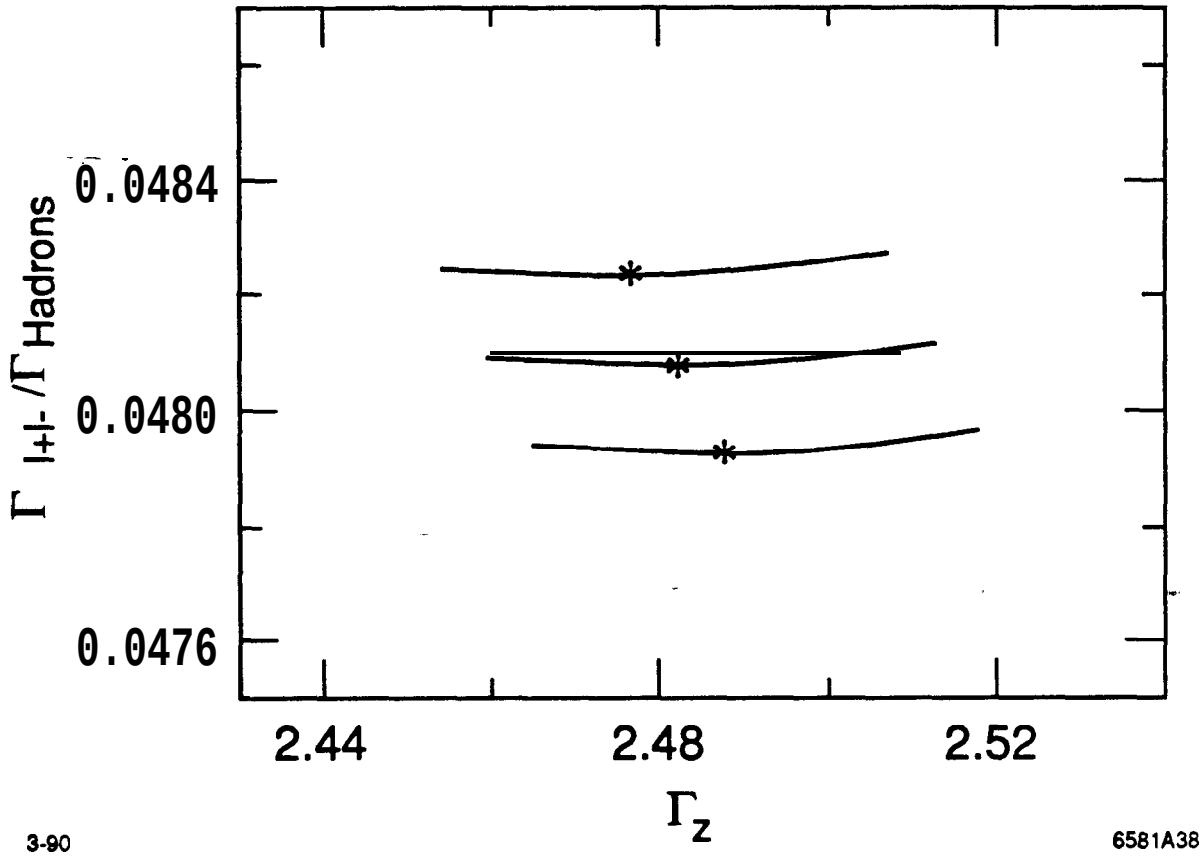

Figure 38. Enlargement of the standard model prediction from Fig. 23, showing the dependence on m_t, varied from 50 to 200 GeV, and on the QCD correction to the hadronic widths, which is varied over the 1 σ error in (3.3).

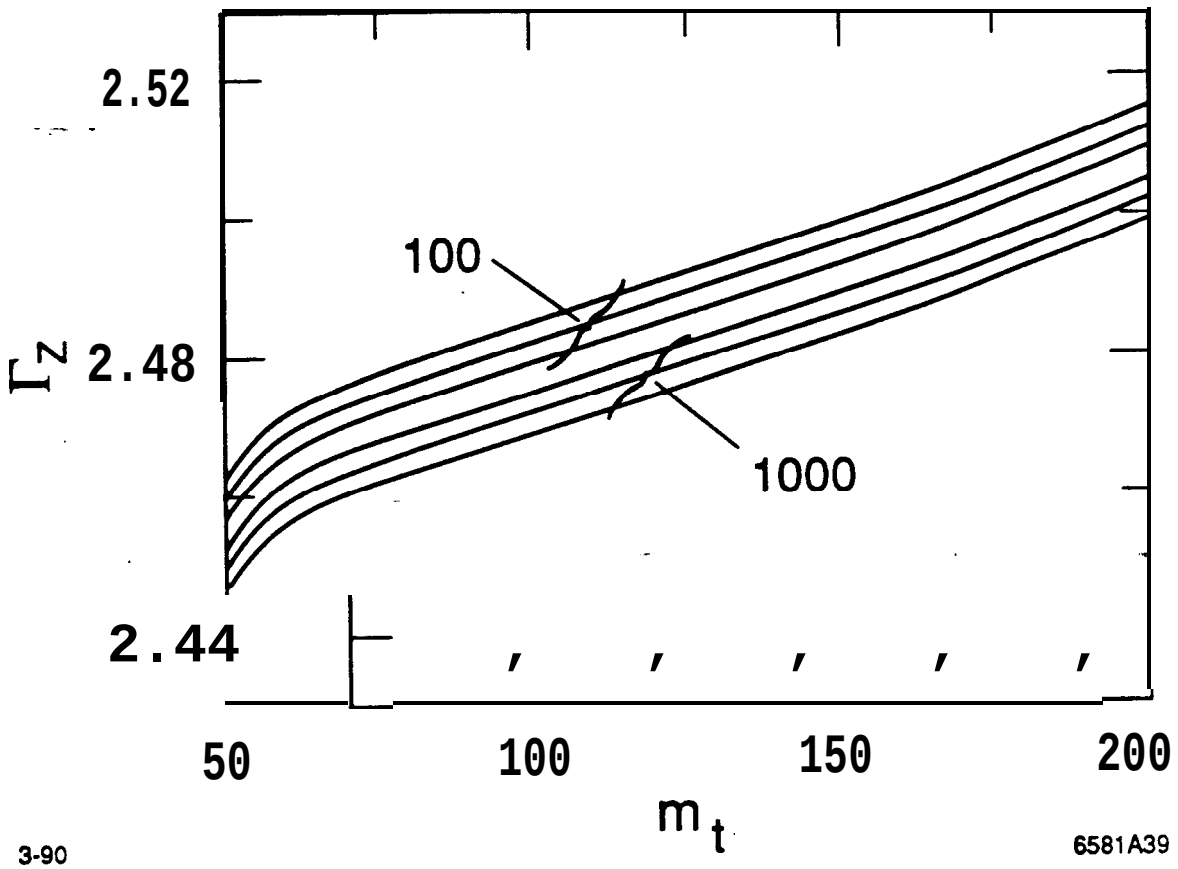

Figure 39. Dependence of the Z^0 total width on m_t and mg. The notation is as in Fig. 31.

give the single most incisive test of the radiative corrections to the standard model. Perhaps it is fortunate that this parameter can be measured in many different and complementary ways.

5.8. A RENORMALIZATION UNIQUE TO THE t QUARK

There is one interesting example of a weak interaction renormalization which falls outside the scope of the effective amplitude (5.53), specifically because it involves the top quark and can be enhanced by a power of (m_t^2/m_W^2) when m_t is large. This is the one direct correction which involves the top quark: the renormalization due to t of the vertex for $Z^0 \to b\bar{b}$. The correction arises from the diagrams shown in Fig. 40, plus the additional diagrams required to make a gauge-invariant set., This correction is particularly interesting because it has the t quark as its specific origin. Up to this point, all of the renormalizations we have studied receive contributions from general vacuum polarization diagrams; in some sense, they are integrals over all types of new physics. We have concentrated on the contributions of the top quark and the Higgs boson, but this has been mainly for pedagogical reasons; it is not unlikely that s_*^2 and other weak parameters also receive contributions from other types of new physics. In an unlucky situation, these contributions might even be of the opposite sign. It is fortunate, then, that there is one correction which can arise only from the top quark and allows an unambiguous test of the rapport between the value of the top quark mass (when it is eventually measured) and a weak interaction l-loop correction.

The diagrams of Fig. 40 and their partners have been evaluated by Akhundov, Bardin, and Riemann,[45] Bernabéu, Pich, and Santamaría,[46] and Beenakker and Hollik.[47] I will quote only the asymptotic formulae here and refer you to these papers for more exact results. Their effect is simply described by noting that these diagrams involve W exchange and so, if we ignore the mass of the b, they couple only to the left-handed components of the b quark. Thus, the effect of these

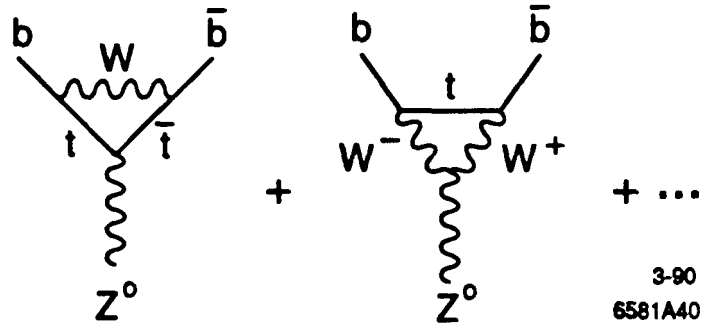

Figure 40. Renormalization of the vertex for $Z^0 \to b\bar{b}$, due to l-loop diagrams involving the top quark.

diagrams is a multiplicative renormalization of the vertex for $Z^0 \to b_L \bar{b}_R$:

$$\mathcal{M} = \frac{-ie_*^2}{c_* s_*} Z_\mu \bar{b} \gamma^\mu b_L \cdot \left[\left(\frac{1}{2} - \frac{1}{3} s_*^2 \right) - F \right] , \tag{5.59}$$

where, in the limit of large m_t,

$$F \cong \frac{\alpha}{16\pi} \frac{1}{s^2} \frac{m_t^2}{m_W^2} \tag{5.60}$$

In principle, this correction alters the relation between $s_*^2(m_Z^2)$ and the forward-backward asymmetry at the Z^0 for $e^+e^- \to b\bar{b}$. However, since the Z^0 couples much more strongly to b_L than b_R, a small change in the larger coupling has an insignificant effect on the polarization asymmetry A_{LR}^b and, through this, on A_{FB}^b. The size of the effect is indeed of order 10^{-4} in A_{FB}^b. However, the correction does noticeably affect the Z^0 branching fraction to $b\bar{b}$ if the top quark mass is large. In Fig. 41, I have plotted the variation of the ratio $\Gamma(Z^0 \to b\bar{b})/\Gamma(Z^0 \to \text{hadrons})$ with m_t. The individual partial widths are affected by the dependence of Z_* and s_*^2 on m_t, as was illustrated for the total width in Fig. 39. However, Z_* cancels in this ratio, and most of the dependence on s_*^2 cancels as well. I have illustrated this in Fig. 41 by comparing the m_t dependence of the Z^0 branching fractions to

$b\bar{b}$ and $d\bar{d}$. The latter is essentially flat as a function of m_t. Thus, a measurement of the Z^0 branching fraction to $b\bar{b}$ is almost entirely a measure of the top quark vertex correction.

Unfortunately, this is a tough experiment. The magnitude of the effect is a 4% decrease in the $b\bar{b}$ fraction for a t quark mass of 200 GeV. If the measurement is done by tagging b quarks with leptons, the leptonic branching ratio must be known to 1%. If the b quarks are identified by their vertices, the lifetime must be known to a few percent. This measurement thus challenges both the large data sets that will be available at LEP and the precision vertex information that will be provided by the SLC. I hope that careful experimenters will take up this challenge and isolate this curious but interesting effect.

5.9. Determination of $\sin^2\theta_w$ from Neutrino Scattering

No review of precision measurements in weak interactions would be complete.,. without some discussion of the constraints imposed by experiments on neutrino-nucleon deep-inelastic scattering. It is fair to say that the precision study of the weak neutral current really began with the precision measurement of the ratio of neutral to charged current neutrino cross sections by the CDHS[48] and CHARM[49] experiments. Deep inelastic scattering has new difficulties which are not shared by experiments on the weak gauge bosons. These all stem from the fact that the target is a nucleon, and so the analysis of the scattering process eventually falters on our uncertain quantitative understanding of QCD. However, it is amazing to me what accuracy can actually be achieved by a combination of clever insights and careful analysis. Since the analysis of these deep inelastic scattering experiments is rather subtle, I have no room for a complete discussion here. For those who wish further information, I recommend the most recent paper of the CDHS collaboration,[50] which also gives references to the earlier literature.

The deep inelastic scattering experiments have concentrated on measuring the

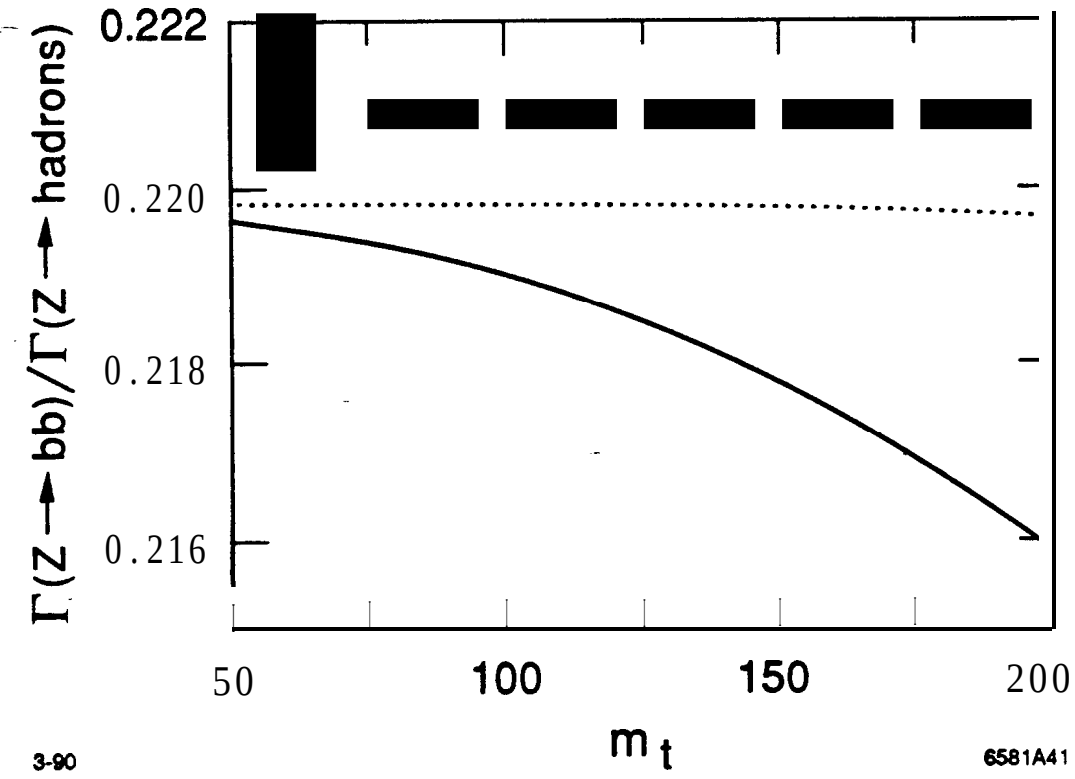

Figure 41. Dependence of the Z^0 width to $b\bar{b}$, as a fraction of the total Z^0 width to hadrons, as a function of m_t. The solid line includes the $b\bar{b}Z$ vertex corrections; the dashed line shows the result of omitting this effect, while retaining the top quark renormalization of $s^2_*(m^2_Z)$.

ratio of neutral to charged current cross sections

$$R^{\nu} = \int dxdy \frac{d\sigma(\nu, NC)}{dxdy} \Big/ \int dxdy \frac{d\sigma(\nu, CC)}{dxdy} , \tag{5.61}$$

where x and y are the standard dimensionless kinematic variables and the integral is taken over the experimental acceptance. These cross sections are readily estimated in the naive parton model: If $f_q(x)$ is the parton distribution of the species q in the proton, the cross sections, for neutrino-proton scattering, at lowest order in weak interactions, are proportional to

$$\begin{aligned}
\frac{d\sigma(\nu, CC)}{dxdy} &= \frac{G_F^2 sx}{\pi}\Big(f_d(x) + (1-y)^2 f_{\bar{u}}(x)\Big) \\
\frac{d\sigma(\nu, NC)}{dxdy} &= \frac{G_F^2 sx}{\pi}\Big([(\tfrac{1}{2} - \tfrac{2}{3}\sin^2\theta_w)^2 f_u(x) + (\tfrac{1}{2} - \tfrac{1}{3}\sin^2\theta_w)^2 f_d(x)] \\
&\quad + (1-y)^2 [(\frac{2}{3}\sin^2\theta_w)^2 f_u(x) + (\frac{1}{3}\sin^2\theta_w)^2 f_d(x)] \\
&\quad + (1-y)^2 [(\frac{1}{2} - \frac{2}{3}\sin^2\theta_w)^2 f_{\bar{u}}(x) + (\frac{1}{2} - \frac{1}{3}\sin^2\theta_w)^2 f_{\bar{d}}(x)] \\
&\quad + [(\frac{2}{3}\sin^2\theta_w)^2 f_{\bar{u}}(x) + (\frac{1}{3}\sin^2\theta_w)^2 f_{\bar{d}}(x)]\Big) ,
\end{aligned} \tag{5.62}$$

plus contributions from heavier quark species. In the neutral current cross section, the two sets of terms for each quark refer to left- and right-handed species, respectively. The two prefactors are identical by virtue of (2.9). However, this is the only simplification available, and otherwise the integrands of (5.61) are complicated functions of x and y. When we include the QCD corrections to (5.62), these integrands will also depend on Q^2. How, then, can we extract any information to 1% accuracy?

The required strategy was set out in a beautiful paper by Llewellyn Smith.[51] In this paper, Llewellyn Smith encourages us to think about a world containing only u and d quarks. This allows three important simplifications in the computation

of R". First, if we consider, instead of the proton, an isoscalar target, $f_u = f_d$, $f_{\bar{u}} = f_{\bar{d}}$, and the only x-dependence in the ratio of the two parton model cross sections above occurs through the function $f_q(x)/f_{\bar{q}}(x)$. In fact, the only x- and y-dependence appears in the particular combination

$$\frac{(1-y)^2 + f_q/f_{\bar{q}}}{1 + (1-y)^2 f_q/f_{\bar{q}}} . \qquad (5.63)$$

The second simplification occurs if we recognize that (5.63) is precisely the parton model expression for the ratio of antineutrino versus neutrino charged current cross sections. Thus, if we define

$$r = \frac{\sigma(\bar{\nu}, \mathrm{CC})}{\sigma(\nu, CC)} , \qquad (5.64)$$

R^ν can be expressed, within the parton model, as $R'' = R^\nu_{\mathrm{LS}}(\sin^2\theta_w)$, where $R^\nu_{\mathrm{LS}}(\sin^2\theta_w)$ is the simple function

$$R^\nu_{\mathrm{LS}}(\sin^2\theta_w) = \frac{1}{2} - \sin^2\theta_w + \frac{5}{9}\sin^4\theta_w(1+r) . \qquad (5.65)$$

Similarly, the ratio of neutral to charged current antineutrino cross sections is equal to

$$R^{\bar{\nu}}_{\mathrm{LS}}(\sin^2\theta_w) = (\frac{1}{2} - \sin^2\theta_w)r + \frac{5}{9}\sin^4\theta_w(1+r) . \qquad (5.66)$$

I have quoted these results as applying to the theoretical total cross sections; however, they apply equally well if the differential cross sections in the numerator and denominator are integrated over the same experimental acceptance. Thus, the dependence of R^ν on acceptance is completely summarized in the parameter r, which can be directly measured. It is noteworthy that r is rather different for the two CERN neutrino experiments:

$$r = \begin{cases} 0.393 \pm 0.014 \ \mathrm{CDHS} \\ 0.456 \pm 0.011 \ \mathrm{CHARM} \end{cases} , \qquad (5.67)$$

reflecting the lower energy threshold of the CHARM detector.

These two insights produce a remarkable simplification, but they have been derived within the naive parton model, and so they would not be of much use without the crucial third step: In a world with only u and d quarks, the above expression for R^{ν} can be derived *using isospin arguments only* by directly comparing strong interaction matrix elements. Thus, this expression is insensitive to QCD corrections.

In a realistic setting, one must of course correct the Llewellyn Smith expression for R^{ν} to take account of the non-isoscalar components of the target, the presence of strange quarks in the proton, and the soft radiative corrections. However, all of these are small corrections to a well-understood basic formula. The most troublesome correction is that due to charm production. Since the energy region of the CERN experiments overlaps the charm threshold, charm is produced at relatively low energy and so the production must be described phenomenologically, with parameters fit to the experimental data. This produces a sizeable systematic error, of order ± 0.003, in the final determination of $\sin^2 \theta_w$.

Once these corrections have been made, the value of R^{ν} may be compared to the theoretical prediction, modified by the inclusion of hard radiative corrections. Using (5.49) (and making the oversimplification that $Q^2 << m_W^2$), these give

$$R^{\nu} = \rho_*(0)^2 R^{\nu}_{\mathrm{LS}}(s^2_*(0)), \qquad (5.68)$$

where R^{ν}_{LS} is the function given in (5.65) and ρ_*, s^2_* are the effective amplitudes defined in the previous sections. The dependence of (5.68) on m_t and m_H, for the CDHS value of r, is shown in Fig. 42.

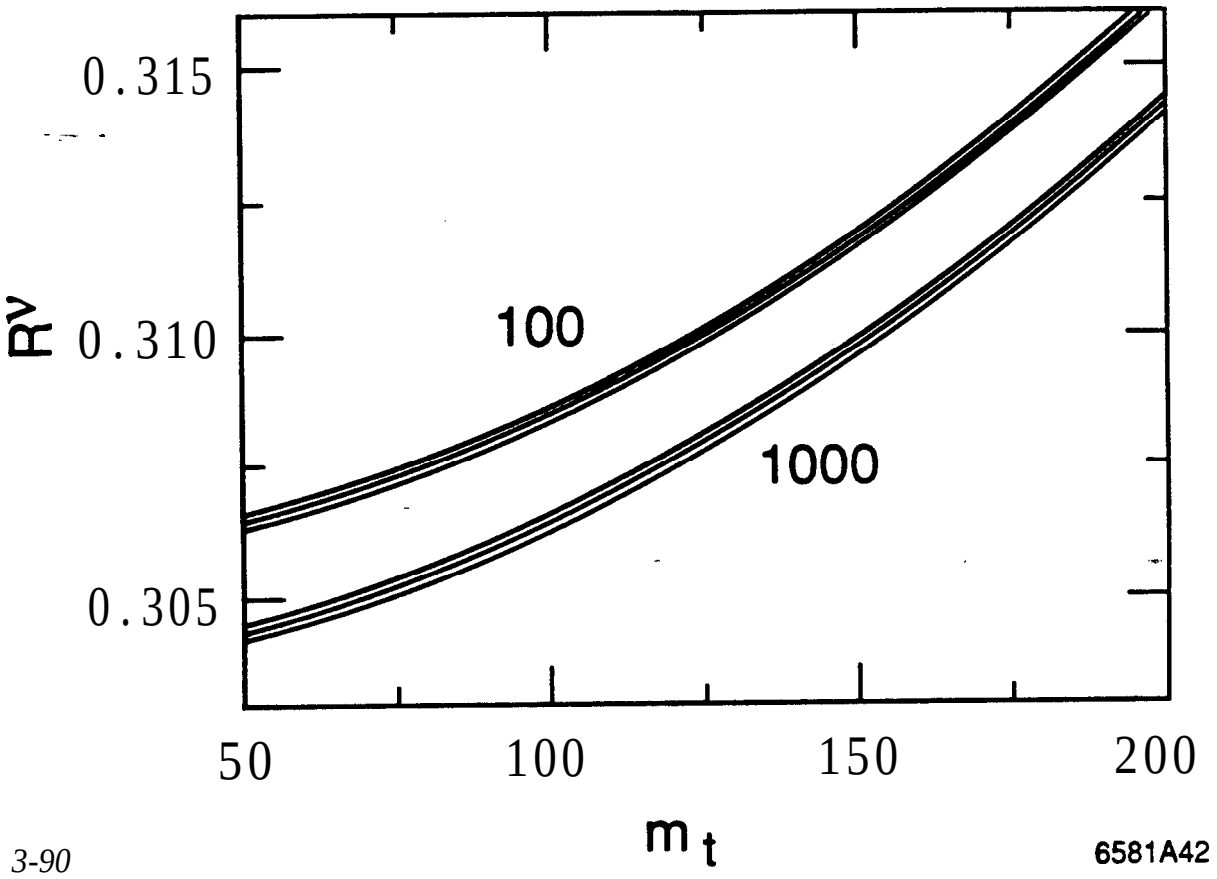

Figure 42. Dependence of R^ν on m_t and m_H, using the CDHS value of the parameter r. The notation is as in Fig. 31.

5.10. Reconciliation of Weak Interaction Measurements

In the previous few sections, we have seen how to compute the weak interaction radiative corrections to a variety of observable quantities. Many of these predictions depended rather strongly on the mass of top quark. It is thus important to ask two questions: First, are the observed values of these quantities simultaneously consistent with a single value of $\sin^2\theta_w$? Second, is this consistency contingent on some limits on the top quark mass, so that it actually constrains the possible range of values for m_t?

To address this question, we first need to know the value of the standard model radiative corrections due to conventional species-light quarks and leptons and weak gauge bosons. It is impossible to give a complete computation of these effects--or even to summarize the result-compactly. (For a rather complete discussion, see ref. 6.) However, because these effects are relatively small compared to the sensitivity of current experiments, one may account them roughly by quoting the relation of the parameters of the effective amplitude to $\sin^2\theta_w|_Z$ for particular.-, values of m_t and m_H. For $m_t = 40$ GeV, $m_H = 100$ GeV:

$$\begin{aligned} \sin^2\theta_w|_S &= \sin^2\theta_w|_Z + 0.0050 \\ s_*^2(0) &= \sin^2\theta_w|_Z + 0.013 \\ s_*^2(m_Z^2) &= \sin^2\theta_w|_Z + 0.0036 \\ Z_* &= 1.009 \\ \mathrm{p,(O)} &= 1.000 \ . \end{aligned} \tag{5.69}$$

Given these offsets, one can then compute the dependence of observables on m_t, m_H, and other corrections using the formulae I have presented in previous sections. I have cribbed these offsets from the current version of the program EXPOSTAR, described in Ref. 52. Because the effective amplitude does not include non-oblique corrections in an exact way, the actual values required for these offsets may vary by about 10% depending on the particular process considered; in addition, the corrections actually depend on. $\sin^2\theta_w$ and in (5.69) are simply evaluted near the

physical value. This method is too crude to use in analyzing a particular precision experiment, but it is useful to give a quantitative feeling for the sensitivity of each experiment to standard and nonstandard radiative corrections.

To assess the consistency of our present weak interaction measurements, Ellis and Fogli [53] have suggested making the following plot: Given the highly accurate values of α and G_F, plus one additional measurement, one can compute the value of $\sin^2 \theta_w|_S$. This computation of course depends on m_t, m_H—and on the assumption that there are no other large corrections from beyond the standard model. Assuming the standard model and fixing m_H, one may then plot the extracted value of $\sin^2 \theta_w|_S$ as a function of m_t. In Fig. 43, I have constructed this plot by taking each of the three best-measured weak boson parameters-mg, the ratio m_W/m_Z, and R^ν—as third input. The bands correspond to 1 σ measurement errors, and I have assumed m_H = 100 GeV. For m_Z and m_W, I have used the values (2.10) and *(4.4).* (Note that m_W/m_Z determines $\sin^2 \theta_w|_S$ directly.) For R", I have used the value

$$R^\nu = 0.3081 \pm 0.004 , \qquad (5.70)$$

which I obtained by converting the CHARM measurement of *R"* to the value appropriate for the CDHS value of r. The calculation is simple, but instructive for anyone who wishes to understand this subject in detail, and I hope I have provided enough information here that you can reproduce it straightforwardly. For comparison, I have reprinted in Fig. 44 a 'professional' version of this analysis done by Paul Langacker.[54] The main difference between the two figures comes in the band from neutrino scattering, where Langacker has included the world sample of neutrino and antineutrino experiments, taken proper account of the Q^2-dependence of the radiative correction, and refitted the charmed quark mass as $\sin^2 \theta_w$ varies. It is also instructive to replot this analysis against the variable $\sin^2 \theta_w|_Z$, and this is done in Fig. *45.*

The results of this analysis are striking. The ratio m_W/m_Z gives a horizontal band in the Ellis-Fogli plot. The band due to R^ν is also almost horizontal, by virtue

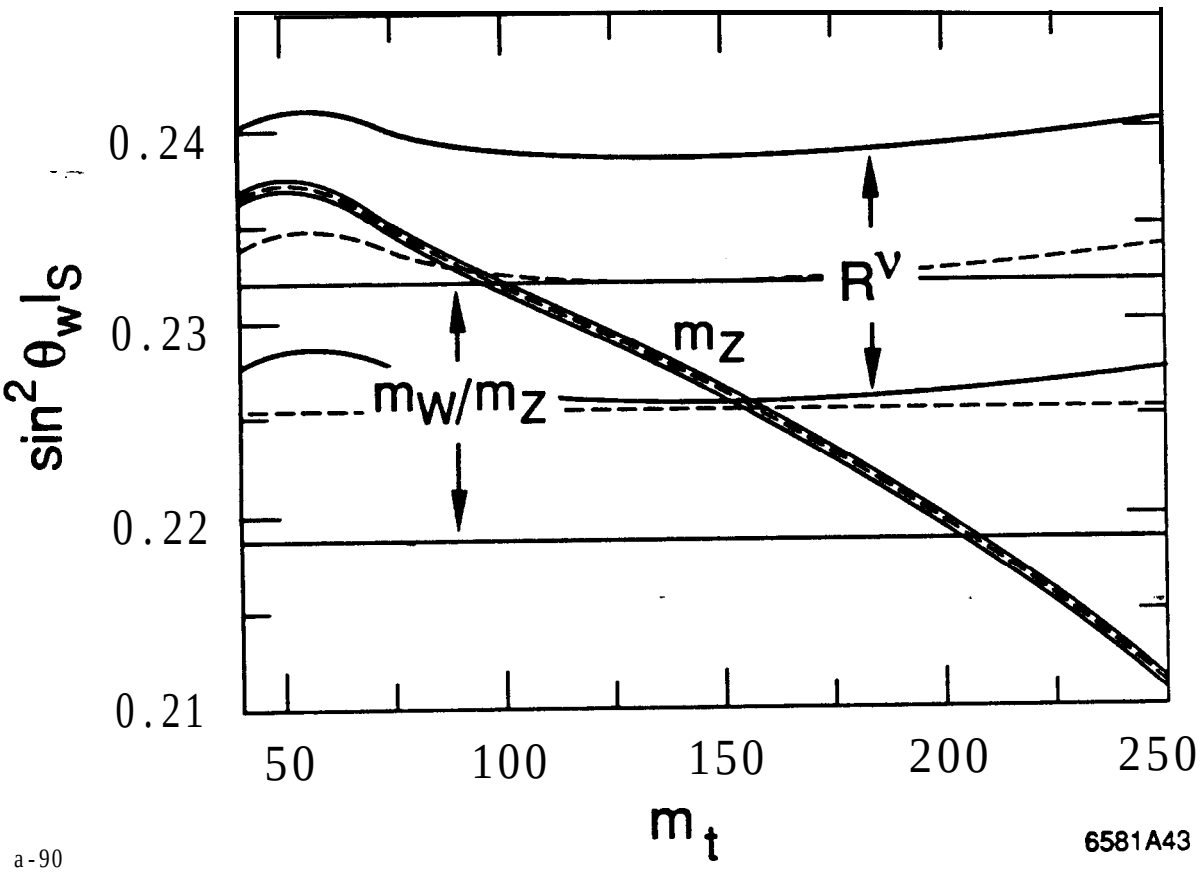

a-90

Figure 43. Interval in $\sin^2\theta_w|_S$ allowed at 1 σ confidence based on the measured values of m_Z, m_W/m_Z, and R^ν. The intervals are plotted as a function of m_t, assuming m_H = 100 GeV.

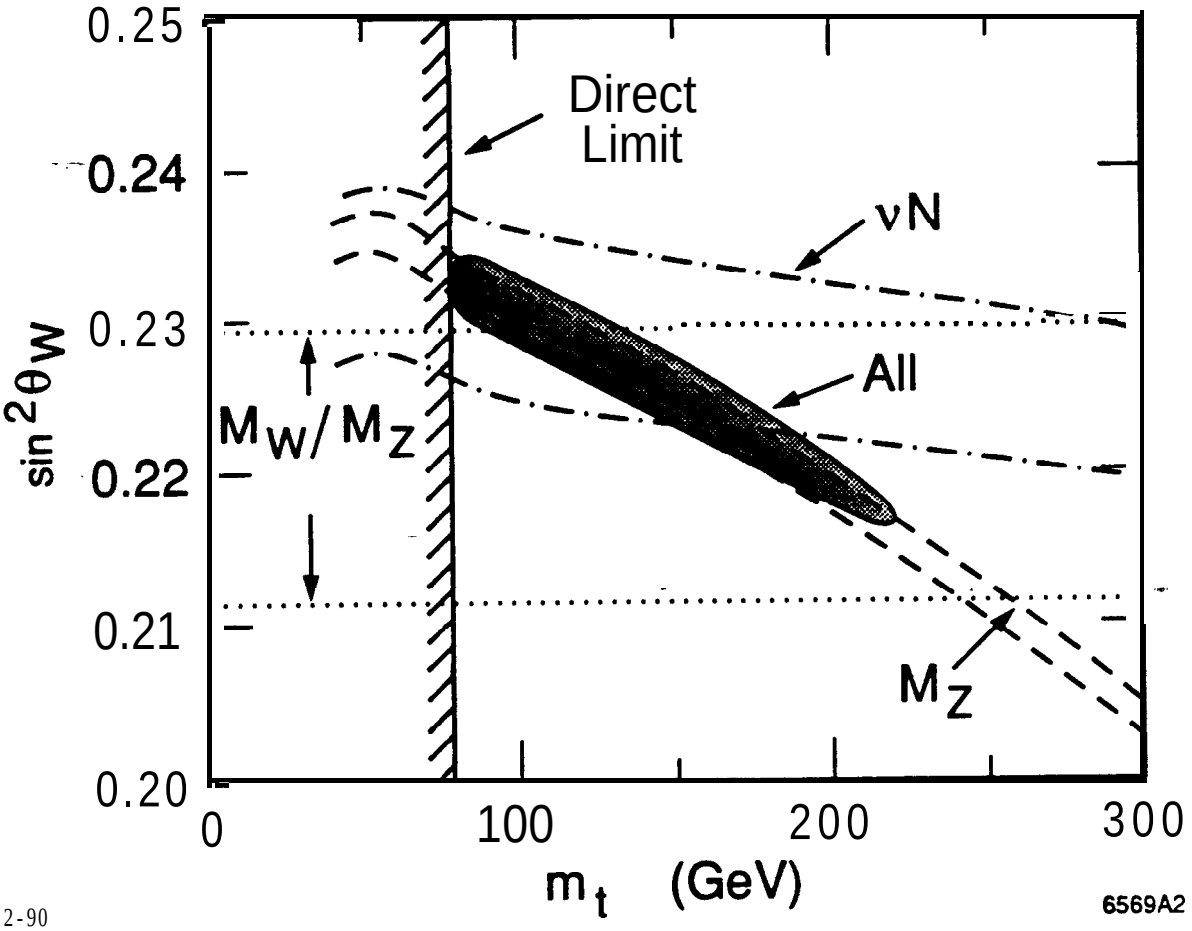

Figure 44. Interval in $\sin^2 \theta_w|_S$ allowed at 1 σ confidence based on the measured values of m_Z, m_W/m_Z, and neutrino deep-inelastic cross sections, from Ref. 54. The intervals are plotted as a function of m_t, assuming m_H = 100 GeV. The shaded region is the 90% confidence allowed region in the plane of $\sin^2 \theta_w|_S$ versus m_t.

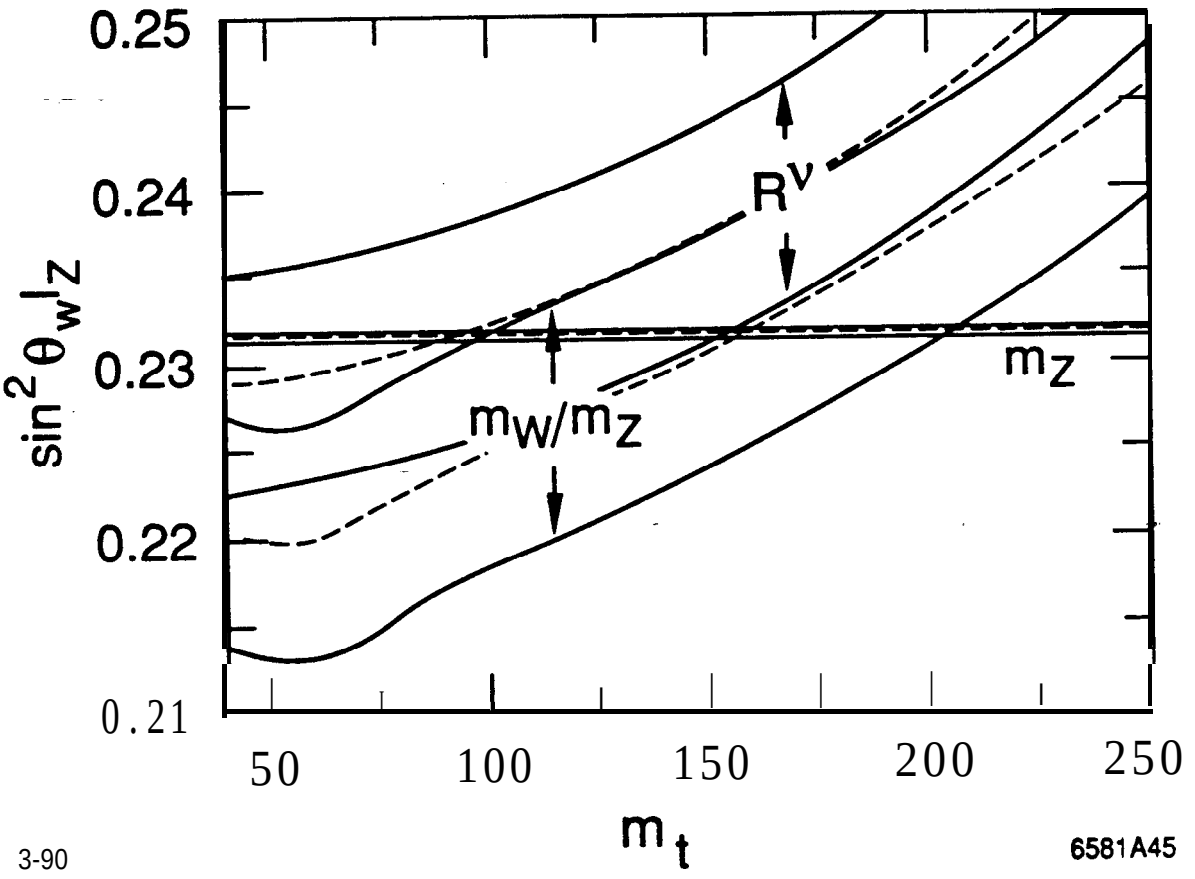

Figure 45. Interval in $\sin^2\theta_w|_Z$ allowed at 1 σ confidence based on the measured values of m_Z, m_W/m_Z, and R^ν. The notation is as in Fig. 43.

of the accidental compensation of the strong m_t dependence of p,(O) by the strong m_t dependence of the relation between $s_*^2(0)$ and $\sin^2\theta_w|_S$. On the other hand, the band from m_Z falls sharply on this plot, reflecting the steep dependence of $\sin^2\theta_w|_S$ on m_t shown in Fig. 36. Bands extracted from direct measurements of $s_*^2(m_Z^2)$ (from Z^0 asymmetries) or $s_*^2(0)$ (from electron-neutrino scattering) will have a similar steep decrease across the plot. The Z^0 mass measurement becomes seriously inconsistent with the neutrino measurements for $m_t > 200$ GeV. At a somewhat lower level of confidence, the measurements of m_Z and m_W become inconsistent if the top quark mass is too low. In Ref. 54, Langacker has reported a 90% confidence interval 51 GeV $< m_t <$ 186 GeV for m_H = 100 GeV; these limits are weakened slightly by variation of the Higgs boson mass. Ellis and Fogli[53] have, somewhat less conservatively, quoted the result $m_t = 132 \pm 34$ GeV. The result that the top quark mass is bounded from above by the consistency of weak interaction radiative corrections is not new; for example, the 1987 analysis of Amaldi, et *al.*,[9] gave the restriction $m_t <$ 180 GeV at 90% confidence. However, in the new data this,, restriction arises not as the integrated effect of many different experiments but rather as the direct contradiction of two well-measured observables.

How can we obtain more precise information on the top quark and other sources of weak interaction radiative corrections? To indicate the expectations for the near future, I have presented in Fig. 46 the expectation for the mid-1990's, when m_W has been measured to ± 50 MeV at the Tevatron or at LEP II. I have also added a band from A_{LR}, which I assume has been measured to ± 0.003 at the SLC. I cannot judge how much high-statistics neutrino scattering experiments at Fermilab can improve the value of $\sin^2\theta_w$ extracted from *R"*. At the moment, a large part of the error in this measurement is systematic, though this systematic error should be diminished by using the new high-energy neutrino beam from the Tevatron to measure the deep inelastic cross section well above charm threshold. However, I have indicated the effect of a measurement of $R^{\bar{\nu}}$, the neutral to charged current ratio in antineutrino-nucleon scattering, to f0.003. This measurement is difficult, since the systematic uncertainties of *R"* are larger for antineutrinos; however, it is

a powerful probe of m_t and other effects that renormalize p+(O), since the function $R_{LS}^{\bar{\nu}}$ defined in (5.66) is almost independent of $\sin^2 \theta_w$ in the region of physical interest.

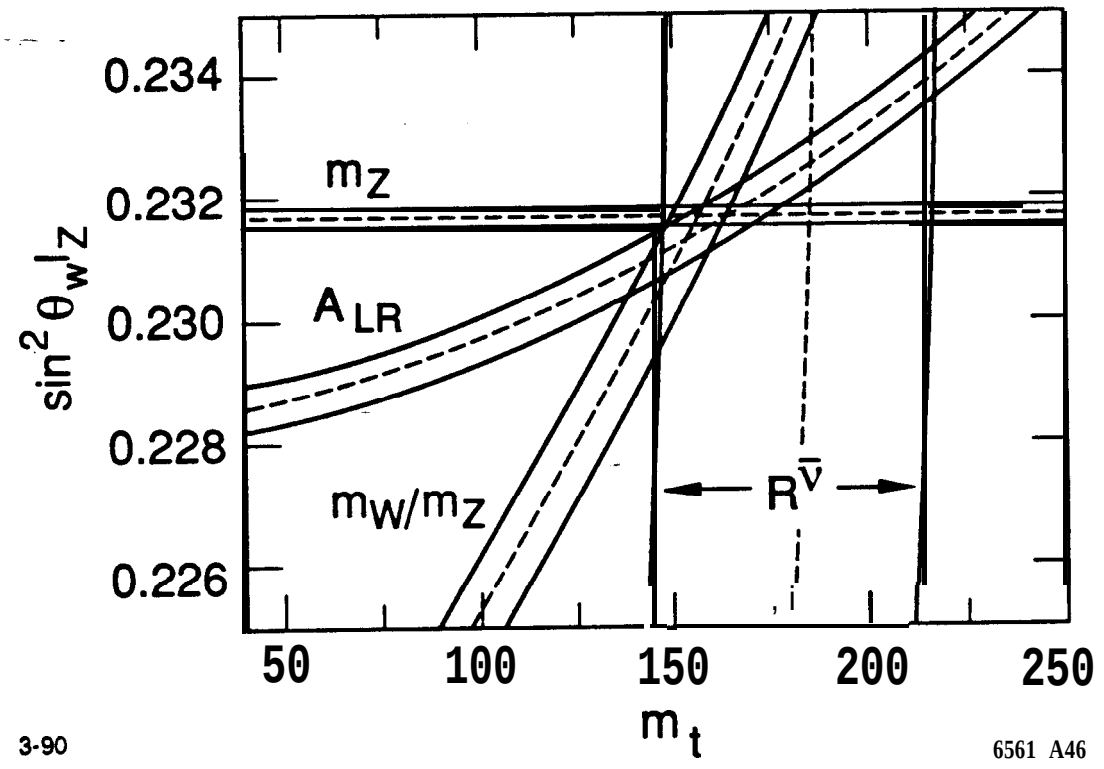

Figure 46. Future prospects for constraints on $\sin^2\theta_w|_Z$. The 1 σ confidence intervals are plotted versus m_t as in Fig. 43. The bands indicated come from m_Z, m_W/m_Z, A_{LR}, and $R^{\bar{\nu}}$. The expected errors in these quantities are described in the text; the central values are, of course, chosen arbitrarily.

6. Conclusions and Prospects

The comprehensive analyses discussed in the previous section bring this review to a natural conclusion. We began by discussing the general features of the standard model and the detailed properties of the lowest order predictions. We then made a lengthy digression on the extraction of the Z^0 mass from the resonance line-shape. Following this, we computed a certain class of weak interaction radiative corrections and saw how these influence the detailed predictions of the electroweak theory. Along the way, I included a brief discussion of the effects of an extended gauge sector, to remind you that new physics may appear not only in the loops, but also in the lowest order formulae.

When the top quark is eventually discovered and its mass measured, we will have an interesting confrontation between this mass value and the size of precisely measured weak corrections. However, it is possible, and even almost expected, that this comparison will fail. Through the example of the top quark loop corrections, we have seen that the weak interactions may be strongly perturbed by loop effects of heavy species. These effects may in fact be our first view of new physics beyond the standard model. In the last two figures, I have presented two manifestations of an additional quark doublet which might appear at very large mass. Figure 47 shows the effect of this doublet on the m_W and A_{LR}, assuming that m_Z is well known and that the top quark contribution is known and subtracted. Figure 48 shows a more futuristic application of weak interaction radiative corrections in the context of future, very high energy e^+e^- colliders. At energies of order 1 TeV in the center-of-mass, a heavy quark doublet of mass m_Q which is still above threshold produces a radiative correction to the amplitude for $e^+e^- \to W^+W^-$, for which the enhancement factor m_Q^2/m_W^2 expected from (5.43) constitutes a substantial modification of the differential cross section.[55] In both cases, the measurement of l-loop corrections allows a glimpse of physics at energies well beyond the nominal collision energy of the e^+e^- reaction.

I have high hopes, then, for this new era of precision weak interaction exper-

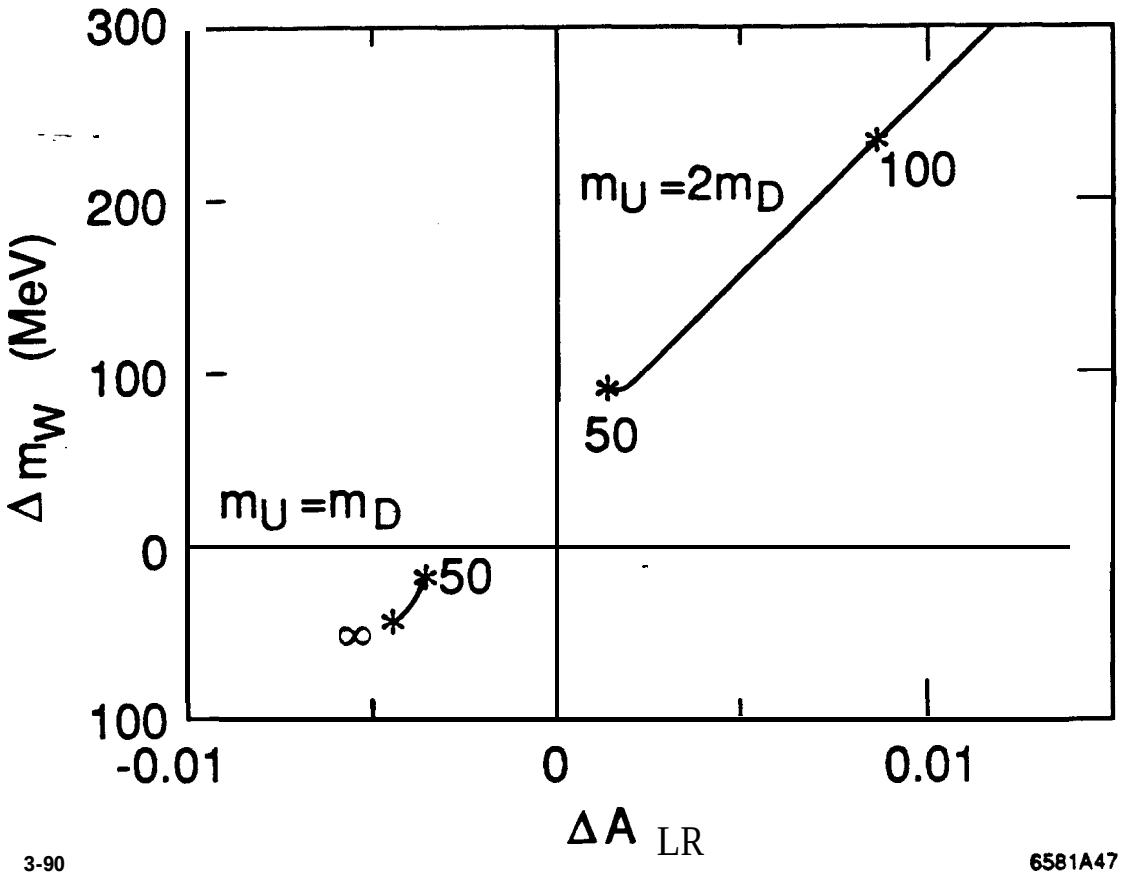

Figure *47.* Effect of a heavy quark doublet (U, D) on the rapport between A_{LR} and m_W, as a function of the mass of the D. The effects are plotted as shifted from the standard model prediction. The two curves refer to m_D/m_U = *0.5* and m_D/m_U = 1. The value of m_D at the starred points is indicated.

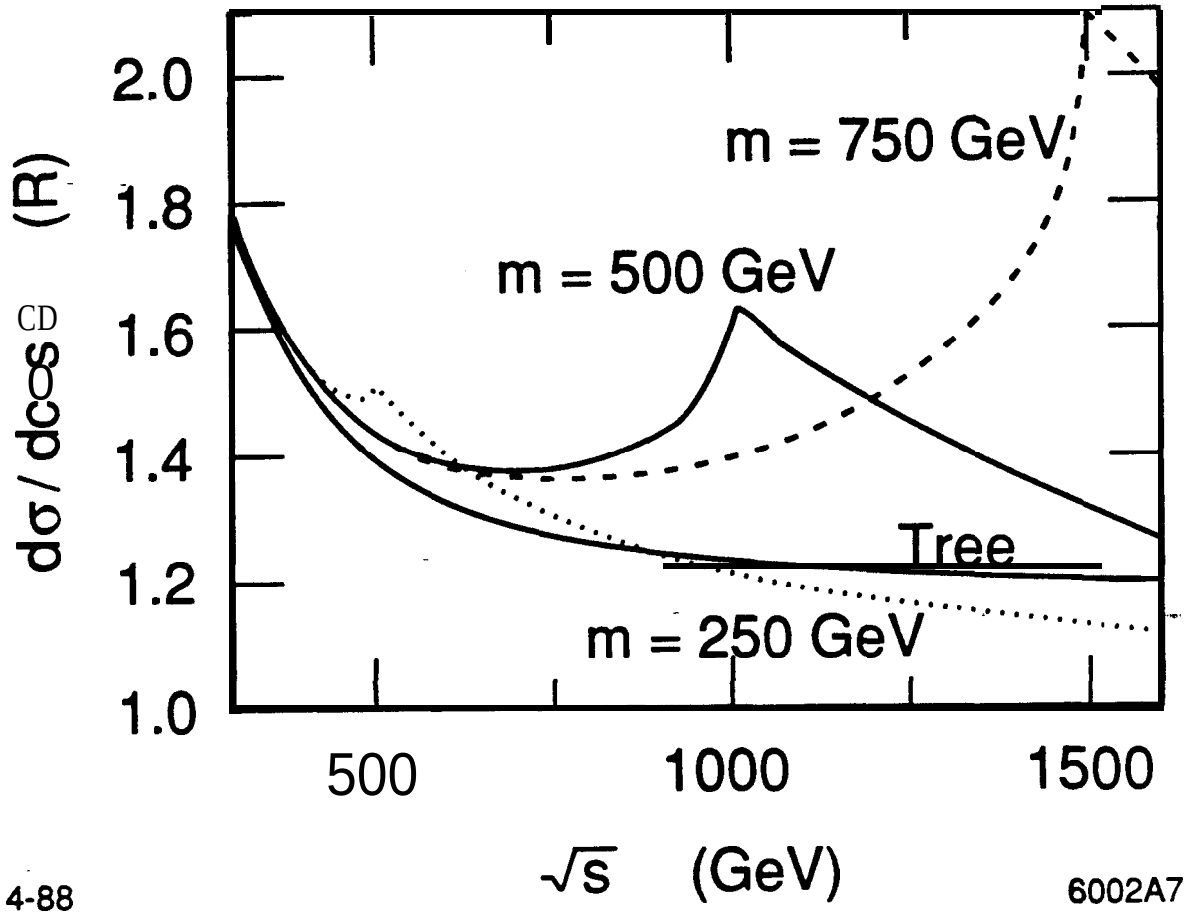

Figure 48. Effect of a heavy quark doublet on the differential cross section for $e^+e^- \rightarrow W^+W^-$, at cos θ = 0. The various curves assume $m_D = m_U = m$; the cross section is computed in units of R.

iments, in which the weak interactions become a tool to probe for the next scale of fundamental physics. I wish my experimental colleagues the skill, perseverence, and, above all, the good luck to follow this road to its promised end.

Acknowledgements:

I am grateful to many colleagues, at SLAC and elsewhere, for discussions which have contributed to my understanding of this subject. Among these people, I am particularly grateful to Gary Feldman, Traudl Hansl, Emlyn Hughes, Paul Langacker, Bryan Lynn, and Morris Swartz for sharing their considerable expertise on the topics discussed here, and to Yossi Nir and Tatsu Takeuchi, for their patient criticism of the manuscript.

REFERENCES

1. A. Sirlin, *Nucl. Phys.* **B71,** 29 (1974), *Nucl. Phys.* **B100,** 291 (1975).
2. A. Sirlin, *Phys.* Rev. **D22,** 971 (1980).
3. M. Veltman, *Acta Phys. Pol.* **B8,** 475 (1977).
4. M. Veltman, *Nucl. Phys.* **B123, 89** (1977).
5. W. Hollik, DESY preprint DESY 88-188 (1988), to appear in *Fortschr. Phys.*
6. *Z* Physics at *LEP* 1, Vol. 1, G. Altarelli, R. Kleiss, and C. Verzegnassi, eds. CERN Report CERN 89-08 (1989).
7. P. Sikivie, L. Susskind, M. Voloshin, and V. Zakharov, *Nucl. Phys.* **B173,** 189 (1980).
8. J. E. Kim, et al., Rev. Mod. *Phys.* 53, 211 (1981).
9. U. Amaldi, et al., *Phys.* Rev. **D36,** 1385 (1987).
10. G. Costa, et al., *Nucl.* Phys. **B297, 244** (1988).
11. J. Alexander, et al. (Mark II), *Phys.* Rev. *Lett.* 63, 2173 (1989).
12. P. Aarnio, et al. (DELPHI), CERN preprint CERN-EP/89-134 (1989).
13. D. Decamp, et al. (ALEPH), CERN preprint CERN-EP/89-169 (1989).
14. L3 Collaboration, L3 preprint # 004 (1989).
15. M. Z. Akrawy, et *al.* (OPAL), CERN preprint CERN-EP/90-27 (1990).
16. G. Bonneau and F. Martin, *Nucl. Phys.* **B27, 381** (1971).
17. G. Altarelli and G. Parisi *Nucl. Phys.* B126, 298 (1977).
18. E. A. Kuraev and V. S. Fadin, Sov. *J. Nucl.* Phys. 41, 466 (1985).
19. V. N. Gribov and L. N. Lipatov, Sov. *J. Nucl. Phys.* 15, 438 (1972); L. N. Lipatov, Sov. *J. Nucl. Phys.* 20, 94 (1974).
20. R. N. Cahn, *Phys.* Rev. D36, 2666 (1987).

21. F. A. Berends, G. J. H. Burgers, and W. L. van Neerven, *Phys. Lett.* **185B,** 395 (1987).

22. F. A. Berends, in ref. 6.

23. J. Alexander. G. Bonvicini, P. Drell, and R. Frey, *Phys.* **Rev. D37, 56** (1988).

24. M. Bohm and W. Hollik, *Nucl. Phys.* B204, 45 (1982).

25. P. Langacker, R. W. Robinett, and J. L. Rosner, *Phys.* Rev. D30, 1470 – (1984).

26. M. E. Peskin, in Proceedings of *the* Fifteenth *SLAC* Summer Institute on *Particle Physics* (August, *1987),* E. C. Brennan, ed. SLAC Report No. 328 (1987).

27. Talks presented at the 1990 meeting of the Division of Particles and Fields of the APS, Dallas (January, 1990). These results are still preliminary.

28. G. Beall, M. Bander, and A. Soni, *Phys.* Rev. *Lett.* 48, 848 (1982).

29. P. Langacker, *Phys.* Rev. **D30, 2008** (1980).

30. M. Cvetič and B. W. Lynn, *Phys.* Rev. D35, 51 (1987).

31. G. Altarelli, R. Casalbuoni, D. Dominici, F. Feruglio, and R. Gatto, CERN preprints CERN-TH-5591/89 (1989), 5626/90 (1990).

32. W. Marciano, *Phys.* Rev. **D20, 274** (1979).

33. W. Marciano and A. Sirlin, *Phys.* Rev. **D22, 2695** (1980).

34. H. Burkhardt, F. Jegerlehner, G. Penso, and C. Verzegnassi, *Z. Phys.* C43, 497 (1989).

35. B. W. Lynn, G. Penso, and C. Verzegnassi, *Phys.* Rev. D35, 42 (1987).

36. E. Eliasson, *Phys. Lett.* **147B,** 65 (1984).

37. J. A. Grifols and J. Sola, *Nucl. Phys.* **B253, 47** (1985).

38. B. W. Lynn, M. E. Peskin, and R. G. Stuart, in *Physics* at *LEP,* J. Ellis and R. Peccei, eds. CERN Report CERN 86-02 (1986).

39. G. Passarino, *Phys.* Lett. B228, 89 (1989).

40. S. Fanchiotti and A. Sirlin, *Phys.* **Rev. D41,** 319 (1990).

41. W. Marciano and A. Sirlin, *Phys. Rev. Lett. 46,* 163 (1981).

42. R. E. Taylor, personal communication.

43. J. Jersak, E. Laermann, and P. M. Zerwas, *Phys. Lett.* **98B,** *363* (1981), Phys. Rev. D25, 1218 (1982).

44. D. Kennedy and B. W. Lynn, *Nucl. Phys.* B322, 1 (1989).

45. A. A. Akhundov, D. Yu. Bardin, and T. Riemann, *Nucl. Phys.* B276, 1 (1986).

46. J. Bernabéu, A. Pich, and A. Santamaría, *Phys.* Lett. **200B,** 569 (1988).

47. W. Beenakker and W. Hollik, *Z. Phys.* **C40,** 141 (1988).

48. H. Abramowicz, et *al.*, *Phys. Rev.* Lett. 57, 298 (1986), *Z. Phys. C35, 443* (1987).

49. J. V. Allaby, *et al., Phys. Lett.* **177B, 446** (1986), *Z. Phys.* **C36,** 611 (1987).

50. A. Blondel, et *al.,* CERN preprint CERN/EP 89-101 (1989).

51. C. H. Llewellyn Smith, *Nucl. Phys.* B228, 205 (1983).

52. D. Kennedy, B. W. Lynn, C. J. C. Im, and R. G. Stuart, *Nucl. Phys.* **B321,** *83* (1989).

53. J. Ellis and G. Fogli, *Phys.* Lett. **213B, 526** (1988), **232B,** 139 (1989).

54. P. Langacker, *Phys. Rev.* Lett. 63, 1920 (1989).

55. C. Ahn, M. E. Peskin, B. W. Lynn, and S. Selipsky, *Nucl. Phys.* **B309,** 221 (1988).